ERDC TR-09-6

US Army Corps
of Engineers®
Engineer Research and
Development Center

Mobility Performance Algorithms for Small Unmanned Ground Vehicles

Paul W. Richmond, George L. Mason, Barry A. Coutermarsh,
Jason Pusey, and Victoria D. Moore

May 2009

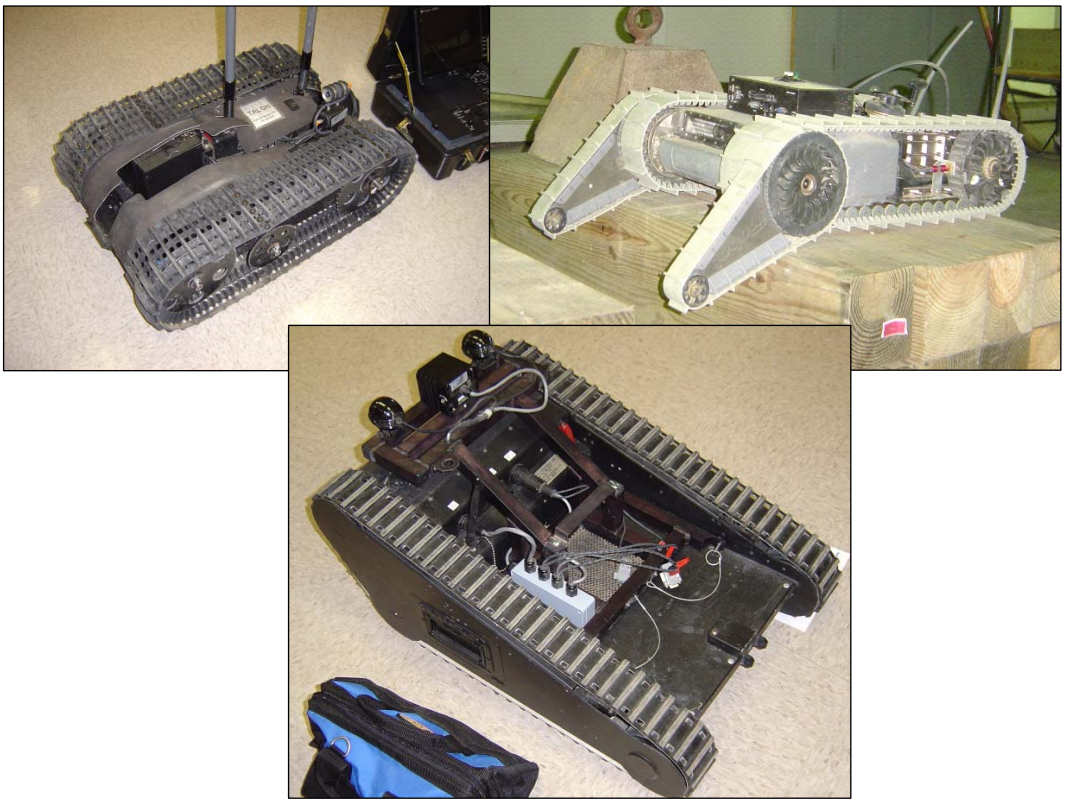

Engineer Research
and Development Center

ERDC TR-09-6
May 2009

Mobility Performance Algorithms for Small Unmanned Ground Vehicles

Paul W. Richmond, George L. Mason, and Victoria D. Moore

Geotechnical and Structures Laboratory
U.S. Army Engineer Research and Development Center
3909 Halls Ferry Road
Vicksburg, MS 39180-6199

Barry A. Coutermarsh

Cold Regions Research and Engineering Laboratory
U.S. Army Engineer Research and Development Center
72 Lyme Road
Hanover, NH 03755-1290

Jason Pusey

Army Materiel Systems Analysis Agency
U.S. Army Research, Development and Engineering Command
392 Hopkins Road
Aberdeen Proving Ground, MD 21005-5071

Final report

Prepared for Headquarters, Department of the Army
Office of the Deputy Chief of Staff, G-3/5/7, ATTN: DAMO-SB
400 Army Pentagon
Washington, DC 20310-0400

Under Project No. UO-2005-37, Small Unmanned Ground Vehicles Models and Data

Abstract: Future Combat Systems will include Small Unmanned Ground Vehicles (SUGV). Several have already been deployed, including the TALON®, an 80-lb SUGV; PackBot® at 50 lb, and Gator™ at 2500 lb. As doctrine, tactics, techniques, and procedures continue to evolve, there exists a need to represent the performance of these vehicles in Army models and simulations. Army simulations such as COMBAT^{XXI} and OneSAF will use the Standard Mobility Application Programmers Interface (STNDMob API) for estimating vehicle performance. Currently, only the Gator can be represented by a STNDMob vehicle class, and it is modeled as a manned vehicle.

This report describes the results of a study undertaken to identify and discuss mobility performance algorithms applicable to SUGV in the weight range of 10 to 5000 lb. Algorithms used by the NATO Reference Mobility Model and the STNDMob were examined. Most of the algorithms currently used in STNDMob were found to be applicable to SUGV. However, it was found that vehicle performance data and algorithms for additional material surfaces and obstacles need to be developed; specifically, models and data for wheeled vehicle skid steering, interior building floor and roof surfaces, and stair climbing are needed. Previously unreported SUGV test results for TALON, MATILDA, and PackBot are presented, and performance estimates described herein compared well using currently available algorithms in STNDMob. Recommendations for new algorithms and improvements to current mobility algorithms are presented.

Contents

Figures and Tables

Figures

Tables

Preface

This report was prepared by Dr. Paul W. Richmond, Dr. George L. Mason, and Victoria D. Moore of the Geotechnical and Structures Laboratory (GSL), U.S. Army Engineer Research and Development Center (ERDC); Barry A. Coutermarsh, Cold Regions Research and Engineering Laboratory (CRREL), ERDC; and Jason Pusey of the Army Materiel Systems Analysis Agency, U.S. Army Research, Development and Engineering Command.

The research reported herein was conducted for the U.S. Army's Battle Command, Simulation, and Experimentation Directorate (DAMO-SB), Project No. UO-2005-37, Small Unmanned Ground Vehicles Models and Data. Project oversight was provided by the U.S. Army Training, Readiness and Analysis Command Analysis Center, Monterey, and the Urban Operations Focus Area Collaborative Team. This report serves as the final project report.

Work was conducted under the general supervision of M. Wendell Gray, Chief, Mobility Systems Branch, GSL; Dr. Larry N. Lynch, Chief, Engineering Systems and Materials Division, GSL; Dr. William P. Grogan, Deputy Director, GSL; and Dr. David W. Pittman, Director, GSL.

COL Gary E. Johnston was Commander and Executive Director of ERDC. Dr. James R. Houston was Director.

Acronyms and Abbreviations

ALFUS	Autonomous Levels for Unmanned Systems
AMSAA	Army Materiel Systems Analysis Agency
ANS	Autonomous Navigation Systems
API	Application Programmers Interface
BC	Battle Command
BTRA	Battlefield Terrain Reasoning and Analysis
CASTFOREM	Combined Arms and Support Task Force Evaluation Model
CCTT	Close Combat Tactical Trainer
CI	Cone Index
CIV	CRREL Instrumented Vehicle
C/JMTK	Commercial Joint Mapping Tool Kit
COMBAT^{XXI}	Combined Arms Analysis Tool for the XXIst Century
CRREL	Cold Regions Research and Engineering Laboratory
CSA	Cambridge Scientific Abstracts
CTDB	Compact Terrain Data Base
DBP	Drawbar pull
DoD	Department of Defense
DTIC	Defense Technical Information Center
EDCS	Environmental Data Coding Standard
EDM	Environmental Data Model
ERDC	U.S. Army Engineer Research and Development Center
FCS	Future Combat Systems
GSL	Geotechnical and Structures Laboratory
GVW	Gross Vehicle Weight
METADEX	Metals Abstracts Index
MODSAF	Modular Semi-Automated Forces
M&S	Models and Simulations
NATO	North Atlantic Treaty Organization
NiMH	Nickel Metal Hydride
NIST	National Institute for Standards and Technology
NRMM	NATO Reference Mobility Model
OneSAF	One Semi-Automated Forces
OTB	OneSAF Testbed Baseline
RCI	Rating Cone Index
RI	Remold Index

SEDRIS	Source for Environmental Data Representation and Interchange
SPAWAR	Space and Naval Warfare Systems Command
SPIE	International Society for Optical Engineering
STNDMob	Standard Mobility
SUGV	Small Unmanned Ground Vehicle(s)
UGV	Unmanned Ground Vehicle
UHRB	Ultra High Resolution Building
UO–FACT	Urban Operations Focus Area Collaborative Team
VCI	Vehicle Cone Index
VDC	Volts Direct Current
VEHDYN 4	Vehicle Dynamics Model version 4
WARSIM	Warfighters Simulation
XML	Extensible Markup Language

Unit Conversion Factors

Multiply	By	To Obtain
degrees (angle)	0.01745329	radians
feet	0.3048	meters
g's (standard free fall)	9.80665	meters per second squared
horsepower (550 foot-pounds force per second)	745.6999	watts
inches	0.0254	meters
inch-pounds (force)	0.1129848	newton meters
miles per hour	0.44704	meters per second
ounces (mass)	0.02834952	kilograms
pounds (force)	4.448222	newtons
pounds (force) per square inch	6.894757	kilopascals
pounds (mass)	0.45359237	kilograms

1 Introduction

The U.S. Army Battle Command, Simulation, and Experimentation Directorate's Urban Operations Focus Area Collaborative Team (UO-FACT) recognized that the modeling and simulation of the performance of small unmanned ground vehicles (SUGV) is a deficiency that should be corrected. The intent of this study was to examine models, algorithms and data and their use in simulating SUGV mobility performance and begin to address this deficiency.

Future Combat Systems (FCS) will include SUGV, several having already been deployed, including the TALON®, an 80-lb SUGV; PackBot® at 50 lb, and Gator™ at 2500 lb. Additionally, the FCS projects that 40% of the military fleet may eventually be robotic. As doctrine, tactics, techniques, and procedures evolve, there exists a need to represent the performance of these small vehicles in Army Models and Simulations (M&S).

The COMBAT^{XXI} and OneSAF simulations will use the Standard Mobility Application Programmers Interface (STNDMob API) for estimating vehicle performance in future studies. Currently, only the Gator can be represented by a STNDMob vehicle class, in which it is modeled as a manned vehicle. Additionally, Pusey (2005) studied issues associated with modeling small remote-controlled vehicles in the Combined Arms and Support Task Force Evaluation Model (CASTFOREM) simulation. He listed issues that need to be resolved before unmanned ground vehicles can be simulated in a force-on-force model, including extending vehicle performance models and analyzing/modeling levels of autonomy. Thus, models of the mobility performance of small ground vehicles must be enhanced and modified or existing models validated before performance of small unmanned vehicles can be simulated with confidence.

This report presents the results of a study undertaken to address the issues associated with modeling the performance of SUGV in Army simulations. For this study, SUGV are considered to be unmanned vehicles in the 10- to 5000-lb weight range. This report presents (1) the results of a literature review, (2) analysis of data collected from previously undocumented mobility performance tests of three SUGV (TALON, MATILDA and PackBot), (3) a discussion of existing full-sized vehicle performance algorithms, and (4) applicability of the performance algorithms to SUGV.

STNDMob vehicle input data files and simulated performance predictions for the three SUGV are presented and discussed in the main text and Appendixes A-C. Additionally, the simulations included performance predictions for the M151 (the original military Jeep) and for the CRREL Instrumented Vehicle (CIV), a 1978 Jeep Cherokee (Blaisdell 1983; Shoop 1993). Although these are manned vehicles, they fall within the SUGV weight range defined for this study. Complete validation of these predictions was not possible due to lack of test data; however, in the opinion of the authors the predictions appear reasonable. Algorithms and models that need further investigation are identified.

2 Background

Mobility as a noun is defined[1] as the quality of moving freely. Traditionally, military ground-vehicle mobility performance has been

- quantified by maximum capable speed in/on given terrain and weather conditions;
- based on semi-empirical models of vehicle capabilities, vehicle-terrain interaction (traction and resistance), driver behavior, and other factors;
- based on a force-balance model (traction versus resistance) along with vehicle characteristics that lead to an equation of tractive force versus speed.

Ground vehicle performance is dependent not only on vehicle characteristics but also upon operator desires such as safety and comfort. How the vehicle interacts with a myriad of possible terrain types (roads, soils, snow, etc.) and conditions (soils of various strength, wet or dry surfaces) results in a large number of "conditions" that need to be examined.

The NATO Reference Mobility Model (NRMM) is the Army model and simulation standard for predicting vehicle mobility. The Standard Mobility API is a model based upon parametric or regional-based terrain and NRMM output. STNDMob includes some of the underlying NRMM algorithms and was developed to specifically support the COMBAT^{XXI} and OneSAF entity level simulations.

Mobility performance models

NATO Reference Mobility Model

The NRMM (Ahlvin and Haley 1992) is a comprehensive computer model that predicts vehicle speed performance on roads, trails, and cross-country in all weather conditions, including terrain conditions associated with winter. The model primarily calculates available traction and motion resistance caused by operation on soft (deformable) surfaces. The traction-versus-slip relationships (see Appendixes B and C) are used, in

[1] *Dictionary.com Unabridged (v 1.0.1)*. Retrieved October 05, 2006, http://dictionary.reference.com/browse/mobility.

conjunction with power-train capabilities to generate an overall maximum traction-versus-speed prediction. The motion resistance is used in combination with other resisting forces (e.g., vegetation, slope) to determine the maximum possible force controlled by speed. Model outputs are velocities traveling up- and down-slope, average velocity, and a numerical code related to the speed-controlling algorithm.

The NRMM is based on data and analysis of the performance of manned standard military vehicles, and some of the underlying algorithms were also developed using scale models in laboratory settings. Recent work by ERDC reexamined these early, fine-grained soils, nondimensional vehicle terrain interaction algorithms to develop a vehicle terrain interface software package for use in a ride motion simulator (Richmond et al. 2004). Haueisen et al. (2005) reported on a case study of the PackBot, modeled with the NRMM, concluding that the greatest obstacle for broad use of the NRMM as an evaluation tool (for small vehicles) is the lack of terrain data at suitable fidelity.

The NRMM is the Army standard mobility model for M&S applications and is the basis of many current ground-vehicle-performance values in current simulations (e.g., the Warfighters Simulation, WARSIM, and the Close Combat Tactical Trainer, CCTT). The Standard Mobility API (discussed below) is also based upon the NRMM and requires data files that have been precomputed using the NRMM.

Vehicle Dynamics Model (VEHDYN 4)

The principal intent of the VEHDYN 4 model is to estimate limits to vehicle speeds based upon driver tolerance of vibration (ride) or shock. VEHDYN 4 can also be used to compare simulated model performance with measured dynamics data, such as accelerations, velocities, and displacements of various vehicle locations and/or components and average absorbed power. Recent enhancements (Creighton et al., in preparation) have added the ability to develop the obstacle force table required by the NRMM and to take into account deformable terrain, in addition to a wireframe animation capability.

The three principal outputs required for NRMM and the Standard Mobility API (which is discussed below) are as follows:

1. Ride performance: Ride is defined as the random semi-uniform vibrations transferred by the vehicle to the driver or other occupants as a result of traveling over an uneven surface. One of the principal measures of ride comfort is absorbed power. A criterion of 6 W (watts) of absorbed power has been established as an upper bound of vibration that will permit crew members to effectively perform their tasks. Experimental test results have shown that there is quite often only a small increase in speed at 15 or 20 W over that at 6 W, because the 6-W absorbed power levels usually occur when the vehicle's suspension begins "bottoming out" and producing discrete shock loads. The 6-W ride curve for the M151 Jeep[1] is shown in Figure 1. It is possible to generate multiple ride curves at different watt levels and to allow the "driver" to choose the amount of power he is willing to absorb.
2. Shock performance: Shock is defined as a sudden, severe change in vibration transferred from the vehicle to the driver or other occupants as a result of an impact with a discrete obstacle such as a boulder, log, rice paddy dike, or ditch. One of the principal measures of shock tolerance is the maximum peak acceleration. A criterion of 2.5 g's vertical acceleration has been established as an upper bound of shock for manned vehicles. This limit was determined through research and experimental testing at the U.S. Army Engineer Waterways Experiment Station in the early 1960s. The 2.5-g speed for an M151 Jeep crossing a 6-in. obstacle is about 10 mph, and a 4-in. obstacle will not produce a 2.5-g level. Figure 2 shows the shock curve for the M151, based on height, using a semicircular obstacle. Murphy and Ahlvin (1976) reported that shock level is relatively insensitive to obstacle shape and that height is a suitable descriptor.
3. Obstacle forces and clearances: As a vehicle crosses an obstacle (see Figure 3, which specifies obstacle dimensions), it encounters additional forces associated with slope climbing and the possibility of interference with its chassis (clearance). A table of clearance values, maximum forces, and average forces is developed for a series of obstacles whose sizes are based on the vehicle geometry itself—the intent being to span the full range of obstacles that are negotiable, including some that are not—allowing interpolation between obstacle sizes. Table 1 gives partial obstacle-force data for an M151 vehicle.

[1] Although no longer used by the U.S. Army, the M151 jeep is within the weight range of "small" vehicles for which there is a significant amount of mobility data (see Table 1). It is used for illustrative purposes and comparison in this study.

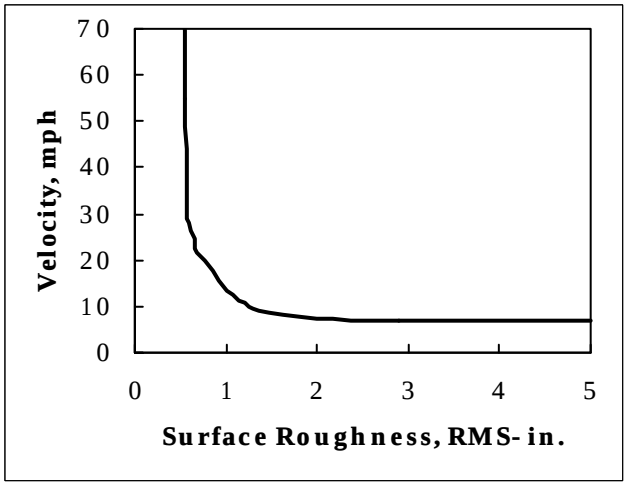

Figure 1. Ride curve for the M151 Jeep.

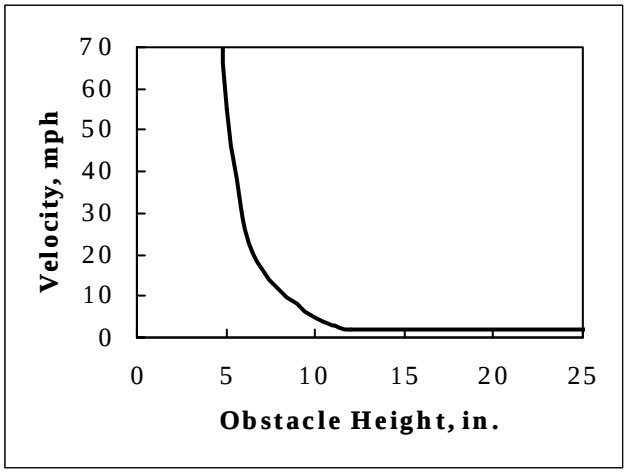

Figure 2. Shock curve for the M151 Jeep.

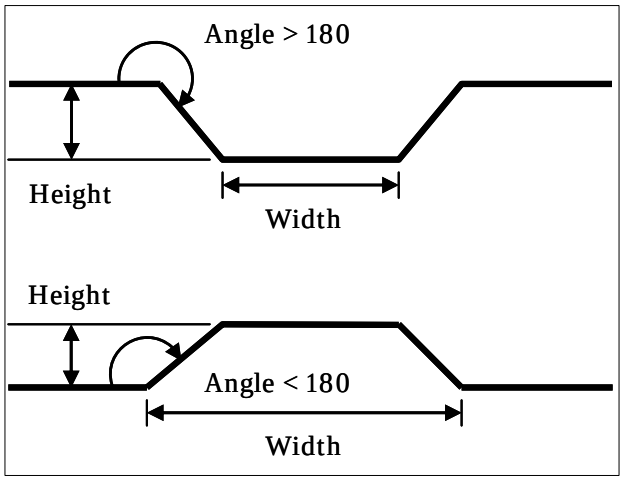

Figure 3. NRMM symmetric obstacles.

Table 1. Partial obstacle-force data for the M151.

Clearance in.	Maximum Override Force, lb	Average Override Force, lb	Height in.	Angle rad	Width in.
8.38	1295.7	285.8	3.15	1.95	5.88
-3.05	2626.8	389.9	15.75	1.95	5.88
-20.45	2616.0	471.7	33.46	1.95	5.88
8.38	1295.7	285.8	3.15	2.48	5.88
-2.69	1405.3	362.5	15.75	2.48	5.88
-13.97	1340.6	402.4	33.46	2.48	5.88

Standard Mobility API

The Standard Mobility API (STNDMob) (Baylot et al. 2005; Richmond et al. 2005) was developed over the past several years and is enhanced periodically to support emerging Army M&S. STNDMob level 1 and 2 fidelity is currently used by COMBAT^{XXI} and OneSAF. Higher levels of fidelity indicate increased sophistication of the vehicle, terrain data, and the mobility algorithms used. Level 3 fidelity of the STNDMob is one of the ERDC Battlespace Terrain Reasoning and Analysis (BTRA) modules handed off to the Commercial Joint Mapping Tool Kit (C/JMTK), a future component of Battle Command (BC) systems for terrain analysis and mission planning. As development continues on COMBAT^{XXI} and OneSAF, there will be a need to simulate SUGV with STNDMob. (STNDMob fidelity level 3 and 4 has also been delivered to OneSAF and COMBAT^{XXI} developers.)

STNDMob level 3 groups vehicles into bins and uses a representative vehicle as a basis for making performance predictions; these are shown in Table 2. Fidelity level 4 uses the same data file format and algorithms, but data for the actual vehicle (in lieu of a representative vehicle) are used for predictions.

Table 2. Vehicle bins and representative vehicles for STNDMob level 3.

Vehicle Bin No.	Vehicle	Name/Description
1	M1A1	High-mobility tracked
2	M270 MLRS	Medium-mobility tracked
3	M60 AVLB	Low-mobility tracked
4	M1084 MTV	High-mobility wheeled

Vehicle Bin No.	Vehicle	Name/Description
5	M985 HEMTT	Medium-mobility wheeled
6	M917 Dump Truck	Low-mobility wheeled
7	M1084/M1095	High-mobility wheeled w/towed trailer
8	M985/M989	Medium-mobility wheeled w/towed trailer
9	M911/M747 HET	Low-mobility wheeled w/towed trailer
10	M113A2	Tracked amphibious combat vehicle
11	LAV25	Wheeled amphibious combat vehicle
12	Kawasaki ATV	Light ATV

As mentioned above, the STNDMob is based on algorithms and data derived from the NRMM, the Army standard for vehicle mobility modeling. STNDMob vehicle performance files are created using a special output file format of the NRMM. The data currently contained in these files for fidelity levels 3 and 4 fidelity are shown in Table 3.

Table 3. Vehicle data parameters.

Parameter	Description or allowable value
Configuration	
Type	Vehicle type: “Tracked” or “Wheeled.”
Towing_Trailer	“Yes” or “No.”
Plow_Blade_Capable	“Yes” or “No.”
Plow_HPcoef	Power-train power reduction coefficient penalty for using the plow (1.0 = no reduction).
Primary_Use	Truck, amphibious (or similar design) combat vehicle, heavy equipment transporter, or other use.
Mfg_Type	The country of origin or manufacturer of the vehicle.
Dimensional_Data	
Gross_Weight	Gross weight (newtons, N) of the vehicle.
Units	The number of vehicle units connected (a truck towing a trailer has two units).
Unit_Length	The length (inches, in.) of each unit.
Max_Unit_Width	The maximum width (in.) of all units.
Unit_Ground_Clearance	The minimum ground clearance (in.) of all units.
Push_Bar	The maximum push-bar force (pounds) the vehicle can withstand overriding vegetation and the height (in.) from the ground to the center

Parameter	Description or allowable value
Force Height	of the push-bar.
Engine_Power	Net engine horse power (horsepower).
Rotating_Mass_Factor	A factor that increases the vehicle's mass based on the inertia of rotating components, used in the calculation of vehicle acceleration.
Center_Of_Gravity Lateral Height	The lateral and vertical center of gravity measured from the geometric center of the vehicle and from the ground (in.).
Tipping_Angle	The angle (radians) at which a vehicle will tip over in a static position.
Axle_Width	The vehicle's axle length (in.) from the center of the left wheel to the center of the right wheel.
AvgTireCorneringStiffness	The vehicle's average tire cornering stiffness (N/degree).
AssemblyWeight	The weight (N) on each axle or track assembly.
CenterToCenterTreaWidth	The center-to-center distance (meters, m) between tracks or wheels on each assembly.
TrackGroundLength	The length of a track on the ground (m).
NumTires	The number of tires on an axle assembly; normally 2, but 4 for duals, 0 for a tracked assembly.
TireUndeflectedDiameter	Undeflected diameter (m) of the tires on each axle.
MinimumTurnRadius	Minimum turning radius (m).
MaxSustainedTireSpeed-Duration	The duration (seconds) at which the maximum tire speeds based on inflation pressure were determined (included in Traction_Data, see below).
Speed_Caps	
On_Road	Maximum on-road speed (kilometers per hour, kph).
Fording	Maximum fording speed (kph).
Swimming	Maximum swimming speed (kph).
Ride_Limited	An array of speed limits based on power absorbed and surface roughness.
UrbanRide_Limited	An array of speed limits based on power absorbed and urban debris spacing.
Obstacle_Maneuver	
Fording_Depth, m	The vehicle combination maximum fording depth (m).
Obstacle_Data	An array of resistive forces, obstacle heights, approach angles, and widths.
Obstacle_Shock	An array of obstacle heights and speed limits (based on a 2.5-g vertical acceleration limit).

Parameter	Description or allowable value
Traction_Data	Multiple arrays of traction and resistance data based on throttle position, and the subsequent tag names. For each of these conditions the traction arrays contain: Maximum braking coefficient Maximum traction coefficient Minimum traction coefficient Maximum tire speed (based on U.S. Army doctrine for tire inflation and terrain) Resistive force coefficient Tractive force speed curve coefficients (see Equation 1)
Terrain_Type	On-road or off-road.
Surface	Corresponds to SurfaceCondition (see Appendix A).
RoadType	Superhighway, primary, or secondary road.
Soil	For each of the five NRMM soil classes that map to USCS soil types with soil strengths ranging from a cone index (CI) or rating cone index (RCI) between 5 and 300 (12 values).
Surface	Winter conditions.
SnowTraction	Ice, ice covered with dry snow, hard-packed snow, and dry snow.
SnowResistance	An array of resistance data for snow based on underlying soil cone index, snow depth, and snow density.

Figure 4 illustrates the variation of tractive force required to achieve a given speed. These relationships will change as a function of soil type, soil strength, surface condition, and throttle setting. These curves are represented by a hyperbola, and Equation 1 shows the equation as a function of traction coefficient. Additionally, these relations are bounded by maximum and minimum traction coefficient values.

$$V = \frac{b_0}{(T - b_1)} - b_2 \tag{1}$$

where:

V = vehicle velocity

b_0, b_1, b_2 = curve fit parameters that are generated by the NRMM.

Sets of these curves are generated for the range of terrain-surface conditions as described in Table 3 (see the Traction_Data parameter). Traction coefficient is simply the traction force divided by the total weight supported by wheels or tracks. Maximum traction coefficient is the maximum traction that can be developed on a given surface. The minimum traction is

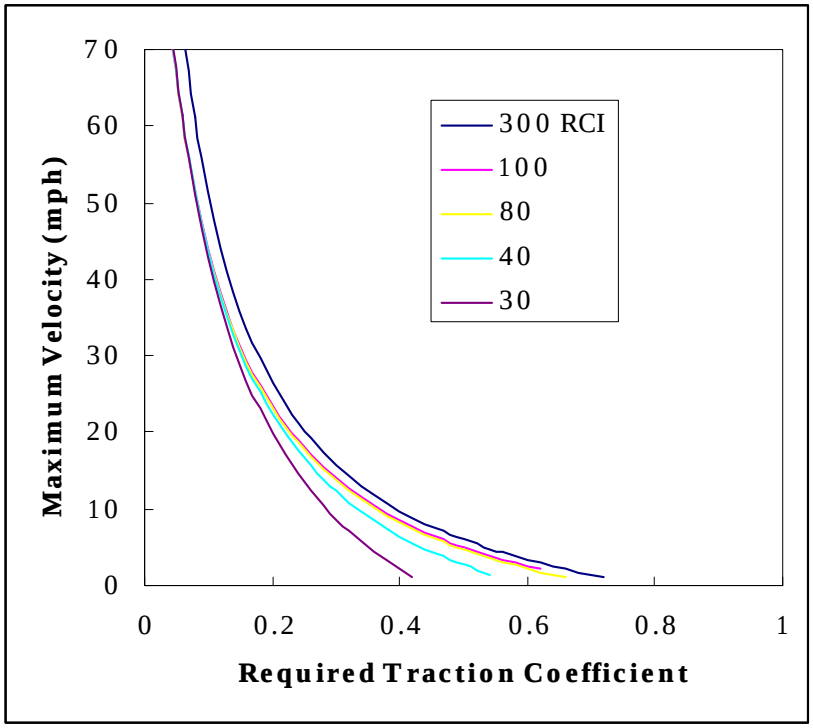

Figure 4. Tractive force versus speed for the M1084 on dry sandy clay.

the amount of traction needed to just move the vehicle; towing resistance is this value plus the resistance of slope, vegetation, obstacles, etc.

Vehicle entity level simulation

To simulate the movement of an individual or group of ground vehicles in an entity level force-on-force simulation, more than maximum capable vehicle speed is required. These requirements can be divided into several submodels, as represented in Figure 5.

Three major modules are represented in Figure 5: a route planning module for long-range planning, a local planner, and a move-vehicle module. In some regards, the movement planning and subsequent movement of a vehicle in these simulations can be considered, in themselves, a form of an autonomous navigation system. This report focuses on the move-vehicle module; however, for some vehicle performance studies, there is a need to understand the effects of the vehicle control mechanism on the local planner. Therefore, driver and autonomous navigation effects on performance are also discussed.

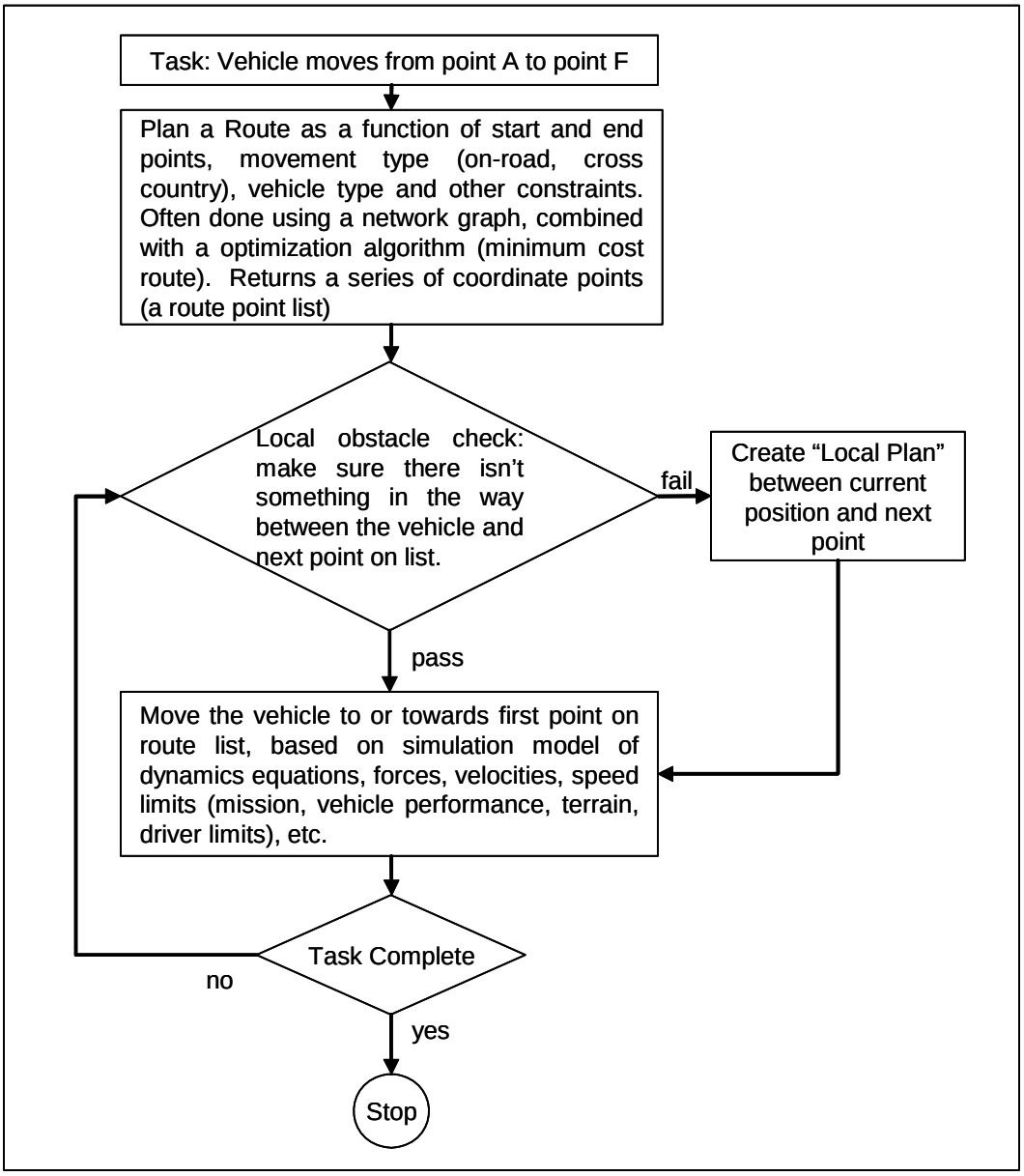

Figure 5. A generic conceptual movement model for an entity level simulation.

The "local planner" requirements can be described by a simple scenario. Consider a stopped vehicle in the path of "your" vehicle that is moving at some speed. In a vehicle operated by a real human onboard, the driver would, at a minimum, cause the vehicle to swerve to avoid a crash. Prior to or during the maneuver, the driver may also cause the vehicle to slow down. If the driver's reaction time and knowledge of the vehicle performance on the given terrain are not sufficient, the vehicle may crash into the stopped vehicle. Another example of the "local planner" is a manned-vehicle performance analysis over an area that has randomly or uniformly spaced obstacles. NRMM accounts for the "local planner" in this case by

reporting an effective speed, also known as speed made good. An example of randomly spaced obstacles is vegetation in a forested area, which in NRMM is represented by a matrix of stem sizes and spacing. Some stem sizes can be driven over while others must be driven around. The NRMM vegetation speed module calculates a speed based on these assumptions and returns the minimum speed associated with maneuvering or riding over the vegetation.

For SUGV, the effects of the method of control (teleoperated, autonomous, semiautonomous) on local planning also need to be modeled. These parameters are discussed in Chapter 6 as driver effects. For a teleoperated vehicle, the operator is primarily dependent on visual cues, with few other sensory inputs, resulting in reduced speeds or increased probability of a driver error due to reaction time (relative to an onboard human operator). In a fully autonomous vehicle, reduced reaction times can be related to sensor input analysis and decision-making time. Fields (2002a) discusses representing interaction of humans and robots in the OneSAF Testbed Baseline (OTB) by including unplanned interactions between the simulated robot and a human operator, for mobility assistance and target identification as an analysis tool for human control of multiple robotic systems.

While entity level force-on-force simulations inherently simulate human behaviors, using these models and the computer code to simulate robotic behavior relates to the “Task” in Figure 5. That is, the models determine how or why an entity should move or conduct some other task. Fields (1999, 2000, 2002b), and Fields and Haug (2003) discuss and demonstrate robotic behavior simulated in OTB.

3 Literature Review

The objective of the literature review was to find performance data on small unmanned ground vehicles that would be useful in development and validation of SUGV performance models. During that search, many of the reports that were looked at contained useful descriptions and information, but often no quantitative data. Those reports are included in the Bibliography. The databases searched were Compendex, Defense Technical Information Center (DTIC), and Cambridge Scientific Abstracts (CSA) Technology Research Database.

Compendex is a comprehensive bibliographic database of engineering research containing references and abstracts to over 5000 engineering journals, conferences, and technical reports. Coverage includes engineering, applied science, chemical and process engineering, computers and data processing, applied physics, electronic and communications, civil, mechanical, aerospace, automotive, and materials engineering. Online coverage is from 1969 to the present.

The DTIC is a provider of Department of Defense (DoD) technical information. The database contains reports generated for and by the DoD. The DTIC serves as a vital link in the transfer of information among DoD personnel, DoD contractors and potential contractors, and other U.S. Government agency personnel and their contractors.

The CSA Technology Research Database is a comprehensive database made up of three components: the CSA Materials Research Database with METADEX, CSA High Technology Research Database with Aerospace, and the CSA Engineering Research Database. The database content covers the relevant serial and nonserial literature available from 1962 to the present. Subject coverage includes civil engineering, computer applications, mechanical engineering, robotics and automation, and transportation engineering as well as other major engineering fields.

Numerous variations of the keywords below were used in the searches:

- unmanned ground vehicle
- sugv
- ugv

- speed
- mobility
- robot
- remote
- autonomous
- scale
- model

Additionally, the International Society for Optical Engineering (SPIE, http://spie.org/) has sponsored conferences and/or conference sessions devoted to unmanned ground vehicles, and these proceedings are a significant source of much of the published work of interest. The Joint Robots Program (https://robot.spawar.navy.mil/) is another source/repository of information related to robotic vehicles; this was also the source of the robots discussed in Appendix B.

The bibliography for this report cites those publications that appeared to have the potential for impact on this study; those that actually did are cited appropriately within the report text. However, many of the publications were lacking information at the level of detail required for this study.

4 Small Vehicle Characteristics

Table 4 presents information describing current "small" vehicles for comparison. This information was assembled principally from publications cited else where in this report and from Web pages. Also indicated is the availability of mobility model input files.

Table 4. Manned and unmanned vehicles in the 10- to 5000-lb GVW range.

Name/Description	GVW[1] lb	Max Speed[2] mph	Auto. Level[3]	Power[4]	No. of Axles	Steering Type	Filenames for Vehicle Performance Models
M1084 MTV, wheeled 4x4	22,740[5]	58	M	IC	2	A[6]	NRMM: MTV.v VEHDYN 4: lmtv.vd4 STNDMob: NRMM004.xml
CIV (1978 Jeep Cherokee), instrumented for mobility testing, wheeled 4x4	5,274	>65	M	IC	2	A	NRMM: CIV_VTI.dat STNDMob: NRMM701.xml
Ford Ranger 2006, wheeled 2x4	4,740	>65	M	IC	2	A	None
Isuzu 2006, wheeled 2x4	5,000	>65	M	IC	2	A	None
MULE, wheeled, 6x6	5,000	—[7]	A	IC	3	skid	None
DEMO III XUV, 4x4	3,400	40	A	IC	2	A[8]	None
M151 Jeep, wheeled 4x4	3,180	57	M	IC	2	A	NRMM: m151a2.dat STNDMob: NRMM702.xml
MDARS-E, wheeled	2,640	9.3	A	24-hp, IC	2	A	None
Mini-Flail, wheeled or tracked	2,500	5.5	T	IC	2	skid	NRMM: mini-flail.inc
Gladiator, wheeled or tracked	1,600	14	SA	IC	—	skid	None
M274 Mule, wheeled	900	13	M	IC	2	A	None
SARGE, wheeled	650	—	T	IC	2	A	None
Kawasaki 650 wheeled 4x4	1,116	72	M/T	IC	2	A	NRMM: kawasaki-650.dat STNDMob: NRMM012.xml
EOD MTRS, tracked	145	—	T	Elect	—	—	None
Pioneer AT-2, wheeled	65	2.6	T	Elect	2	skid	None
PackBot, tracked	48	6	T	Elect	1.5	skid	NRMM: pack-wf.dat, pack-wof.dat STNDMob: NRMM803.xml, NRMM804.xml

Name/Description	GVW[1] lb	Max Speed[2] mph	Auto. Level[3]	Power[4]	No. of Axles	Steering Type	Filenames for Vehicle Performance Models
MATILDA, tracked	40	2	T	Elect	1	skid	NRMM: matilda.dat STNDMob: NRMM802.xml
TALON, tracked	115 -140	4	T	Elect	1	skid	NRMM: talon.dat STNDMob: NRMM801.xml
Markbot, wheeled	32	—	T	Elect	2	A	None
Zackbot, wheeled	—	—	T	Elect	2	A	None
ODIS-T3, wheeled	40	—	T	Elect	3	omni	None

[1] Consider these weights approximate, as variations will occur due to mounting of sensors, manipulators, etc.

[2] Obtained from various Internet sources; consider these values as relative indicators.

[3] M - manned, T - teleoperated, A - fully autonomous, SA - semiautonomous (teleoperated or fully autonomous).

[4] IC - internal combustion engine; Elect - electric motor-driven.

[5] Included because it is the STNDMob class 4 (high-mobility wheeled) representative vehicle.

[6] A = Ackerman.

[7] Unknown, or not available.

[8] A special case of Ackerman steering; all wheels can be turned, but the vehicle is primarily operated with the steering on the two rear axles locked.

5 Terrain

Definition of terrain features and attributes

Small Unmanned Ground Vehicle models must represent performance on the same terrain types as full-sized vehicles, along with the surfaces associated with buildings (floors, stairs, roofs, and conduits (ducts and pipes)). Current mobility models do not address these building surface types. Terrain surfaces and attributes are defined for both COMBAT^{XXI} and OneSAF by the OneSAF Terrain Environmental Data Model (EDM).

Terrain data required for the STNDMob are based on the Source for Environmental Data Representation and Interchange (SEDRIS) Environmental Data Coding Standard (EDCS). The OneSAF Terrain Environmental Data Model (EDM) is also based on that standard. The OneSAF EDM was developed with the knowledge that OneSAF vehicle speeds would be based on the NRMM and, as such, its terrain features contain appropriate attribution for predicting mobility performance of full-sized manned vehicles. The terrain parameters currently required by STNDMob full-sized vehicles are described in Appendix A.

For SUGV performance, building materials may also provide the terrain surface. Therefore, the OneSAF Ultra High Resolution Building (UHRB) EDM features and attributes need to be considered when developing SUGV performance models. The UHRB EDM that supports OneSAF has specific features and attributes that can influence movement rates of small vehicles. Table 5 lists the material or construction types that can be specified in OneSAF for floors, stairs, roofs, and ducts. Similar materials have been grouped together, and the test data column indicates whether mobility performance data are available or required. Additionally, these surfaces can be dry or wet, and roofs may be ice or snow covered, adding additional modeling requirements.

SUGV mobility over roofs will depend greatly upon the surface material and slope of the roof. Many of the roof types defined in Table 6 are based on their internal makeup, but not the surface material on a roof. For example, built-up roofs may be made of asphalt, coal tar, or polyvinyl chloride (PVC) membrane.

Table 5. Trafficable building materials from the OneSAF UHRB Environmental Data Model.

Floor Construction Type	Stair Construction Type	Roof Assembly Type	Ventilation Duct Wall Building Component - Primary Material Type	Test Data
Brick				Required
Cobble				Required
Concrete	Concrete	Clay and concrete tile[1]	Concrete	Available
Dimensional lumber, engineered lumber, wood	Engineered lumber, lumber	Wood shake, wood shingle	Lumber	Required
Earthen				Available
Steel	Steel		Steel, aluminum, sheet metal	Required[2]
Carpet[3]				Required
Ceramic tile				Required
Fired clay tile				Required
Sheet vinyl, vinyl tiles				Required
Slate		Slate		Required
Thatch		Thatch		Required
	Steel with concrete fill			Required
			Fiberglass	Required
		Asphalt shingle		Required
		Built-up acrylic		Required
		Built-up aggregate		Required
		Built-up asphalt		Required
		Built-up coal tar		Required
		Built-up fabric		Required
		Built-up mineral surface inorganic cap sheet		Required
		Liquid applied		Required
		Metal panel and shingle		Required
		Mineral surface roll roofing		Required
		Polymer modified bitumen		Required
		Spray polyurethane foam		Required
		Thermoset single-ply		Required

[1] This is considered one material in the EDM.

[2] Data required for both sheet steel and steel grating.

[3] The EDM does not distinguish between high- and low-pile carpet; see below regarding increased resistance to movement based on pile height.

Table 6. Roof assembly type definitions.

Proposed Trafficability Roof Category	Roof Assembly Label (EDCS code)	EDCS Definition
1	ASPHALT_SHINGLE (1)	Constructed of underlayment plus self-adhering polymer-modified bitumen sheet, smooth roll roofing, or asphalt shingles.
2 (possibly 1 or 3)	BUILT_UP_ACRYLIC (2)	Constructed of a built-up acrylic coating.
3	BUILT_UP_AGGREGATE (3)	Constructed of a built-up aggregate surfacing.
3	BUILT_UP_ASPHALT (4)	Built-up from one or more of the following materials: asphalt-coated fiberglass base sheet, asphalt fiberglass felt, asphalt-saturated and asphalt-coated base sheets, asphalt-saturated organic felt, asphalt, asphalt adhesive, asphalt cement, asphalt coating, or asphalt primer.
3	BUILT_UP_COAL_TAR (5)	Built-up from the following materials: coal-tar, coal-tar cement, and coal-tar-saturated organic felt.
3?[1]	BUILT_UP_FABRIC (6)	Constructed of a built-up fabric.
3	BUILT_UP_GLASS_MAT (7)	Built-up from the following materials: glass mat, coal tar, and glass mat (venting type).
1	BUILT_UP_MINERAL_SURFACE_ INORGANIC_CAP_SHEET (8)	Built-up from mineral surface inorganic cap sheets.
4	CLAY_AND_CONCRETE_TILE (9)	Constructed of underlayment and clay or concrete tile.
5	LIQUID_APPLIED (10)	Constructed using liquid applications.
6	METAL_PANEL_AND_SHINGLE (11)	Constructed of one or more of the following materials: galvanized steel, prepainted steel, or aluminum-zinc alloy-coated steel; metal panel and/or shingle.
1, 3	MINERAL_SURFACED_ROLL_ ROOFING (12)	Constructed of underlayment and mineral-surfaced roll roofing.
3	POLYMER_MODIFIED_BITUMEM (13)	Constructed of polymer-modified bitumen.
7	SLATE (14)	Constructed of underlayment and slate shingles.
2, 5?	SPRAY_POLYURETHANE_FOAM (15)	Constructed using spray polyurethane foam.
8	THATCH (16)	Constructed using thatching materials (for example: straw, reeds, and/or palm leaves); thatch.
9, 2?	THERMOSET_SINGLE_PLY (17)	Constructed of thermoset single ply.
10	WOOD_SHAKE (18)	Constructed of underlayment, interlayment, and wood shakes.
10	WOOD_SHINGLE (19)	Constructed of underlayment and wood shingles.
[1] A question remains as to the category; testing is required.		

Frequently, built-up roofs have a ballast or wearing surface of stone or paver blocks to protect the surface. This data model does not specify the surface material. Table 6 provides the EDCS descriptions for each of the roof assembly labels. Column 1 presents an attempt to categorize the assembly types into groups that are expected to produce similar mobility performance.

Figure 6 shows a building with three types of built-up roof surfacing. In the foreground left is stone ballast, foreground right shows a concrete paver block surface, and in the background is a PVC membrane without ballast. As the picture shows, the three surfaces have very different characteristics. Numerous obstacles to movement are visible on the roof, such as protruding vents. A raised expansion joint is present in the middle of the picture, between the foreground and background roof sections. Additionally, some roofs will have a surface that is directional, and these surfaces could present quite a different mobility challenge depending upon the direction of travel relative to the orientation of the roof surface.

Figure 6. Built-up roof with three surfaces.

Figure 7 shows a tile roof common in the southwestern United States. Mobility would be different if an SUGV were traversing across the roof or up and down the slope. The transverse tiles at the ridgeline could be a significant obstacle for a small vehicle traversing over the ridge.

For floor covering types such as carpet, the structure or framework can make a significant difference to performance. According to wheelchair performance studies reported by the United States Access Board (2003), floor covering types such as linoleum, low-pile carpet (0.1-in. pile height[1]),

[1] Further specifications of this low-pile carpet are as follows: 10 stitches per inch, 16-oz face weight excluding backing and glue, and is on a jute (backing).

Figure 7. Tile roof illustrating tile orientation.

and high-pile carpet (0.5-in. pile height[1]), required an increase in force to maneuver (resistance to motion).

These findings (Table 7) were determined using the traversal of bare concrete as a baseline. From these results, it appears that linoleum and concrete equally require minor effort; low-pile carpet requires a noticeable, though moderate, increase in effort; and high-pile carpeting requires a significant increase in effort. Typically, vehicle motion resistance is dependent on weight and is reported as a ratio (resistance force/weight). However, the weight on the wheels for this study was not reported.

Table 7. Effects of wheelchair maneuver on selected floor types (U.S. Access Board 2003).

Floor Type	Force Increase (Concrete as Baseline)
Linoleum	+3%
Low-pile carpet	+20%
High-pile carpet	+62%

[1] Further specifications of this high-pile carpet are as follows: 10 stitches per inch, 40-oz face weight excluding backing and glue, and is on ActionBac (a type of carpet backing).

Fidelity

While the above section discussed the definition of terrain features and their attributes needed to estimate SUGV performance, the fidelity of these data was not discussed. As a first approximation, terrain features need to be represented at the same order of magnitude as vehicle dimensions. For example, the ground clearance and wheel base influence the ability of a vehicle to cross a ditch or crater (obstacle). An obstacle to a full-sized vehicle may look like steep terrain to a small vehicle. A curb is no obstacle to a tank, but will be to a small vehicle. Fields (1999) recognized these issues and developed a procedure for enhancing Compact Terrain Data Bases (CTDB) for use in the ModSAF simulation. While the ModSAF simulation is no longer in use, Fields discusses the need for increasing terrain fidelity of elevation, soil types and features, and associated issues for simulating Demo III XUV (see Table 4) performance.

6 Analysis of Performance Algorithms

Overview

Many of the issues related to SUGV center on their size. It is an interesting paradox that their size is both an advantage and disadvantage when compared with the performance of a full-sized vehicle. For example, traveling through tall thick grass can be a significant challenge to an SUGV but of little effect to a full-sized vehicle. On the other hand, a large pipe across the intended path of travel can be a significant obstacle to a full-sized vehicle where an SUGV that can travel up vertical surfaces could get on top and use the pipe as a pathway. The models of mobility performance of small vehicles need to characterize these issues to provide an accurate prediction of the mobility potential of these vehicles. While previous sections of this report presented information regarding vehicle parameters, terrain types and attributes, this section discusses the algorithms and supporting data required to simulate vehicle performance.

Driver effects

Aside from actually selecting the desired speed, a vehicle's driver can have a significant effect on the maximum speed a vehicle is driven at; some of these were discussed previously (ride and shock limits, as well as "local planning"). Currently, for full-sized manned vehicles STNDMob driver parameters are represented by a set of driver variables based on NRMM scenario input values. These parameters associated with the vehicle driver condition or preferences, are shown in Table 8. These are directly related to NRMM scenario variables. The default driver values match the NRMM default values.

Table 8. Driver variables.

Variable Name	Description	Default Value
driverName	An identifier of either a specific driver which corresponds to a driverState XML file supplied with STNDMob. New drivers can easily be added.	Default
recognitionDistance	The distance in meters used to estimate stopping distance (can lower maximum speed). This distance should be set to the smaller of atmospheric visibility or the distance to an object in the vehicles path (e.g., a building or stopping point).	100 m
duration	For safe tire operation, STNDMob provides "limits" on speed which correspond to tire design and deflection (inflation pressure). Reduced tire inflation enhances off-road mobility and its use is implied in determining	28800.0 sec

	the traction data (Table 3). Using reduced inflation pressure in off-road conditions is accepted U.S. Army doctrine, and on some vehicles, a central tire inflation system is available. Duration is the time in seconds, which the driver has determined to run at speeds which are greater than the maximum safe tire speed, The maximum safe tire speed, VTIRE, is applied only if the vehicle is operated for extended periods of time at reduced deflections, in which case a speed limit is assigned to ensure tire protection. The total duration value must be maintained and updated outside of the STNDMob code.	
brakePosition	The brake position or amount of braking to use.	90%
decelerationRate	The maximum deceleration rate the driver will endure.	2 g's
minVegetationSpeed	The minimum speed the driver will use to override vegetation.	1.8 m/sec
reactionTime	The reaction time for braking,	0.75 sec
roughnessComfort	In consideration of the amount of absorbed power due to natural terrain surface roughness the driver/equipment is willing to endure over a given amount of time, a "ride" speed, VRIDE, is set. This limit is usually about 8 hr for 6 W of absorbed power by the driver/equipment. STNDMob obtains this speed from a lookup table in the vehicle data, as a function of surface roughness. Urban Ride-limited speed VURBAN is also a lookup. Here, however, the roughness is caused by rubble or debris from buildings subjected to weapons effects.	6 W
shockComfort	Similarly, STNDMob considers the amount of shock that a driver or equipment can or is willing to sustain when encountering an obstacle. The impact of the vehicle's traction element and the obstacle varies and usually increases as the height of the obstacle increases. Thus, the impact speed, VOBS, will decrease as the height of the obstacle increases and will eventually become zero at a given height. STNDMob provides this as a lookup table as a function of obstacle height and speed.	2.5 W
throttleSetting	0–100% throttle applied	100%
driverCommandSpeed	In consideration of the driver's preferred or regulated speed, a driver's commanded speed (km/hr) for the vehicle has been added. This speed will override the maximum speed of the vehicle if it is lower. However, if the driver commanded speed his higher, the maximum speed takes rank.	200 km/hr

To address the effects of "driver" control on SUGV, three control methods can be considered: teleoperated, semiautonomous, and autonomous. Also important is the type of performance analysis being done. For example, is the need only for a "speed made good" value (based on some "average terrain," such as the NRMM vegetation model) or do the effects of sensing, planning, and maneuvering under very specific conditions need to be modeled—such as, avoid an obstacle in a force-on-force model. Kelly and Stentz (1997) provide a starting point for this analysis, and while they applied these concepts only to a fully autonomous vehicle, they can also apply to teleoperated vehicles.

Massey et al. (2005) discuss and present data relative to performance in teleoperated vehicles comparing head aimed and joy stick control simulated vehicles. Of particular interest is the presentation of some older Defense Advanced Research Projects Agency data (citation not included in Massey et al. 2005). These data compare the modes of operation to manned vehicles, suggesting joy stick control is only 30% effective as a manned vehicle.

Autonomous definitions

There is no general standard for defining autonomy for robotic systems. However, interest in creating an autonomous definition has recently grown. The National Institute for Standards and Technology (NIST) has assisted in the formation of autonomous level definitions for the FCS Autonomous Navigation Systems, or ANS (shown in Table 9). The FCS ANS threshold goals are to achieve capabilities inherent in levels 1–6, with the objective goals reaching as far as level 9. The level 1 autonomy is the most basic and simplest form of autonomy where a human is teleoperating the robot through a physical wire connection just as an old toy car would be controlled. As the levels increase, more functionality is added to the robot, such as driving sensors, driver warnings, way-point navigation, path planning, etc.

Table 9. Descriptions of autonomy (Albus et al. 2003).

Level	Description	Risk	Situational Awareness	Decision Making	Capability	Example
1	Tethered remote control/teleoperation	Low	None	None	Tethered operator steering, speed and braking commands	Teleoperate with tethered operator
2	Remote control/teleoperation	Low	Driving sensors	None	Remote operator steering, speed and braking commands	Remote with tethered operator
3	Advanced remote control/teleoperation	Low	Local state	Basic Health and vehicle state reporting	Remote operator steering, speed and braking commands using vehicle state knowledge	Teleoperate with operator knowledge of vehicle state situation awareness
4	Supervised semi-autonomous operation for externally planned routes	Low	World model database basic perception sensors	ANS-commanded steering based on externally planned dense waypoint path	Basic path following requires operator help with hazards and obstacles	Dense waypoint remote from leader robotic convoying

Level	Description	Risk	Situational Awareness	Decision Making	Capability	Example
5	Supervised semi-autonomous operation for locally planned routes	L/M	Perception sensor suite detects hazards and obstacles	Local planning / re-planning World model. Correlation with local perception	Robust leader-follower requiring operator help with hazards and obstacles	Path following remote form leader robotic convoying
6	Unsupervised hazard avoidance/negotiation	Med	Local perception correlated with world model database	Path planning based on hazard estimation	Basic open and rolling terrain semi-autonomous navigation with operator intervention	Basic open and rolling terrain
7	Basic autonomous operations	Med	Local perception and world model database used in hazard and object avoidance/ negotiation processing	Path planning and negotiation of complex terrain and objectives	Open rolling terrain with obstacle negotiation, limited mobility speed with some operator help	Robust open rolling terrain
8	Fusion of sensors and data	M/H	Local vehicle sensor fusion	Robust planning and negotiations of complex terrain environmental conditions, hazards, and objects	Complex terrain with obstacle negotiation, limited mobility, speed, and little operator help	Basic complex terrain semi-autonomy
9	Cooperative operations	High	Data fusion of similar data among cooperative vehicles (such as unmanned air vehicles)	Advanced decisions based on shared data from other similar vehicles	Robust complex terrain with full mobility and speed, autonomous coordinated group accomplishment of ANS goals with high-level supervision	Basic complex terrain semi-autonomy
10	Autonomous collaborative operations	High	Fusion of ANS data and RSTA [1] information among Operational Force UGVs	Collaborative reasoning, planning, and execution	Accomplish mission objectives through collaborative planning and execution with no operator oversight	Autonomous mission accomplishment with differing individual goals

[1] Reconnaissance, surveillance, and target acquisition.

NIST has created a working group, openly inviting experts in the field of robotics from government, industry, and academia, called the Autonomous Levels for Unmanned Systems (ALFUS).[1] ALFUS is working on establishing a methodology to define the autonomy for all unmanned

[1] Autonomous Levels For Unmanned Systems (ALFUS). NIST Web site (21 Nov 2006), http://www.isd.mel.nist.gov/projects/autonomy_levels/.

systems based on the level of complexity of the mission the unmanned system is capable of performing, the level of human-robot interaction, and the level of complexity of the operating environment. The ALFUS inaugural workshop was held on 18 Jul 2003.

Canonical maneuvers

To analyze the maneuverability of a robotic system is not a trivial problem. A command vector for a robotic vehicle may include steering, throttle, braking, individual wheel velocities, or other parameters, where each of the input elements of the command vector is a time continuous function. The dynamic equations of the robotic vehicle can be quite complex and sometimes nontrivial. Therefore, analyzing the maneuverability of a robotic system entails solving the vehicle dynamic equations subject to time-varying inputs and terrain-following loads. To simplify the dynamic equations, a canonical form of the obstacle avoidance maneuver trajectories can be used. Examples of canonical or standardized maneuvers where simplified equations can be formed are listed below.

- Panic stop
- Turning stop
- Impulse turn
- Reverse turn

The equations for the canonical maneuvers may be limited to specific terrain conditions and vehicle speeds since the canonical maneuver equations are approximations of more complex vehicle dynamic equations. Other maneuvers, where simplified equations may be formed, are listed below.

- Passing another moving vehicle (double lane change)
- Parallel parking
- Single lane change

It may prove beneficial to include additional maneuvers in the NRMM code to expand the performance prediction of vehicles. Even without the addition of new vehicle maneuvers, there are existing subroutines within NRMM that can be modified to better represent robotic vehicles.

Response, reaction, and maneuver times

Capturing the performance of an autonomous robotic vehicle is in some ways not much different from measuring the performance of a manned vehicle. As a manned vehicle drives on a path, the driver sees the environment, comprehends what is observed, decides how to react, and then executes the decision and continues on. All this is done by the driver continuously in an extremely short period of time. A similar process has to be completed by an ANS, but the difference is that the ANS is much slower and generally does not comprehend nearly as much as a human does.

Measuring how fast an autonomous robot is able to respond to its environment is a key measure for determining its performance. A vehicle may be able to physically drive over a terrain at high speeds, but if the driver (human or ANS) is not able to respond fast enough to the environment, the speed will be limited. The total system response time of an ANS-driven vehicle can be separated into two discrete events. The first event includes the robot seeing, understanding, deciding what to do, and sending the command to the actuators to begin execution of its decided plan. The second event includes the completion of the response trajectory, however it is defined. It might be helpful to consider the total system response time as a "perceive-think-act" loop.

The time period from the instant that an obstacle appears in the field of view of the perception sensors to the instant at which the vehicle is considered to have completed the avoidance trajectories is defined as the total system response time. The total time it takes for an autonomous robotic vehicle to respond to its environment in order to complete a task is made up of a reaction time (T_{react}) and a maneuver time ($T_{maneuver}$). The total system response time (T_{resp}) is therefore defined as the sum of the reaction time and the maneuver time.

$$T_{resp} = T_{react} + T_{maneuver} \tag{2}$$

The reaction time incorporates the time from when the robot senses the environment to the time when the actuators respond to the given command. The maneuver time begins after the reaction time ends and accounts for the time it takes the robot to complete the execution of the particular maneuver.

The reaction time and maneuver time can be further defined as the following:

$$T_{react} = T_{sens} + T_{perc} + T_{plan} + T_{cont} + T_{act} \quad (3)$$

where:

T_{sens} = time it takes sensing the environment
T_{perc} = time it takes perceiving what the sensor data mean
T_{plan} = time it takes deciding what to do
T_{cont} = time it takes commanding the actuators
T_{act} = time it takes for the actuator to respond.

Substituting Equation 3 into Equation 2 yields the following expression for the total system response time:

$$T_{resp} = T_{sens} + T_{perc} + T_{plan} + T_{cont} + T_{act} + T_{maneuver} \quad (4)$$

Figure 8 presents a flow diagram to further explain the terms that comprise the total system response time. To further clarify the definitions presented above, consider the example of a vehicle executing a panic stop. In a panic stop maneuver, the vehicle is initially traveling at a constant speed in a straight line, then decides to fully apply the brakes and skids or slows to a complete stop. Consider a robotic vehicle driving in a straight path and detecting an object in its path with its sensors. The time passed counts for the T_{sens} time. Next, the robot interprets the data as a rock (T_{perc}) and decides to slam on the brakes (T_{plan}). Then, the robot sends the signal to apply the brakes (T_{cont}), and the actuators begin pushing the brake pedal (T_{act}). Finally, the vehicle decelerates until it comes to a complete stop ($T_{maneuver}$). This example breaks down the components of the total system response time. The current NRMM or STNDMob algorithms, which make use of response time, are discussed in the next section.

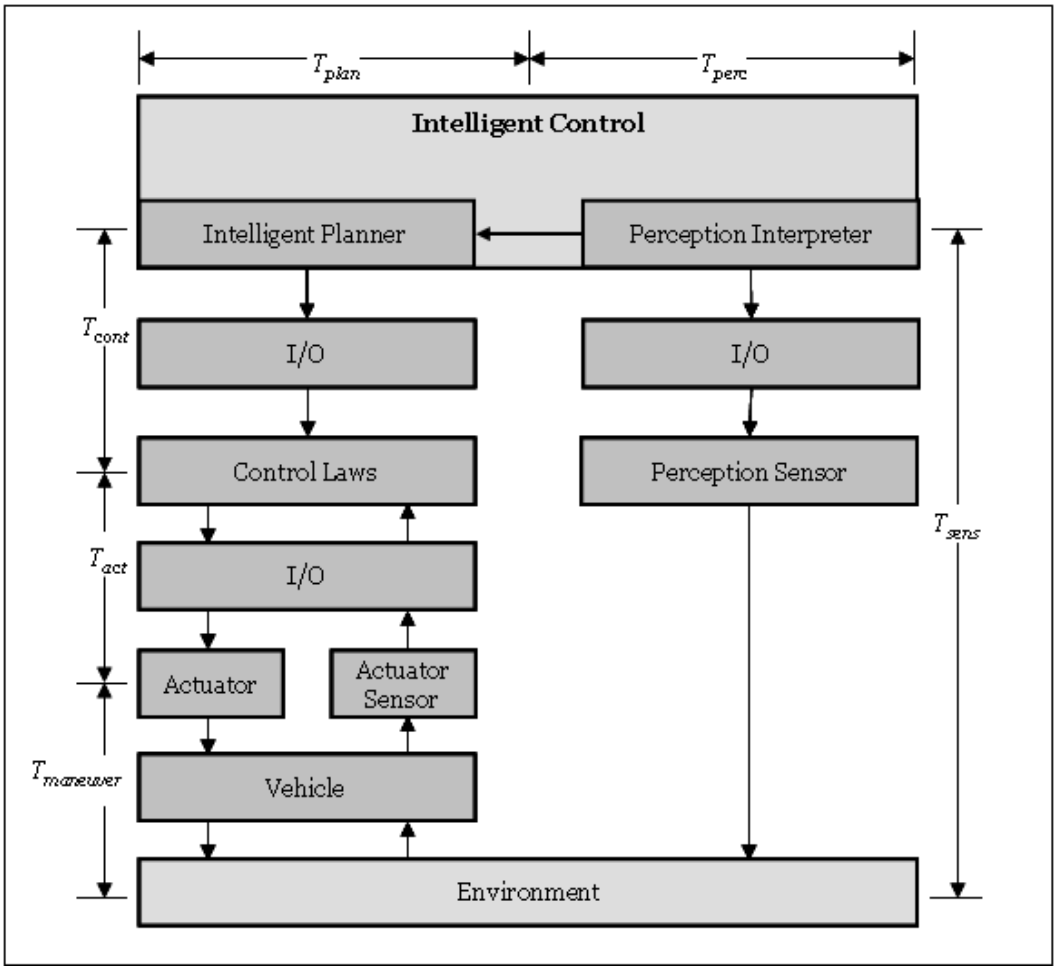

Figure 8. Response time elements (after Kelly and Stentz 1997).

Mobility performance algorithms

Table 10 identifies the performance algorithms or effects required for SUGV performance modeling and summarizes the issues—or identifies where further development or testing is needed. Further discussion (of some of the algorithms) continues in the following paragraphs. While STNDMob is the target model for use in Army simulations, it is based on the NRMM. Thus, algorithms are discussed in the context of the most appropriate model (NRMM or STNDMob). For simulations, there are generally two performance parameters of interest: the maximum speed the vehicle can be driven and the velocity for the next time step (given the current velocity, terrain, and driver parameters).

As a result of ERDC testing (Appendix B) NRMM, VEHDYN 4, and STNDMob vehicle files were created for the test vehicles (TALON, MATILDA, and PackBot). Comparisons with simulation results, data, and other observations are discussed in a later section of the report.

Table 10. Mobility performance algorithms for SUGV in STNDMob.

Algorithm or Effect	Full Size Implemented in STNDMob	SUGV Mobility Performance Issues
Tractive force vs. speed equation hyperbolic curve fit	Yes	Need to confirm that a hyperbolic curve fit is appropriate for all cases and, for electric-powered vehicles, these are principally empirical. So, all soil categories/conditions need to be compared with test data. Also need to represent building surfaces from Table 5.
Dry and wet road surface friction coefficients for driving and braking	Yes	Need to confirm/examine all terrain and building surfaces.
Soil and road surface resistance (self-propelled)	Yes	Soil and road surface resistance is accounted for in the tractive force speed curve; building surfaces could be handled similarly.
Soil and road surface resistance (towed)	Data is available, but not yet accessible through the API	Need to consider electric motor-driven vehicle issues related to towing.
Snow resistance	Yes	Snow resistance is currently based on snow density and depth; a lightweight tracked vehicle resistance model developed for small robotic vehicles is available (Lever and Shoop 2006).
Obstacle forces	Yes	Validation; appropriate-sized obstacles required.
Plowing Force	Yes	Assume not required. Current plow model needs data specific to plow type and size (full width, track width, etc.); its principal purpose is for mine clearing.
Slope effects (gravity)	Yes	No changes required; can use slope test data for validation.
Wheeled vehicle cornering resistance	Yes	Current algorithm does not apply to skid steer vehicles.
Tracked vehicle cornering resistance	Yes	Need to confirm that current model is applicable to small vehicles.
Acceleration and deceleration	Yes	No changes required; basic physics equations. Other algorithms set the required parameters.
Speed limited by sliding on curves	Yes	Algorithms are based on a semistatic force balance; they are applicable to all size vehicles.
Speed limited by tipping	Yes	Algorithms are based on a semistatic force balance; they are applicable to all size vehicles.
Speed limit on curves (AASHO 1966)	Yes	Not applicable. Sliding and tipping speeds (above) are sufficient; modify STNDMob API to ignore this algorithm for SUGV.

Algorithm or Effect	Full Size Implemented in STNDMob	SUGV Mobility Performance Issues
Vegetation limited speed	Yes	Base override forces added to terrain resistance or determination of the speed attainable by maneuver around the vegetation. Override forces obtained from empirical; may not be applicable to small vehicles.
Visibility limited speed	No	This limit is related to the ability of a driver to stop a vehicle and the distance to an obstacle or maneuver point, combined with atmospheric visibility. For teleoperated or ANS, the ability of sensors raises issues.
Ride (roughness) limited speed	Yes	The algorithm was discussed above, for unmanned vehicles. The appropriate levels absorbed to the vehicle's components needs to be determined.
Shock limited speed	Yes	The algorithm was discussed above, for unmanned vehicles. The appropriate levels of tolerable shock to the vehicle's components need to be determined.
Tire limited speed	Yes	This speed limit is set to model the case of tires that have had their inflation pressure lowered to ensure off-road mobility. The vehicle can be driven at higher than recommended speeds for short periods of time. The time limit (duration) is set as a driver parameter (Table 8).

Tractive force versus speed equations

Part I of Appendix C discusses steady-state electric motor equations and performance in conjunction with tractive force speed curves. Based on that discussion, it was concluded that the hyperbolic tractive force speed curve fitting process used in STNDMob is also appropriate for small electric-powered vehicles. The test data presented in Appendix B also support this conclusion.

Maximum traction and braking coefficients

For off-road conditions, the braking coefficient is the sum of the maximum traction coefficient and the resistance caused by the terrain. For on-road conditions, these values are based on accepted vehicle design parameters and are presented in Table 11. Shown also are the maximum traction values reported in Appendix B and for the Kawasaki 650. Actual braking coefficient is determined by adding other resistances and taking into

account driver limits. McBride et al. (2003) estimate reported traction coefficients for the PackBot on concrete from slope tests as 0.78 and 0.66–0.8 from pull tests. An indication that the traction coefficients for light vehicles are very sensitive to surface texture was observed during the ERDC testing, and may explain these differences observed for the PackBot.

If the 0.9 value specified by NRMM is used, a conservative estimate of maximum traction is obtained. Further data are needed to confirm the coefficients used for other surface conditions. Note that these values are appropriate for both concrete and asphalt surfaces.

Table 11. On-road maximum traction and braking coefficients.

	NRMM	Measured			
Condition	Wheeled or Tracked	Kawasaki 650	TALON	MATILDA	PackBot
Maximum traction dry	0.90[1]	0.96[2]	1.2	No data	1.0
Maximum braking dry	0.75	No data	No data	No data	No data
Maximum traction wet	0.50	No data	No data	No data	No data
Maximum braking wet	0.45	No data	No data	No data	No data

[1] This value can be lower based on the tractive force speed curve (vehicle capability).

[2] At optimal slip (about 15%), from GSL Mobility Systems Branch, unpublished data obtained from Jody Priddy (Jody.D.Priddy@usace.army.mil).

Surface resistance

For surface resistance on level terrain, there are three conditions to consider: road or nondeformable surfaces (most building surfaces would also be considered nondeformable), deformable soil, and snow or ice. NRMM computes hard surface resistance coefficient values for wheeled vehicles as a function of the tire inflation pressure and the road type (super highway, primary, or secondary). Adjustments are made for cornering (turning). For tracked vehicles, constant values are used (0.045 for secondary roads and 0.0375 for super highway and primary roads), and adjustments are also made for turning. The STNDMob vehicle files contain the appropriate values without turning effects, and the STNDMob API contains the algorithms to make the corrections based on radius of the turn (discussed below). The issue for these conditions is whether the algorithms and constants used give appropriate values for small vehicles. Additionally, the possibility of nonpneumatic (solid rubber) tires arises, for which there appear to be no data.

The basis of NRMM off-road vehicle performance is a series of empirical equations based on vehicle parameters, soil type, and soil strength (cone index, CI, or rating cone index, RCI). These equations estimate the maximum drawbar pull a vehicle can achieve for a given soil type and strength. A comparison of the RCI with the vehicle cone index (VCI) indicates whether the vehicle can negotiate the given soil condition for a given number of passes. (See Appendix B for further discussion.)

Maximum braking force including the driver

NRMM calculates the maximum braking force including the driver (NRMM Routine IV12[1]). It has been observed in testing that a driver may not use the total braking force the vehicle is capable of producing due to driver choice or skill level. For example, the driver may not wish to apply the maximum braking force for reasons such as the desire to keep some in reserve for "safety sake," or the negative acceleration is uncomfortable, or the driver does not want a lunch box to slide off the seat onto the floor, or the driver skill level. The maximum braking force including the driver is calculated from the following:

$$B_{MX} = \min\left(DCL_{MAX} \times W, \frac{T_{BF} SFTYPC}{100}\right) \quad (5)$$

where:

B_{MX} = total braking force used
DCL_{MAX} = maximum braking acceleration (g's) that the driver will accept
W = total gross vehicle weight
$SFTYPC$ = percentage of potential braking force driver will use
T_{BF} = maximum braking traction available.

For an autonomous robotic vehicle, the amount of braking force applied will not be governed by the driver, since there is no human physically on the vehicle. The amount of braking force applied by the robotic vehicle could be limited, but this in general may not be true. However, data or parameters from an ANS could be used to populate the driver variables in Table 8.

[1] See Ahlvin and Haley (1992) for complete descriptions of the NRMM routines.

Speed limited by visibility

NRMM routine IV13 calculates the speed limited by visibility. In this calculation, the vehicle's maximum speed is a function of several factors that depend on a human driver. The driver's total recognition distance, visibility distance, driver eye height, and reaction time between recognition and the application of the brakes are based on human capabilities. For an autonomous robotic vehicle, these terms are dependent on the number of sensors, the range, accuracy, field of view, field of regard, scan rate, etc., of each sensor, the computer processing speed, and other variables.

The human recognition distance is computed using the following equation:

$$D_r = D_v \frac{h_e}{60} \tag{6}$$

where:

D_r = total recognition distance (inches)
D_v = visibility distance (inches), and is the smallest of the distance to an object to be avoided, a point at which to stop, or the meteorological visibility
h_e = driver eye height (inches).

The "60" is based on a "standard" but undocumented technique of determining recognition distance at an eye height of 60 in., when developing NRMM terrain data files. Equation 6 adjusts the value relative to the driver eye height in the vehicle of interest.

A robotic vehicle may have more than one sensor, each at a different height location. The robot's sensor visibility distance depends on the particular sensor in question. These factors influence the robot's total recognition distance and should be incorporated in an appropriate representation (in lieu of Equation 6). The maximum speed limited by visibility is calculated by solving for V in the following equation:

$$D_r = t_r V + \frac{V^2}{2B_{MX}} \tag{7}$$

where:

D_r = recognition distance (Equation 6)
t_r = reaction time between recognition and application of brakes
V = maximum speed limited by visibility
B_{MX} = braking force (Equation 5).

The reaction time between recognition and application of the brakes t_r in Equation 7 is the reaction time for an average human driver located in the vehicle. For a robotic vehicle, the total response time T_{resp} from Equation 3 could be used in place of t_r. Solving Equation 7 for V will provide the maximum speed limited by visibility at which the vehicle will be able to come to a complete stop in a straight line. It does not incorporate the other maneuvers where the vehicle is turning or in a cluttered environment, etc. The maneuver the robotic vehicle is executing and the environment in which the robot vehicle is to move influence the response time and visibility.

Vehicle cornering resistance

For wheeled vehicles, three types of steering can be identified: Ackerman, skid, and omni (all wheels rotate, as in a castor). NRMM and STNDMob do not model lateral forces on a wheel during turning, but do estimate the effect of turning on motion resistance and speed limits based on sliding, tipping, and highway design (Baylot et al. 2005). Currently, NRMM and STNDMob model only the induced longitudinal resistance based on Ackerman steering. This longitudinal component of cornering force can be as much as 20 percent of the vehicle's power requirement (Milliken and Milliken 1995). For small vehicles, Ojeda et al. (2005, 2006) demonstrated the use of the rate of turning and power consumed to determine terrain characteristics in a Pioneer 2-AT[1] skid-steered vehicle. For example, they reported an increase in the resistance coefficient from about 0.02 to 0.22 on dry pavement, as turning rate increased from 0 to 12 deg per second.

Longitudinal resistance during cornering induced by lateral forces is summed over the wheel elements (axles) of wheeled or partially wheeled vehicles (e.g., half-tracks). The longitudinal cornering resistance (F_{RC}) on level terrain is originally from Smith (1970):

[1] See Table 4 for basic characteristics of this 64-lb vehicle.

$$F_{RC} = \frac{\sum \left(\frac{Vm}{R} \right)^2 2\pi}{180nfc \frac{\mu}{0.75}} \tag{8}$$

where:

V = tangential velocity of the vehicle
m = mass of the vehicle supported by an element
R = radius of curvature to the center of gravity of the vehicle
n = number of tires on the element
f = empirical correlation coefficient (0.96)
c = average cornering stiffness (pounds, force/degree)
μ = maximum friction coefficient for current terrain.

Smith (1970) developed this empirical equation for large trucks and, as part of NRMM, it has been used for vehicles as small as ATVs, although there may be no data that support its use for vehicles this size or smaller. The average cornering stiffness (c) is a standard tire parameter associated with full-sized pneumatic tires. It is an important parameter in tire design and higher fidelity models, in which lateral tire forces are required. This value is often hard to obtain and, in this case, for NRMM, a rule of thumb is used:

$$c = \frac{\text{Gross Vehicle Weight}}{\text{Number of Tires}} \times \begin{cases} 0.12 \text{ for Radial Tires} \\ 0.10 \text{ for Bias Tires} \end{cases} \tag{9}$$

While the above rule is known to be appropriate for full-sized vehicles, the authors have yet to find any published data that indicate it would be valid for smaller tires. For vehicles smaller than ATVs, the wheels may not be pneumatic, and this lack of data is problematic for the use of Equation 8. While some researchers (e.g., Hoblet et al. 2003) have made cornering stiffness measurements of radio-controlled vehicle-sized tires, they have not published their results with enough information to determine the cornering stiffness coefficients (values equivalent to the 0.12 or 0.10 in Equation 9).

Omni-steered vehicles are a special case, as all the wheels are turned in the direction of travel during a turn. Hence, additional longitudinal resistance during a turn will be minimal, which suggests a value of 0 for F_{RC} as an

estimate. There are very few omni-steered vehicles, and no discussion was found related to forces on wheels during turns.

For skid-steered, wheeled vehicles, a few research papers have been published relating to calculation of individual wheel velocities, but no in-depth dynamic analysis (such as recently published by Wong and Chang 2001 for skid-steered, tracked vehicles). Attempts to redevelop the equations of Smith (Equation 8) and of Merritt (1946) and Ray (1979) for tracked vehicles (discussed below) as a simply derived estimate were unsuccessful—based on order of magnitude values compared with the data of Ojeda et al. (2005). A carefully developed model of the terrain-vehicle interaction forces is required with validation based on field tests, which is beyond the scope of this work. The work of Ojeda et al. provides a starting point, but without a fully developed model, the empirical data can be assumed to apply only to vehicles similar to the Pioneer 2-AT.

For tracked vehicles, the longitudinal component of the lateral force associated with steering tracked suspension elements (NRMM subroutine IV6R2) is computed using the Merritt equation (Merritt 1946; Ray 1979) in terms of the vehicle tread width-to-length ratio. The set of equations has recently been presented by Baylot et al. (2005) and is not repeated here. Although the equations appear to be empirically based, the initial equations presented by Merritt are physics based and nondimensional. Ray presented a correction factor to Merritt's force equation for radius of curvature, which decreases the force predicted by Merritt as turning radius increases above about 7.6 m (force increases with smaller radii). Ray's basis for this correction is test data that are from full-sized vehicles and reflect the effects of track tension and flexing. There appears to be no reason these equations are not applicable to tracked SUGV. There does appear to be a velocity effect that is not captured by these equations, and at high velocities, the force will be higher than actual, producing a conservative performance estimate. Additionally, it should be noted that Merritt and Ray present additional equations that could be useful in estimating power consumption associated with tracked vehicle turning.

Vegetation limited speed

One factor in the IV7 NRMM routine limits the vehicle speed through a driver tolerance limit to impact. This is the maximum longitudinal acceleration that the driver will tolerate, which is currently set to a level of 2.0 g's, and is hard coded in STNDMob. For a robotic vehicle, this limit

could be exceeded, because there is no human driver physically on the vehicle. There may also be other vertical acceleration factors that constrain robotic vehicles, such as the maximum vertical accelerations that robot components can withstand.

The NRMM provides two sets of algorithms to account for vegetation: area denied and override. The equations for vegetation override were first published by Blackmon and Randolph (1968). The equations are developed for a vehicle striking and overriding a tree of a given diameter. There are two forces: a maximum force and an average force. The maximum force is added to the soil resistance and other forces to determine if the vehicle has enough traction. The vehicle speed is then calculated using the average force (plus all the other resisting forces). In certain soil conditions, it is possible that the average force will contribute to immobilization.

$$F_{average} = \frac{56}{5.8} d^3 \tag{10}$$

where:

$F_{average}$ = force required to override (pounds)
d = stem diameter (inches).

There is also a peak force required for the vehicle to break or override the vegetation during the initial impact. The maximum force against the vehicle push-bar exerted by such an override attempt is given by

$$F_{\max} = (40 - \frac{h}{2}) d^3 \tag{11}$$

where h is the push-bar height (inches).

Tests conducted and algorithms in NRMM would suggest that the TALON, PackBot, and MATILDA movement will be obstructed from vegetation 1 in. or greater in diameter. Tests conducted for the TALON in high grass indicates an average value of maximum drawbar pull of 86 lb, as reported in Appendix B, Table B6—a reduction of 32 lb from average value for hard soil tests. The TALON was the only vehicle for which tests were run in vegetation.

The SUGV tested have a push-bar height of approximately 4 in. Figure 9 relates maximum override force, average override force, and push-bar height using Equations 10 and 11 by assuming a tree diameter of 1 in. Regardless of tree diameter, the maximum required push-bar force to override a tree will always go to zero at a push-bar height of 80 in. Also, at around 60 in., the average force and maximum force will be equal.

Figure 10 illustrates data collected by Blackmon and Randolph (1968) overlaid on Equation 11. Additional tests were conducted on trees varying from 1.5 in. to 5 in. in diameter, illustrated in Figure 10 as diamonds. A push-bar height of 12 in. is substituted into Equation 11 to produce the curve in Figure 10. In general, with the exception of one outlier, these new data appear to validate Equation 11 for small vehicles.

Future research in this area should include the modification of NRMM for stem diameters less than 1 in. These algorithms do appear to encompass the modeling requirements of vehicles greater than 1000 lb. It is the mobility of vehicles less than 1000 lb that appears to require additional tests for validation.

Electric vehicle model

SUGV may be electrically powered, and their performance is dependent on battery charge state. Whereas, in most cases, standard-sized ground vehicles are traction limited (unable to develop enough traction to move and wheels spin), SUGV with low battery charge can additionally face the condition of being power limited (engine stalls or clutch slips). To model these conditions, battery and electric motor performance models will be required. These exist in the literature, but must be implemented with a trafficability model (STNDMob).

Figure 11 shows a conceptual electric-powered SUGV trafficability model that includes motor, battery, and controller modules. The dashed lines in the figure represent the model flow if only the STNDMob API is used. A behavior model (not shown) would be required to control the throttle. A discussion of a full electric motor and battery performance model is beyond the scope of this report.

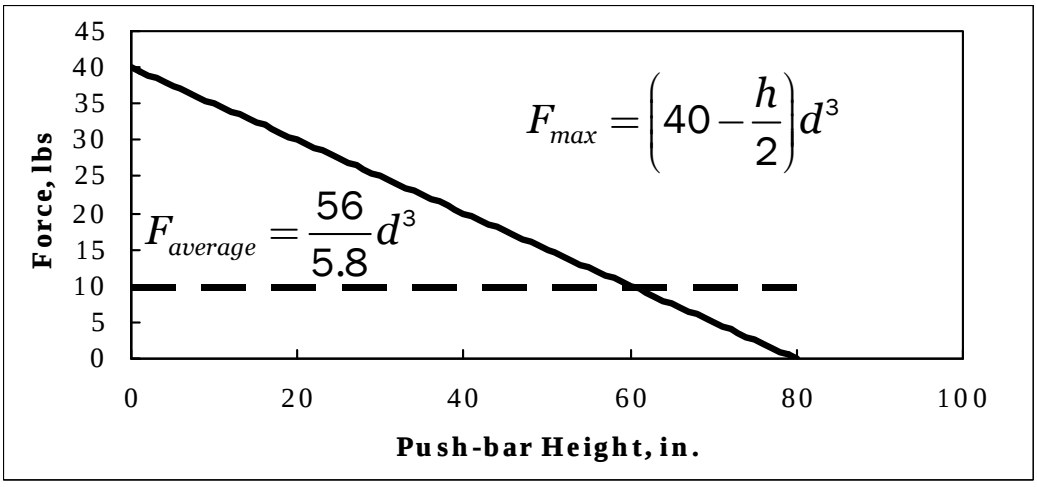

Figure 9. Comparison of equations for a 1-in.-diam tree.

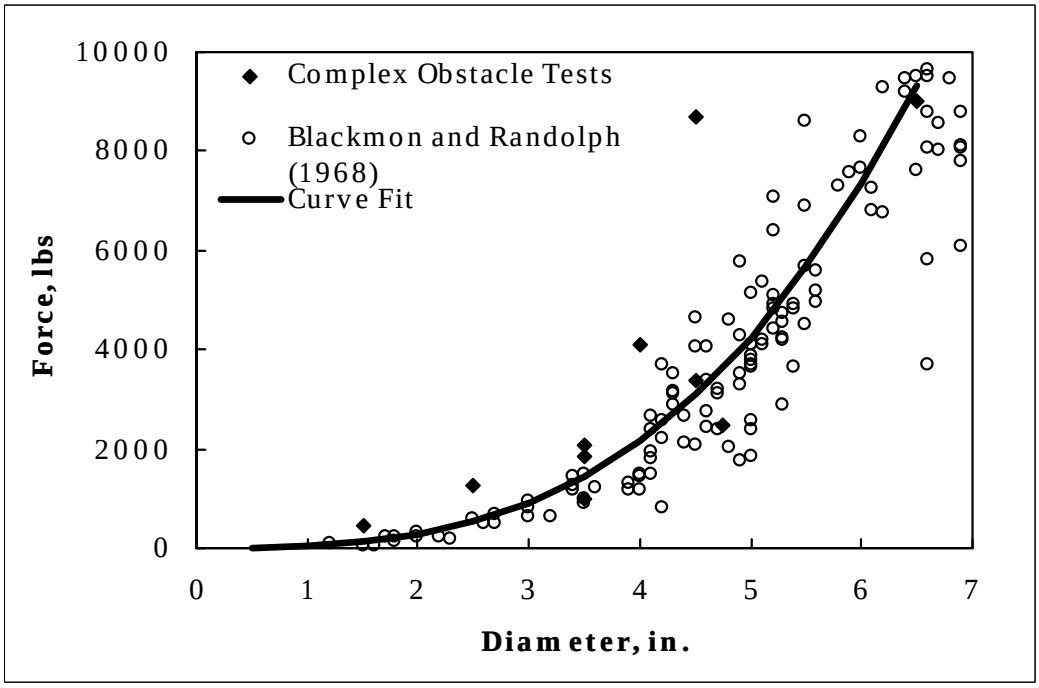

Figure 10. Tree override force.

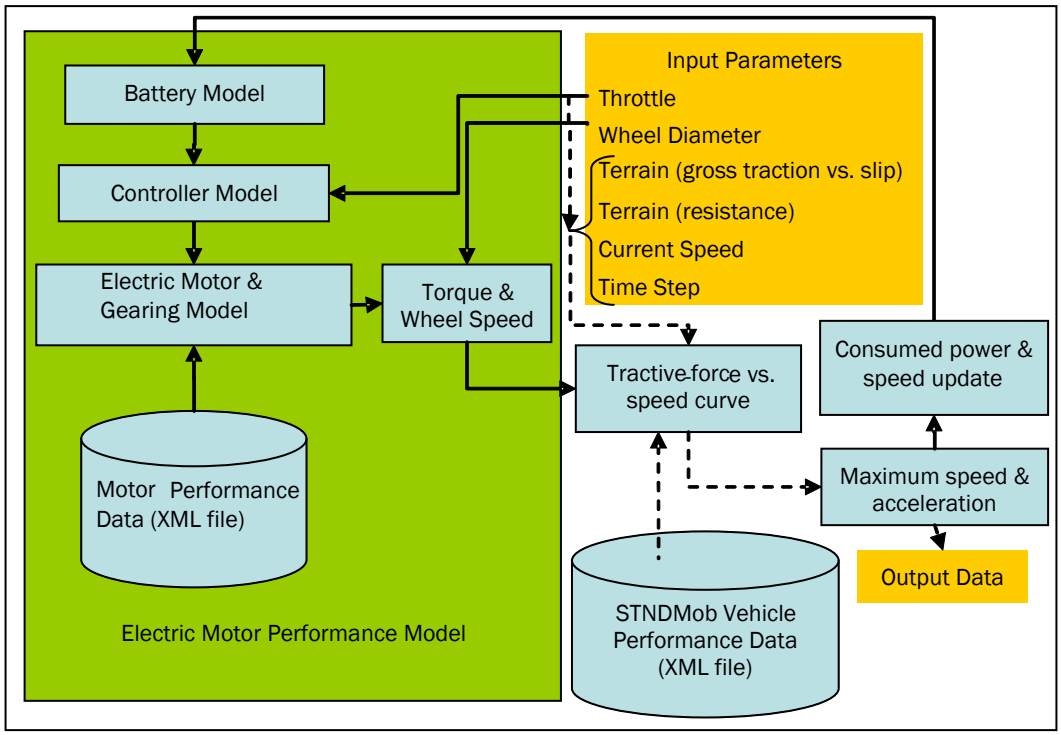

Figure 11. Conceptual electric vehicle trafficability model with dashed lines showing current STNDMob API for full-sized vehicles.

7 Simulated Vehicle Performance

In this section, vehicle performance predictions made using STNDMob and the vehicle data files developed for the MATILDA, TALON, and the PackBot (Appendix B) are presented, and comparisons are made between vehicles with the limited specific test data that are available. Additionally, STNDMob predictions for the M1084 vehicle are compared with those for the CIV and M151 vehicles. The M1084 is used for comparison because it is the STNDMob class 4 (high-mobility wheeled) representative vehicle and would currently represent the CIV and M151. Table 12 contains the terrain conditions simulated. Those STNDMob input parameters (Appendix A) not shown were set to 0 or to values that would have no effect. Performance predictions for the two obstacles (Figure 12) were made for all six vehicles. Additionally, an acceleration simulation on a level concrete surface was produced.

Table 12. Terrain conditions used for performance comparisons.

STNDMob Input Parameter	Values (MATILDA, TALON, PackBot)	Values (M1084, CIV, M151)
vehiclePitch (slope)	0, 10, 30, 50, 70, 80, 90%	0, 10, 20, 30, 40, 50%
soilUSCSType	CH, SC, CL, SM	CH, SC, CL, SM
soilStrengthCone_40	1, 2, 5, 10, 30, 50 psi	20, 50, 70, 100, 150, 250 psi
frozenWaterType	None	None
surfaceType	Cross country, primary road	Cross country, primary road
Surface Condition	Dry, wet	Dry, wet
	Obstacle 1	**Obstacle 2**
obstacleHeightIngress	6 in.	5.75 in.
obstacleHeightEgress	1.25 in.	5.75 in.
obstacleWidth	6 in.	2.125 in.
obstacleApproachAngleIngress	1.50796 rad	2.660705 rad
obstacleApproachAngleEgress	2.877104 rad	2.661418 rad
obstacleMaterialType	Concrete	Concrete
Surface Condition	Dry, wet	Dry, wet

Figure 12. Obstacles 1 and 2.

Slope and soil type speed predictions

Figure 13 compares the slope performance of small but full-sized vehicles with the M1084. The CIV speed was limited to 60 mph-based maximum tire speed information in the data file (which should be reexamined). Significant differences are seen, indicating that smaller vehicles will not be well represented by the M1084 as the representative vehicle of that class. A similar effect is seen for soft soil performance (Figure 14). Again, the CIV speed is limited by maximum tire speed (at a lower tire inflation pressure). Simulations of these smaller full-sized vehicles, whether manned or autonomous, should have their own class or use their specific vehicle file.

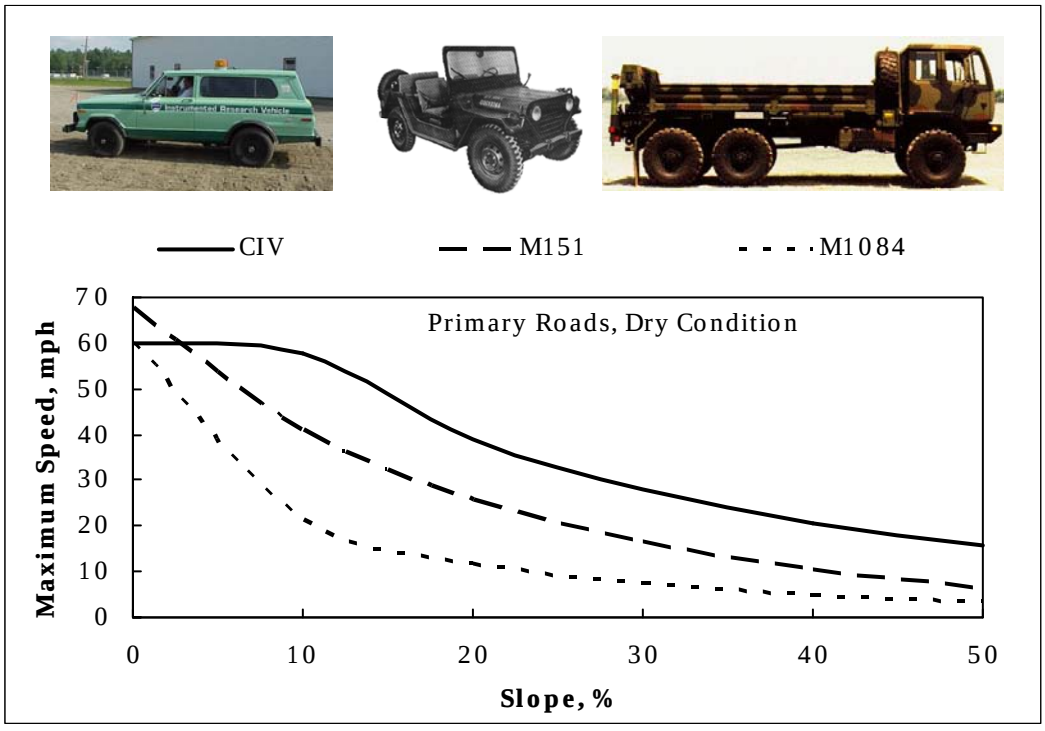

Figure 13. Comparisons of slope performance predictions on dry pavement.

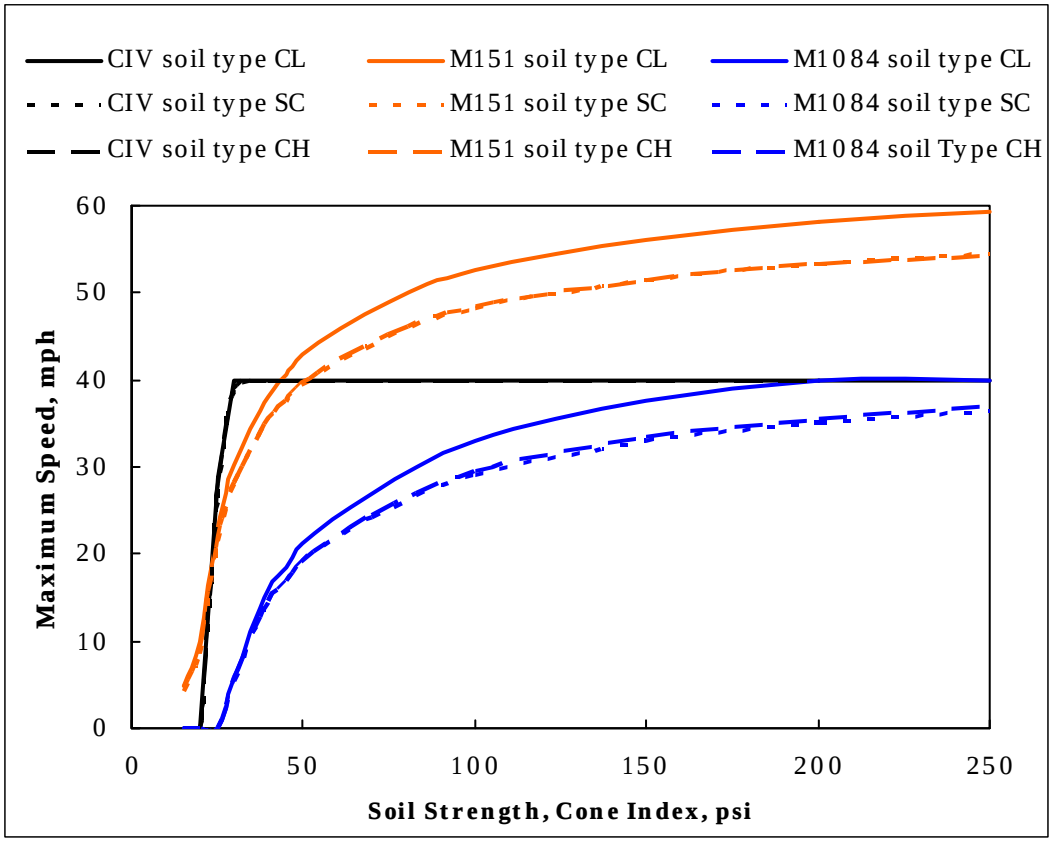

Figure 14. Small full-sized vehicle performance on soft slippery soils.

Figure 15 compares slope performance of the three robotic vehicles and, as expected, the performance closely follows their tractive force speed curves for dry pavement. For wet pavement, the traction is limited by the maximum traction coefficient for wet pavement (Table 11), but there are no data to support this value.

Test data (Appendix B) indicate that the PackBot can ascend a 76 to 85% concrete slope, and McBride et al. (2003) found that the PackBot could climb a 78% concrete slope. Figure 15 indicates the PackBot can climb close to a 90% slope. The difference in the predicted and observed results can be attributed to the hard surface motion resistance. NRMM and, hence, STNDMob use a "standard" value of 0.0375 for tracked vehicle motion resistance on smooth pavement. It is probable that, for small electric-powered tracked vehicles, this value could be higher, although no data appear available. In order for the predicted slope climbing values to match those observed, the motion resistance would need to be on the order of 0.07 to 0.1.

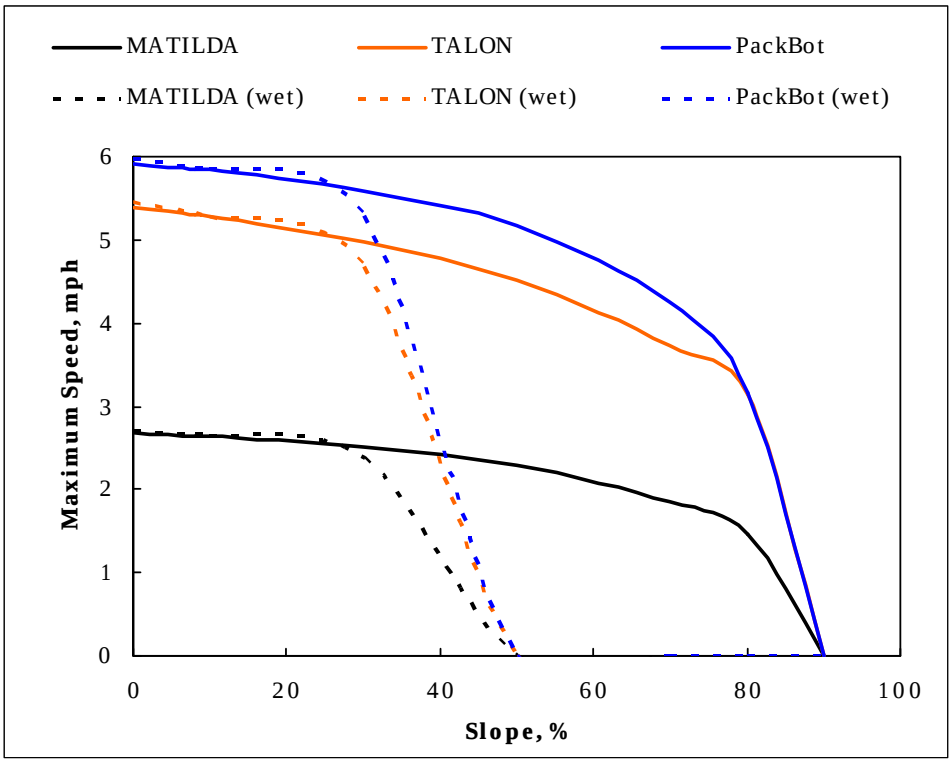

Figure 15. Comparisons of slope performance predictions on dry and wet pavement.

Soft soil performance estimates for the three robotic vehicles are shown in Figure 16, and as observed for pavement, these curves follow the general shape of the tractive force speed curves. Also, note that there is little difference between soil types for each vehicle. Discussed in Appendix C, the shape of these curves is related to the electric motor parameters. This suggests that, for small electric-powered vehicles, the tractive force speed curve, in addition to being normalized for weight, may also be normalized for velocity. Potentially allowing development of "generic" tractive force speed curves, this could then be used with specific vehicle characteristics.

Obstacle speed and negotiability predictions

Two obstacles were selected for simulation, as shown in Figure 12. The dimensions of these obstacles are given in Table 12. Table 13 presents the maximum predicted crossing speeds for each of the vehicles. The SUGV's predictions consist of two speeds: the value to the left of the slash (Table 13) represents the obstacle crossing speed considering "default" driver effects (see Table 8); the value to the right represents the speeds determined only from the specified terrain parameters after considering the resistive force, obstacle override, and obstacle clearance requirements. As stated earlier, driver effects can significantly impact the overall

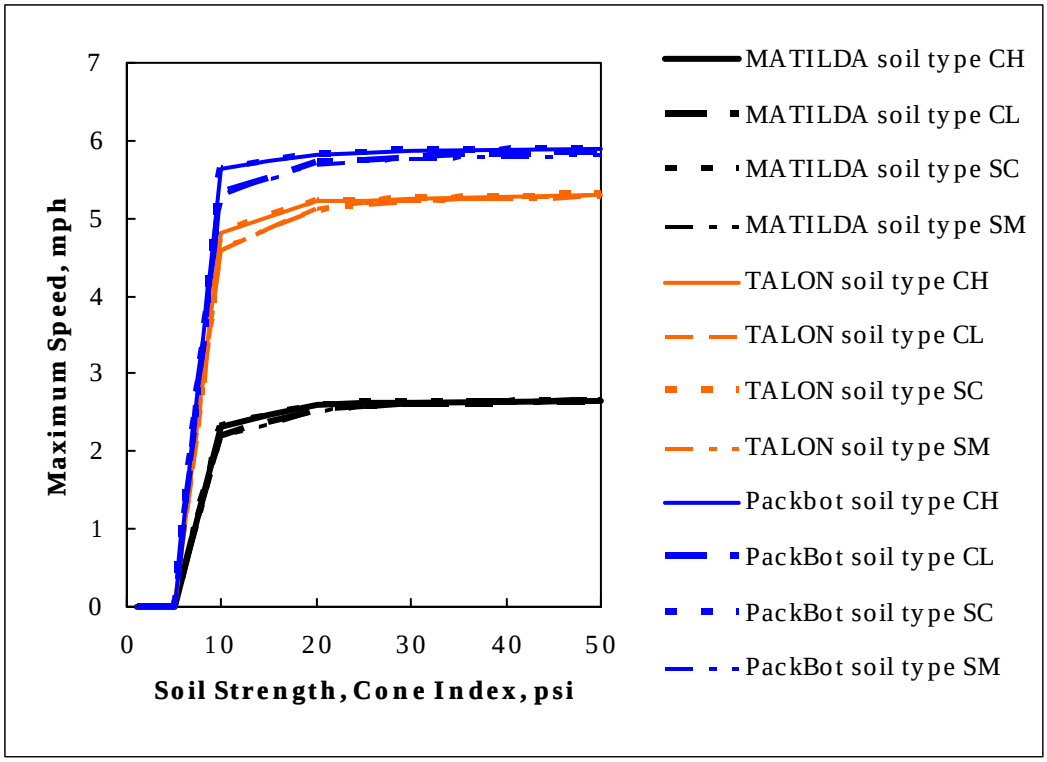

Figure 16. SUGV performance on soft slippery soils.

Table 13. Maximum speed (mph) predictions for obstacle negotiation.

Vehicle	Obstacle 1 Dry	Obstacle 1 Wet	Obstacle 2 Dry	Obstacle 2 Wet
MATILDA	0.5[1]/2.7	0.5/2.7	0.5/2.7	0.5/2.7
TALON	0.5/5.4	0/0	0.5/5.4	0.5/5.4
PackBot	0.5/5.9	0.5/5.9	0.5/5.9	0.5/5.9
M151	26.2	0	33.4	33.4
CIV	13.4	0	14.0	14.0
M1084	22.0	22.0	23.6	23.6

[1] For the SUGV, the first value includes driver limits (from Table 8); the second value considers only terrain parameters.

performance of a vehicle (shock, ride, visibility speed, tire speed, and the driver's commanded speed). In this scenario, shock-performance (vertical acceleration limit) is the cause for the very low speeds. All the crossing speeds are the same (except for the TALON on wet pavement, which was not able to cross).

For the full-sized vehicles, surprisingly the M151 and CIV could not negotiate obstacle 1 when wet. This was found to be caused by the estimated maximum obstacle override force being larger then the available traction.

This is one factor in determining the capability to negotiate an obstacle ("GO/NO-GO" case). If the estimated maximum force required to override the obstacle is larger than the available vehicle traction, vehicle immobilization results. Possible causes for incorrect predictions are the gross granularity used to create the obstacle performance information for the vehicle file, the conservative assumption inherent in the obstacle performance prediction model, and conservative estimates characterizing the terrain traction surfaces (0.5 representing maximum traction on wet pavement). These results suggest that, for small vehicles, more analysis needs to be done when assembling the obstacle crossing data tables (selection of the obstacle size matrix and methodology) than may be required for full-sized tactical military vehicles, for which there is a larger body of data and experience.

Acceleration performance

The acceleration calculations in STNDMob are based on the tractive force speed curves and are described in Appendix C (Part II). Terrain and vehicle parameters, initial velocity, and other factors affect the maximum acceleration prediction. At full throttle, the three SUGV accelerate to maximum speed quickly (Figure 17), achieving their maximum speeds in less than a second, on dry level pavement.

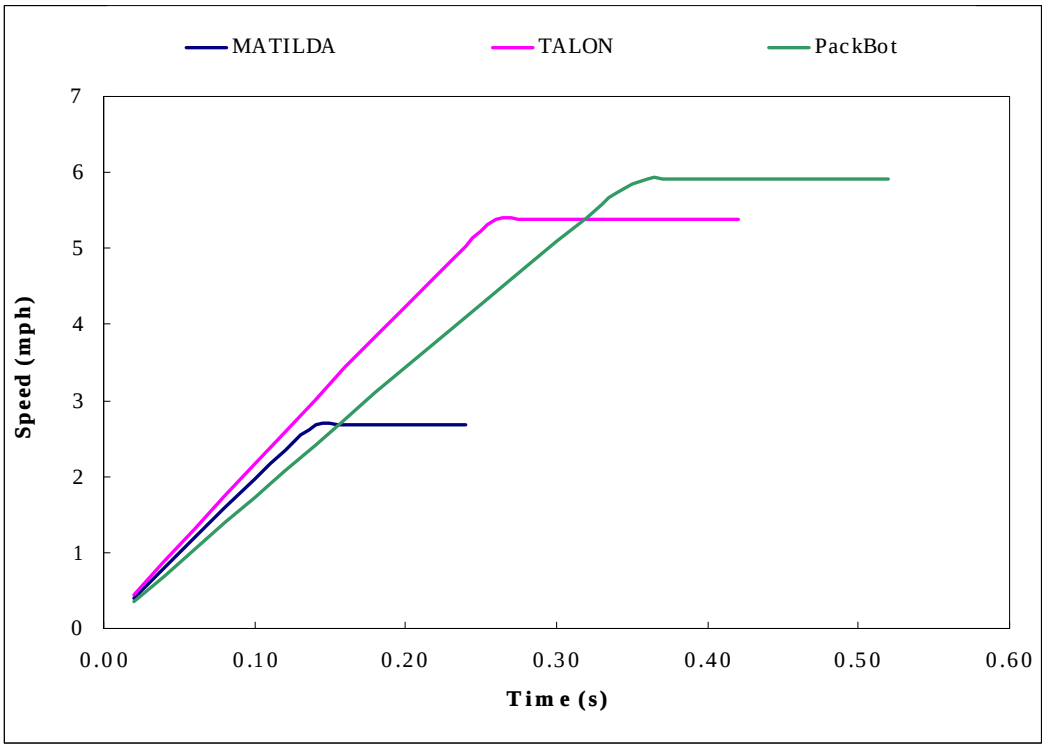

Figure 17. Acceleration of the SUGV.

Table 14 shows the predicted travel time for 120 ft compared with data from Table B2 for straight-line travel. Nearly exact travel times were found for the TALON; however, there is a major difference for the MATILDA. The test data did not indicate why travel times would be longer than expected, although battery charge state is suspected.

Table 14. Comparisons of travel times over 120 ft of dry pavement.

Vehicle	Measured, sec	Predicted, sec
MATILDA	42.0	30.52
TALON	15.38	15.17

8 STNDMob Vehicle File Additions

In an effort to simulate SUGV with STNDMob, the STNDMob vehicle performance file formats were modified to include additional terrain data. All the data associated with full-sized vehicles remain in the file. Additional performance data for floors, roofs, and conduit building materials and the corresponding coefficients for nonslippery and slippery surface types (refer to Table 5 for Trafficable Building Materials Types) have been added (Table 15). The performance coefficients on these surfaces will be represented in the same manner, i.e., as coefficients to Equation 1, as are the surfaces for full-sized vehicles.

Table 15. New materials for the STNDMob vehicle data file.

Terrain Type	Material Types
Floor	brick, cobble, concrete, wood, steel, carpet, ceramic_tile, fired_clay_tile, vinyl, slate, thatch
Roof	clay_concrete_tile, woodshake, slate, thatch, asphalt_shingle, builtup_acrylic, builtup_aggregate, builtup_asphalt, builtup_coal_tar, builtup_fabric, mineral_inorganic_sheet, liquid_applied, metal_pan_shingle, metal_roll_roofing, polymer_modified_bitumen, spray_poly_foam, thermostat_shingle_ply
Conduit	Concrete, lumber, metal, fiberglass

A new XML schema file will validate any newly created vehicle XML file produced for use in STNDMob. STNDMob has been enhanced to handle the new information and to generate performance predictions using these data. Figure 18 depicts how the new terrain data will appear in the XML files. Nonslippery and slippery condition performance data will be based on the presence of water. Winter conditions will be represented as other terrain conditions primarily independent of the underlying surface. The material type coefficients (labeled “info” in Figure 18) will hold the performance data in the same format as other terrain, namely:

- Maximum braking coefficient
- Resistive force coefficient
- Minimum and maximum tractive force
- Tractive force coefficients (b_0, b_1, b_2)
- Maximum tire speed

Additionally, steering type (Ackerman, skid, or omni) will be added as a vehicle configuration variable for wheeled vehicles.

```
</Terrain>
        -<Terrain Type="floor">
      -<Surface condition="nonslippery">
        <Coefficient materialType="brick">info</Coefficient>
        <Coefficient materialType="cobble">info</Coefficient>
        <Coefficient materialType="concrete">info</Coefficient>
        <Coefficient materialType="wood">info</Coefficient>
        <Coefficient materialType="steel">info</Coefficient>
        <Coefficient materialType="carpet">info</Coefficient>
        <Coefficient materialType="ceramic_tile">info</Coefficient>
        <Coefficient materialType="fired_clay_tile">info</Coefficient>
        <Coefficient materialType="vinyl">info</Coefficient>
        <Coefficient materialType="slate">info</Coefficient>
        <Coefficient materialType="thatch">info</Coefficient>
      </Surface>
</Terrain>
  -<Terrain Type="roof">
      -<Surface condition="nonslippery">
        <Coefficient materialType="clay_concrete_tile">info</Coefficient>
        <Coefficient materialType="woodshake">info</Coefficient>
        <Coefficient materialType="slate">info</Coefficient>
        <Coefficient materialType="thatch">info</Coefficient>
        <Coefficient materialType="asphalt_shingle">info</Coefficient>
        <Coefficient materialType="builtup_acrylic">info</Coefficient>
        <Coefficient materialType="builtup_aggregate">info</Coefficient>
        <Coefficient materialType="builtup_asphalt">info</Coefficient>
        <Coefficient materialType="builtup_coal_tar">info</Coefficient>
        <Coefficient materialType="builtup_fabric">info</Coefficient>
        <Coefficient materialType="mineral_inorganic_sheet">info</Coefficient>
        <Coefficient materialType="liquid_applied">info</Coefficient>
        <Coefficient materialType="metal_pan_shingle">info</Coefficient>
        <Coefficient materialType="metal_roll_roofing">info</Coefficient>
        <Coefficient materialType="polymer_modified_bitumen">info</Coefficient>
        <Coefficient materialType="spray_poly_foam">info</Coefficient>
        <Coefficient materialType="thermostat_shingle_ply">info</Coefficient>
      </Surface>
</Terrain>
  -<Terrain Type="conduit">
      -<Surface condition="nonslippery">
        <Coefficient materialType="concrete">info</Coefficient>
        <Coefficient materialType="lumber">info</Coefficient>
        <Coefficient materialType="metal>info</Coefficient>
        <Coefficient materialType="fiberglass">info</Coefficient>
      </Surface>
```

Figure 18. Representation of building materials as terrain types (data are repeated for throttle position and for slippery conditions).

9 Summary and Recommendations

The algorithms in NRMM and STNDMob were examined in light of using them for simulation of SUGV performance. Some of the existing NRMM subroutines can be modified to account for a robotic vehicle. Some of the algorithms require specific data that need to be collected. Additional testing and model analysis (verification) are required, specifically:

- Revisit obstacle crossing in STNDMob. Investigate the use of VEHDYN 4 for a higher fidelity obstacle crossing module (VEHDYN 4 was still under development during the period of this study).
- Data for wet surface conditions are lacking. The use of 0.5 as a maximum traction coefficient on wet pavement may be too conservative for SUGV.
- Data for the surface traction of building materials are required.
- Investigate the use of a generic tractive-force speed curve normalized for both vehicle weight and speed.
- Vegetation (heavy grass, small shrubs, and plants) may affect SUGV speeds much more than full-sized vehicles. Current algorithms are not valid for these types of vegetation.
- Performance in deep snow by tracked SUGV has been investigated by Lever and Shoop (2006); however, these algorithms need to be implemented in STNDMob.

References

Aberdeen Test Center. Army. 1980. *Test operations procedure, drawbar pull.* TOP 2-2-604. Aberdeen Proving Ground MD.

_____. 2002. *Test operations procedure, testing of unmanned ground vehicle (UGV) systems*. TOP 2-2-540 (20 June). Aberdeen Proving Ground, MD [DTIC accession: ADA403776].

Ahlvin, R. B., and P.W. Haley. 1992. *NATO reference mobility model, edition II; NRMM user's guide*. Technical Report GL-92-19. Vicksburg, MS: U.S. Army Waterways Experiment Station.

Albus, J., J. Evans, C. Schlenoff, T. Barbera, E. Messina, and S. Balakirsky. 2003. *Achieving intelligent performance in autonomous driving*. Gaithersburg, MD: National Institute of Standards and Technology Interagency Report 7166.

American Association of State Highway Officials (AASHO). 1966. *A policy on geometric design of rural highways*. Washington, DC.

Barnett, S. 2005. Development of a tow capacity test device for small unmanned vehicles. MS thesis, Virginia Polytechnic Institute and State University.

Baylot, E. A., B. Q. Gates, J. G. Green, P. W. Richmond, N. C. Goerger, G. L. Mason, C. L. Cummins, and L. S. Bunch. 2005. *Standard for ground vehicle mobility*. ERDC/GSL TR-05-06. Vicksburg, MS: U.S. Army Engineer Research and Development Center.

Blackmon C. A., and D. Randolph. 1968. *An analytical model for predicting cross-country vehicle performance; Appendix B, Vehicle performance in lateral and longitudinal obstacles (vegetation). Volume II, Longitudinal obstacles*. TR 3-783. Vicksburg, MS: U.S. Army Engineer Waterways Experiment Station.

Blaisdell, G. L. 1983. *The CRREL instrumented vehicle: Hardware and software*. Special Report 83-3. Hanover, NH: U.S. Army Cold Regions Research and Engineering Laboratory.

Creighton, D. C., G. B. McKinley, and R. B. Ahlvin. *Enhanced vehicle dynamics module: User's guide for computer program VEHDYN 4.0*. ERDC/GSL Technical Report (in preparation). Vicksburg, MS: U.S. Army Engineer Research and Development Center.

Ehsani, M., K. M. Rahman, and H. A. Toliyat. 1997. Propulsion system design of electric and hybrid vehicles. *IEEE Transactions on Industrial Electronics* 44(1):19–27.

Fields, M. 1999. *Modifying ModSAF terrain databases to support the evaluation of small weapons platforms in tactical scenarios*. ARL-TR-1996, Aberdeen Proving Ground, MD: U.S. Army Research Laboratory.

Fields, M. 2000. Designing a behavior development environment to support the Demo III robotics program. In *Proceedings of SPIE – The International Society for Optical Engineering, Unmanned Ground Vehicle Technology III*, ed. G. R. Gerhart and C. M. Shoemaker, 4364:349–358.

_____. 2002a. Modeling the human/robot interaction in OneSAF. In *Proceedings of the 23rd Army Science Conference* (poster).

_____. 2002b. Representing ground vehicle systems in battlefield simulations. In *Measuring the performance and intelligence of systems; Proceedings of the 2002 PerMIS workshop. August 13–15*. NIST Special Publication 990, ed. E. R. Messina and A. M. Meystel.

Fields, M., and B. Haug. 2003. *Developing a chemical reconnaissance behavior for unmanned ground vehicles using the OneSAF battlefield simulation tool*. ARL-TR-2972. Aberdeen Proving Ground, MD: U.S. Army Research Laboratory.

Haueisen, B., G. Hudas. D. Gorsich, R. B. Ahlvin, R. Jones, J. Priddy, G. Mason, and G. Hulburt. 2005. *Case study of the evaluation and verification of a PackBot model in NRMM*. SAE Paper 2005-01-0844. Warrendale, PA: Society of Automotive Engineers.

Headquarters, Department of the Army. 1994. Field Manual No. 5-430-00-1, *Planning and Design of Roads, Airfields, and Heliports in the Theater of Operations – Road Design*.

Hoblet, P., R. T. O'Brien, Jr., and J. A. Piepmeier. 2003. Scale-model vehicle analysis for the design of a steering controller. In *Proceedings of the 35th Southeastern Symposium on System Theory*, 201–205.

Kelly, A., and A. Stentz. 1997. Analysis of requirements for high speed rough terrain autonomous mobility; Part 1: Throughput and response. In *Proceedings of the 1997 IEEE International Conference on Robotics and Automation,* 4:3318–3325.

Lever, J. H., and S. A. Shoop. 2006. Design of lightweight robots for over-snow mobility. In *Proceedings, 10th European Conference of the International Society for Terrain-Vehicle Systems (ISTVS)*, 3–6 October, Budapest, Hungary.

Lever, J., D. Denton, G. Phetteplace, S. Wood, and S. A. Shoop. 2006. Mobility of a lightweight tracked robot over deep snow. *Journal of Terramechanics* 43(4):527–551.

Massey, K., J. Chatten, and M. J. Chatten. 2005. Greatly improved tele-operations efficiency. In *Proceedings of SPIE – The International Society for Optical Engineering, Unmanned Ground Vehicle Technology VII,* ed. G. R. Gerhart, C. M. Shoemaker, and D. W. Gage, 5804:597–602.

McBride, B., R. Longoria, and E. Krotkov. 2003. Measurement and prediction of the off-road mobility of small robotic ground vehicles. In *Proceedings of Performance Measures for Intelligent Systems (PerMIS'03)*. National Institute of Standards and Technology Special Publication 1014, ed. E. R. Messina, and A. M. Meystel. http://www.isd.mel.nist.gov/research_areas/research_engineering/Performance_Metrics/PerMIS_2003/Proceedings/index.html.

McKinley, G. B. 1988. *Mobility models utilizing acceleration and deceleration*. Technical Report GL-88-19. Vicksburg, MS: U.S. Army Waterways Experiment Station.

Merritt, H. E. 1946. The evolution of a tank transmission. In *Proceedings, Institution of Mechanical Engineers,* 154:412–428. London, UK: Institution of Mechanical Engineers.

Milliken, W. F., and D. L. Milliken. 1995. *Race car vehicle dynamics*. Warrendale, PA: SAE International [ISBN 1-56091-526-9].

Murphy, N. L., Jr., and R. B. Ahlvin. 1976. *AMC-74 vehicle dynamics module*. Technical Report M-76-1. Vicksburg, MS: U.S. Army Engineer Waterways Experiment Station.

Ojeda, L., J. Borenstein, and G. Witus. 2005. Terrain trafficability characterization with a mobile robot. In *Proceedings of SPIE – The International Society for Optical Engineering, Unmanned Ground Vehicle Technology VII,* ed. G. R. Gerhart, C. M. Shoemaker, and D. W. Gage, 5804:235–243.

Ojeda, L., J. Borenstein, G. Witus, and R. Karlsen. 2006. Terrain characterization and classification with a mobile robot. *Journal of Field Robotics* 23(2):103–122.

Pusey, J. 2005. Robotics modeling challenges for army combat simulation. In *Proceedings of the 73rd Military Operations Research Symposium (MORS), 21–23 June, West Point, NY.*

Ray, J. R. 1979. *Investigation of the factors involved in steering tracklaying vehicles*. Technical Report 10969. Warren, MI: U.S. Army Tank-Automotive Command [DTIC Accession number AD871157].

Richmond, P. W., R. A. Jones, D. C. Creighton, and R. B. Ahlvin. 2004. *Off-road ground contact forces for a real time motion simulator*. Special Publication 2004-01-2643. Warrendale, PA: Society of Automotive Engineers.

Richmond, P. W., B. Q. Gates, and E. A. Baylot. 2005. *Modeling vehicle terrain interaction in Army simulations*. SAE Paper 2005-01-3556. Warrendale, PA: Society of Automotive Engineers.

Rush, E. S. and A. A. Rula. 1967. *A limited study of effects of soil strength on walking speed*. Miscellaneous Paper No. 4-950, Vicksburg, MS: U.S. Army Engineer, Waterways Experiment Station.

Shoop, S. A. 1993. *Precision analysis and recommended test procedures for mobility measurements made with an instrumented vehicle*. Special Report 92-7. Hanover, NH: U.S. Army Cold Regions Research and Engineering Laboratory.

Smith, G. L. 1970. *Commercial vehicle performance and fuel economy*. SP-355. New York, NY: Society of Automotive Engineers.

U.S. Access Board. 2003. Bulletin 4: Ground and floor surfaces. *ADA accessibility guidelines for buildings and facilities*. http://www.access-board.gov/adaag/about/bulletins/pdf/surfaces.pdf.

Wies, R. W., J. Mitchell, S. Daniels, and J. Hawkins. 2000. Analysis of electric machines and drive systems for unmanned ground vehicle applications. In Proceedings of SPIE – The International Society for Optical Engineering, Unmanned Ground Vehicle Technology II, 24–25 April, ed. G. R. Gerhart, R. W. Gunderson, and D. W. Gage, 4024: 263–272.

Wong, J. Y., and C. F. Chang. 2001. A general theory for skid steering of tracked vehicles on firm ground; Proceedings of the Institution of Mechanical Engineers, Part D. Journal of Automobile Engineering 215(3):343–355.

Bibliography

Adamczyk, P. G., D. Gorsich, G. Hudas, and J. Overholt. 2003. Lightweight robotic mobility: Template-based modeling for dynamics and controls using ADAMS/Car and MATLAB. In Proceedings of SPIE – The International Society for Optical Engineering, Unmanned Ground Vehicle Technology September 2003, ed. G. R. Gerhart, C. M. Shoemaker, and D. W. Gage, 5083:63–74.

Ansorge, K. H., and J. E. Pond. 2000. Robotics vehicle mobility study. In *Proceedings of SPIE – The International Society for Optical Engineering, Unmanned Ground Vehicle Technology II, 24–25 April*, ed. G. R. Gerhart, R. W. Gunderson, and D. W. Gage, 4024:159–169.

Apostolopoulos, D. 2001. *Analytical configuration of wheeled robotic locomotion*, CMU-RI-TR-01-08. PhD diss., The Robotics Institute, Carnegie Mellon University.

Bares, J., and D. Stager. 2004. Expanded field test results from Spinner, a highly mobile, robust unmanned ground vehicle. In *Proceedings, Association for Unmanned Vehicle Systems International (UVSI) Unmanned Systems North America 2004*, 1245–1266.

Bares, J., S. McFadden, T. Stentz, C. Richards, and S. Murray. 2002. Designing crash-survivable unmanned vehicles. In *Proceedings, Association for Unmanned Vehicle Systems International (UVSI), Unmanned Systems North America, July*.

Bares, J., D. Stager, T. Cotton, S. Timoney, S. McFadden, and C. Richards. 2003. Initial field testing results from Spinner, a high mobility hybrid UGCV. In *Proceedings, Association for Unmanned Vehicle Systems International (UVSI) Unmanned Systems North America, July*.

Baten, S. 2000. Autonomous road and contour following with a tracked vehicle. In *Proceedings of SPIE – The International Society for Optical Engineering, Unmanned Ground Vehicle Technology II, 24–25 April*, ed. G. R. Gerhart, R. W. Gunderson, and D. W. Gage, 4024:32–42.

Baylot, A., P. Frederick, R. Kania, B. Theisen, D. Ward, U. Benz, J. Willis, and H. Yamauchi. 2005. Unmanned ground vehicle navigation: Bringing together image analysis, models and simulations, and on-board guidance systems. In *Proceedings, European Simulation Interoperability Workshop, 27–29 June, Toulouse, France* (05E-SIW-044).

Blackburn, M. R., R. Bailey, and B. Lytle. 2004. Improved mobility in a multi degree of freedom unmanned ground vehicle. In *Proceedings of SPIE – The International Society for Optical Engineering, Unmanned Ground Vehicle Technology VI,* ed. G. R. Gerhart, C. M. Shoemaker, and D. W. Gage, 5422:124–134.

Bodt, B. A., and R. S. Camden. 2004. Technology readiness level 6 and autonomous mobility. In *Proceedings of SPIE – The International Society for Optical Engineering, Unmanned Ground Vehicle Technology VI,* ed. G. R. Gerhart, C. M. Shoemaker, and D. W. Gage, 5422:302–313.

Brosinsky, C. A., D. M. Hanna, and S. G. Penzes. 2000. Articulated navigation testbed (ANT): An example of adaptable intrinsic mobility. In *Proceedings of SPIE – The International Society for Optical Engineering, Unmanned Ground Vehicle Technology II, 24–25 April*, ed. G. R. Gerhart, R. W. Gunderson, and D. W. Gage, 4024:86–95.

Brosinsky, C. A., S. G. Penzes, M. Buehler, and C. Steeves. 2001. Integrating intrinsic mobility into unmanned ground vehicle systems. In *Proceedings of SPIE – The International Society for Optical Engineering, Unmanned Ground Vehicle Technology III*, ed. G. R. Gerhart, and C. M. Shoemaker, 4364:19–27.

Browne, M., and K. Moffitt. 1996. A head-mounted display system for UGV control stations. In *Proceedings of the 23rd Annual Association for Unmanned Vehicle Systems International Symposium and Exhibition, 15–19 July, Orlando, FL,* 705–715.

Bullock, R. 1995. Applying PMDC motors. *Power Transmission Design* (May).

Camden, R., B. Bodt, S. Schipani, J. Bornstein, R. Phelps, T. Runyon, F. French, and C. Shoemaker. 2003. *Autonomous mobility technology assessment: interim report*. Technical Report ARL-MR-565. Aberdeen Proving Ground, MD: Army Research Laboratory.

Carlson, J., and R. R. Murphy. 2005. How UGVs physically fail in the field. *IEEE Transactions on Robotics* 21(3):423–437.

Chaudhry, A. I., and J. D. Thele. 1999. High velocity tele-operated rover. In *Proceedings of SPIE – The International Society for Optical Engineering, Unmanned Ground Vehicle Technology*, ed. G. R. Gerhart, R. W. Gunderson and C. M. Shoemaker, 3693:202–211.

Chun, W. H., and T. M. Jochem. 1995 Unmanned ground vehicle Demo II: Demonstration A. In *Proceedings of SPIE – The International Society for Optical Engineering, Mobile robots IX*, ed. W. J. Wolfe, and W. H. Chun, 2352:180–191.

Crow, E. C., K. M. Reichard, J. Kozlowski, C. Rogan, and G. Puri. 2005. Integrated prognostic health monitoring of battery health in ground robots. In *Proceedings of Association for Unmanned Vehicle Systems International Unmanned Systems North America 2005,* 309–323.

Czop, A., K. Hacker, J. Murphy, and T. Zimmerman. 2005. Development of an affordable and supportable EOD unmanned ground vehicle. In *Proceedings of Association for Unmanned Vehicle Systems International Unmanned Systems North America 2005,* 741–755.

Digney, B. L. 2003. Extreme mobility and autonomous operation of unmanned guided vehicles [DTIC Accession Number: ADB296920].

Digney, B. L., and S. Penzes. 2002. Robotic concepts for urban operations. In *Proceedings of SPIE – The International Society for Optical Engineering, Unmanned Ground Vehicle Technology IV*, ed. G. R. Gerhart, C. M. Shoemaker and D. W. Gage, 4715:63–74.

Economou, J. T., P. C. K. Luk, A. Tsourdos, and B. A. White. 2003. Hybrid modeling of an all-electric front-wheel Ackerman steered vehicle. In *Proceedings, Vehicular Technology Conference, 2003. VTC 2003-Fall. IEEE 58th*, 58:3294–3298 [ISBN: 0-7803-7954-3].

Enigma Industries. 2003. Electric drive train simulator. http://www.enigmaindustries.com/manual.htm.

Feddema, J., C. Lewis, and P. Klarer. 1999. Control of multiple robotic sentry vehicles. In *Proceedings of SPIE – The International Society for Optical Engineering, Unmanned Ground Vehicle Technology*, ed. G. R. Gerhart, R. W. Gunderson, and C. M. Shoemaker, 3693:212–223.

Frederick, P. A., R. Kania, B. Theisen, D. Ward, U. Benz, A. Baylot, J. Willis, and H. Yamauchi. 2005. Remote imagery for unmanned ground vehicles (RIUGV). In *Proceedings of the SPIE, Airborne Intelligence, Surveillance, Reconnaissance (ISR) Systems and Applications II,* ed. S. H. Wyatt, 5787:93–104.

Gerhart, G. R., and C. M. Shoemaker, ed. 2001. *Proceedings of SPIE: Unmanned Ground Vehicle Technology III,* 4364. Bellingham, WA: SPIE—The International Society for Optical Engineering.

Gerhart, G. R., C. M. Shoemaker, and D. W. Gage, ed. 2003. *Proceedings of SPIE: Unmanned Ground Vehicle Technology V,* 5083. Bellingham, WA: SPIE–The International Society for Optical Engineering.

Gerhart, G. R., C. M. Shoemaker, and D. W. Gage, ed. 2004. *Proceedings of SPIE: Unmanned Ground Vehicle Technology VI,* 5422. Bellingham, WA: SPIE–The International Society for Optical Engineering.

Ghaffari, M., A. Alhaj, M. Souma, V. Murthy, X. Liao, J. Gaylor, and E. L. Hall. 2004. Design of an unmanned ground vehicle, Bearcat III; theory and practice. *Journal of Robotic Systems* 21(9):471–480.

Glubrecht, D., and D. Jones. 2003. *Affordable hybrid drive system for small to medium sized unmanned ground vehicles (UGV).* Madison, AL: Mesa Associates, Inc. [DTIC Accession Number: ADB290576].

Goodsell, T. G., N. S. Flann, and M. E. Davidson. 1999. Mobility planning for omni-directional vehicles in natural terrains. In *Proceedings of SPIE – The International Society for Optical Engineering, Unmanned Ground Vehicle Technology*, ed. G. R. Gerhart, R. W. Gunderson and C. M. Shoemaker, 3693:2–10.

Gunter, D. D., W. W. Bylsma, K. Edgar, M. D. Letherwood, and D. J. Gorsich. 2005. Using modeling and simulation to evaluate stability and traction performance of a track-laying robotic vehicle. In *Proceedings of SPIE – The International Society for Optical Engineering, Enabling Technologies for Simulation Science IX*, ed. D. A. Trevisani and A. F. Sisti, 5805:66–73.

Henninger, A. E., and R. Madhavan. 2005. Metric for assessing the fidelity of trajectory models for mobile agents. In *Proceedings of SPIE – The International Society for Optical Engineering, Unmanned Ground Vehicle Technology VII*, ed. G. R. Gerhart, C. M. Shoemaker, and D. W. Gage, 5804:23–34.

Hogg, R. W., A. L. Rankin, M. C. McHenry, D. M. Helmick, C. F. Bergh, S. I. Roumeliotis, and L. Matthies. 2001. Sensors and algorithms for small robot leader/follower behavior. In *Proceedings of SPIE – The International Society for Optical Engineering, Unmanned Ground Vehicle Technology III*, ed. G. R. Gerhart and C. M. Shoemaker, 4364:72–85.

Hong, T. H., S. Legowik, and M. A. Nashman. 1998. *Obstacle detection and mapping system*. Interagency Report (NISTIR) 6213. Gaithersburg, MD: National Institute of Standards and Technology.

Hori, Y., Y. Toyoda, and Y. Tsuruoka. 1998. Traction control of electric vehicle: basic experimental results using the test EV "UOT Electric March." *IEEE Transactions on Industry Applications* 34(5): 1131–1138.

Ibanez-Guzman, J., X. Jian, A. Malcolm, Z. Gong, C. W. Chen, and A. Tay. 2004. *Unmanned tracked ground vehicle for natural environments*. Singapore: Defence Science and Technology Agency [DTIC Accession Number: ADA432934, http://handle.dtic.mil/100.2/ADA432934].

Jacoff, A., E. Messina, and J. Evans. 2001. Reference test courses for autonomous mobile robots. In *Proceedings of SPIE – The International Society for Optical Engineering, Unmanned Ground Vehicle Technology III*, ed. G. R. Gerhart and C. M. Shoemaker, 4364:341–348.

Jaczkowski, J. J. 2003. Robotic follower experimentation results: ready for FCS Increment I. In *Proceedings of SPIE – The International Society for Optical Engineering, Unmanned Ground Vehicle Technology V*, ed. G. R. Gerhart, C. M. Shoemaker, and D. W. Gage, 5083:311–321.

Kuhlman, K. R., A. E. Behar, J. A. Jones, F. Carsey, G. A. Hajos, J. J. Flick, and J. Antol. 2004. Tumbleweed—a new paradigm for surveying the surface of mars for in-situ resources, Contribution 1224. In *Space Resources Roundtable VI Program and Abstracts; LPI*.

Lane, G. R., P. Lescoe, and S. Cooper. 1991. Unmanned ground vehicle control technology. In *Proceedings, IEEE National Telesystems Conference*, 1:329–329.

Matthies, L., T. Litwin, K. Owens, A. Rankin, K. Murphy, D. Coombs, J. Gilsinn, T. Hong, S. Legowik, M. Nashman, and B. Yoshimi. 1998. Performance evaluation of UGV obstacle detection with CCD/FLIR stereo vision and LADAR. In *Proceedings, IEEE ISIC/CIRA/ISAS Joint Conference*, 658–670.

McCoy, R., and B. DeGrano. 2005. Autonomous mine detection sensors (AMDS) design and performance. In *Proceedings of SPIE – The International Society for Optical Engineering, Detection and Remediation Technologies for Mines and Minelike Targets X*, ed. R. S. Harmon, J. T. Broach, and J. H. Holloway, Jr., 5794:1008–1017.

Morillon, J. G., O. Lecointe, J. Quin, and M. Tissedre. 2003. Development of high level robotic functions for mobile combat systems. In *Proceedings of SPIE – The International Society for Optical Engineering, Unmanned Ground Vehicle Technology V*, ed. G. R. Gerhart, C. M. Shoemaker, and D. W. Gage, 5083:452–461.

Muench, P., S. Laughery, J. Everson, K. Houle, and F. Ikramulla. 2000. Tele-operation convoy. In *Proceedings of SPIE – The International Society for Optical Engineering, Unmanned Ground Vehicle Technology II*, ed. G. R. Gerhart, R. W. Gunderson, and C. M. Shoemaker, 4024:348–355.

Munkeby, S. H., C. M. Shoemaker, and W. H. Chun. 1994. Unmanned ground vehicle Demonstration II program. In *Proceedings of the IEEE National Telesystems Conference*, 4:149–152.

Neville, N., and M. Buehler. 2003. *Towards bipedal running of a six-legged robot.* Montreal, Canada: McGill Research Centre for Intelligent Machines [DTIC Accession Number: ADA438825, http://handle.dtic.mil/100.2/ADA438825].

Pan, W., Y. Papelis, and Y. He. 2004. A vehicle-terrain system modeling and simulation approach to mobility analysis of vehicles on soft terrain. In *Proceedings of SPIE – The International Society for Optical Engineering, Unmanned Ground Vehicle Technology VI,* ed. G. R. Gerhart, C. M. Shoemaker, and D. W. Gage, 5422:520–531.

Pape, O., J. G. Morillon, P. Houbloup, S. Leveque, C. Fialaire, T. Gauthier, and P. Ropars. 2005. Stability control for high speed tracked unmanned vehicles. In *Proceedings of SPIE – The International Society for Optical Engineering, Unmanned Ground Vehicle Technology VII,* ed. G. R. Gerhart, C. M. Shoemaker, and D. W. Gage, 5804:418–426.

Pastore, T. H., M. Barnes, and R. Hallman. 2005. Mobile robot knowledge base. In *Proceedings of SPIE – The International Society for Optical Engineering, Unmanned Ground Vehicle Technology VII,* ed. G. R. Gerhart, C. M. Shoemaker, and D. W. Gage, 5804:542–549.

Peters, J. 1995. *Analysis of soil-track interaction for computer program TVSTEER.* Technical Report GL-95-6. Vicksburg, MS: U.S. Army Engineer Waterways Experiment Station.

Pratt, S., F. Alibozek, T. Frost, C. Norman, A. Shein, and C. Smith. 2002. Applications of tactical mobile robot technology to urban search and rescue: Lessons learned at the World Trade Center disaster. In *Proceedings of SPIE – The International Society for Optical Engineering, Unmanned Ground Vehicle Technology IV,* ed. G. R. Gerhart, C. M. Shoemaker, and D. W. Gage, 4715:13–20.

Rankin, A. L., C. F. Bergh, S. B. Goldberg, P. Bellutta, A. Huertas, and L. H. Matthies. 2005. Passive perception system for day/night autonomous off-road navigation. In *Proceedings of SPIE – The International Society for Optical Engineering, Unmanned Ground Vehicle Technology VII,* ed. G. R. Gerhart, C. M. Shoemaker, and D. W. Gage, 5804:343–358.

Rosenblum, M., and V. Rajagopalan. 2005. The road more traveled: A foundation for autonomous roadway operations. In *Proceedings of SPIE – The International Society for Optical Engineering, Unmanned Ground Vehicle Technology VII,* ed. G. R. Gerhart, C. M. Shoemaker, and D. W. Gage, 5804:727–740.

Sadhukhan, D., C. Moore, and E. Collins. 2004. Terrain estimation using internal sensors. In *Proceedings of the Tenth IASTED International Conference on Robotics and Applications,* ed. M. Kamel, 195–199.

Shamah, B. 1999. *Experimental comparison of skid steering vs. explicit steering for a wheeled mobile robot*. CMU-RI-TR-99-06. MS thesis, The Robotics Institute, Carnegie Mellon University.

Shinoda, Y., Y. Niwa, and M. Kaneko. 1999. Influence of camera position for a remotely driven vehicle; Study of a rough terrain mobile unmanned ground vehicle. *Advanced Robotics* 13(3):311–312.

Shirkhodaie, A. 2001. Supervised tactical mobility behavior modeling and control of multi-agent robotic vehicles. In *Proceedings of SPIE – The International Society for Optical Engineering, Unmanned Ground Vehicle Technology III*, ed. G. R. Gerhart, and C. M. Shoemaker, 4364:117–126.

Shoemaker, C. M., and J. A. Bornstein. 2000. Overview and update of the Demo III experimental unmanned vehicle program. In *Proceedings of SPIE – The International Society for Optical Engineering, Unmanned Ground Vehicle Technology II*, ed. G. R. Gerhart, R. W. Gunderson, and C. M. Shoemaker, 4024:212–220.

Singh, S., D. Feng, P. Keller, G. Shaffer, and W. Shi, D. H. Shin, J. West, and B. X. Wu. 1991. *A system for fast navigation of autonomous vehicles*. CMU-RI-TR-91-20. Pittsburg, PA: Robotics Institute, Carnegie Mellon University [DTIC Accession Number: ADA243523].

Singh, H., H. Singh, J. Raj, and G. Grant. 2004. Development of a virtual mobile robot laboratory. In *Proceedings of SPIE – The International Society for Optical Engineering, Unmanned Ground Vehicle Technology VI*, ed. G. R. Gerhart, C. M. Shoemaker, and D. W. Gage, 5422:584–593.

Spain, E. H., and T. W. Hughes. 1991. *Objective assessments of mobility with an early unmanned ground vehicle (UGV) prototype viewing system*. San Diego, CA: Naval Ocean Systems Center [DTIC Accession Number: ADA237317].

Spenko, M., K. Iagnemma, and S. Dubowsky. 2004. High speed hazard avoidance for mobile robots in rough terrain. In *Proceedings of SPIE – The International Society for Optical Engineering, Unmanned Ground Vehicle Technology VI*, ed. G. R. Gerhart, C. M. Shoemaker, and D. W. Gage, 5422:439–450.

Spofford, J. R., and B. M. Gothard. 1995. Stopping distance analysis of ladar and stereo for unmanned ground vehicles. *In Proceedings of SPIE – The International Society for Optical Engineering, Mobile Robots IX*, ed. W. J. Wolfe, and W. H. Chun, 2352:215–226.

Taylor, M., K. Lay, J. Struble, W. Allen, and M. Subrt. 2003. Automated field testing of a track-type tractor. In *Proceedings of SPIE – The International Society for Optical Engineering, Unmanned Ground Vehicle Technology V*, ed. G. R. Gerhart, C. M. Shoemaker, and D. W. Gage, 5083:173–182.

Tobler, C. 2004. Development of an autonomous navigation technology test vehicle. MS thesis, University of Florida.

Trentini, M., B. Beckman, B. Digney, and J. Collier. 2004. Novel mobility platforms utilizing intelligent algorithms. In *Proceedings of SPIE – The International Society for Optical Engineering, Unmanned Ground Vehicle Technology VI*, ed. G. R. Gerhart, C. M. Shoemaker, and D. W. Gage, 5422:451–460.

Vandapel, N., R. R. Donamukkala, and M. Hebert. 2003. Quality assessment of traversability maps from aerial LIDAR data for an unmanned ground vehicle. In *Proceedings, IEEE International Conference on Intelligent Robots and Systems*, 1:305–310.

Vandapel, N., R. R. Donamukkala, and M. Hebert. 2006. Unmanned ground vehicle navigation using serial LADAR data. *International Journal of Robotics Research* 25(1):31–51.

Vanerp, J. B. F., and B. Kappe. 1997. *Head-slaved images for low-cost driving simulators and unmanned ground vehicles (Hoofd-gestuurde beelden voor onbemande grondvoertuigen en simulatoren)*. Report TM-97-A041. Soesterberg, The Netherlands: TNO Human Factors Research Institute.

Vasseur, L., P. Gosset, L. Carpentier, V. Marion, J. G. Morillon, and P. Ropars. 2005. Constrained navigation for unmanned systems. In *Proceedings of SPIE – The International Society for Optical Engineering, Unmanned Ground Vehicle Technology VII,* ed. G. R. Gerhart, C. M. Shoemaker, and D. W. Gage, 5804:371–383.

Vong, T. T., G. A. Haas, and C. L. Henry. 1999. *NATO reference mobility model (NRMM) modeling of the Demo III experimental unmanned ground vehicle (XUV)*. ARL-MR-435. Aberdeen Proving Ground, MD: Army Research Laboratory [DTIC Accession Number: ADA362133].

Wells, P., and D. Deguire. 2005. TALON®, a universal unmanned ground vehicle platform, enabling the mission to be the focus. In *Proceedings of SPIE – The International Society for Optical Engineering, Unmanned Ground Vehicle Technology VII,* ed. G. R. Gerhart, C. M. Shoemaker, and D. W. Gage, 5804:747–757.

Wies, R. W., J. Mitchell, S. Daniels, and J. Hawkins. 2000. Analysis of electric machines and drive systems for unmanned ground vehicle applications. In *Proceedings of SPIE – The International Society for Optical Engineering, Unmanned Ground Vehicle Technology II*, ed. G. R. Gerhart, R. W. Gunderson, and C. M. Shoemaker, 4024:263–272.

Wit, J., R. Mandapat, and B. Skibba. 2004. High speed robot assisted teleoperation. In *Proceedings, ANS 10th International Conference on Robotics and Remote Systems for Hazardous Environments,* 427–431.

Witus, G. 1999. Mobility and dynamics modeling for unmanned ground vehicle motion planning. In *Proceedings of SPIE – The International Society for Optical Engineering, Unmanned Ground Vehicle Technology*, ed. G. R. Gerhart, R. W. Gunderson, and C. M. Shoemaker, 3693:32–43.

Witus, G., R. Karlsen, J. Overholt, and G. Gerhart. 2005. Forecasting off-road trafficability from terrain appearance. In *Proceedings of SPIE – The International Society for Optical Engineering, Unmanned Ground Vehicle Technology VII,* ed. G. R. Gerhart, C. M. Shoemaker, and D. W. Gage, 5804:217–226.

Appendix A: Description and Definitions of Input Parameters to the Standard Mobility API

The Standard Mobility API version 3.4 (STNDMob) Java method "calculateMaximumSpeedAcceleration" for fidelity degrees 3 and 4 calculates the maximum steady-state terrain and vehicle limited speed, and the available acceleration at a given current speed. This method is for determining speed when terrain parameters are available as discrete values. Additionally, it populates the field variable "totalResistForceCoeff" (which is effectively the towing resistance and will be useful for simulation of vehicle recovery and towing). STNDMob will need slight enhancement to model towing. The variables required are described in Table A1. Tables A2 and A3 provide additional enumeration for soil wetness and vegetation stem sizes, respectively.

Table A1. STNDMob input variables for fidelity degrees 3 and 4.

Variable Name	Value Type	Description
vehicleTypeID	integer	An identifier of either a specific vehicle type or vehicle bin, which corresponds to a vehicle XML file currently supplied with STNDMob and created using a special output format of the NRMM. In the future, AMSAA will provide validated data files in the proper format.
throttleSetting	integer	A percentage value estimating the how much the accelerator has been compressed by the driver.
plowType	integer	The type of mine plow attached to vehicle: 0 NO PLOW 1 TRACK WIDTH MINE PLOW 2 FULL WIDTH MINE PLOW 3 TRACK WIDTH MINE RAKE 4 FULL WIDTH MINE RAKE
plowdepth	float	The plowing depth (cm).
plowWeight	integer	The mass of the plow (kg), Not used in STNDMob 3.4, (plow data does not have weight, this needs to be modified; this mass will be added to the vehicle mass. Set to 0 for STNDMob 3.4.
vehiclePitch	float	Vehicle pitch (radians) should be based on the vehicle location and heading (effectively the terrain slope).
vehicleRoll	float	Vehicle roll (radians) should be calculated outside of STNDMob, based on vehicle location and heading, vehicle roll is the angle perpendicular to the vehicle pitch.

[1] Currently, the system of units used for input to STNDMob is inconsistent; this will be corrected in future versions. The OneSAF implementation uses only SI units.

Variable Name	Value Type	Description
soilUSCSType	integer	USCS soil type: Input USCS type NRMM internal soil type 0 none 1 GW 5 2 GP 5 3 GM 4 4 GC 1 5 SW 5 6 SP 5 7 SM 4 8 SC 1 9 ML 3 10 CL 3 11 OL 2 12 CH 2 13 MH 2 14 OH 2 15 PT 6 16 not used 17 not used 18 Evaporates 3
soilStrengthCone_40	integer	The average soil cone index down to 40 cm, as the tractive force speed curves (in the XML vehicle files) were generated from terrain where the 0- to 15-cm and 15- to 30-cm (0–6 and 6–12 in.) RCI/CI values were equal. Interpolations are made between the values given in the data file if required. SoilStrengthCone_40 is the average of the EDCS attribute: SOIL_CONE_INDEX_QB_MEASUREMENT_DEPTH - <SOIL_CONE_INDEX> at <MEASUREMENT_DEPTH>: [0,15], [15,30] where measurement depths are in centimeters. [1]
FROZEN_WATER_TYPE	integer	The condition of frozen water on the terrain surface corresponds to the EDCS attribute: FROZEN_WATER_TYPE - The type of frozen <WATER> present. 0 ICE 1 MELTING_SNOW_OR_ICE 2 MIXED_SNOW_AND_ICE 3 NONE_PRESENT 4 SLUSH 5 SNOW 6 SNOW_OVER_ICE
surfaceType	integer	Used to determine if the surface is a type of road, use the EDCS attribute: TERRAIN_ROUTE_TYPE - The type of a <TERRAIN_TRANSPORTATION_ ROUTE>. 0 SURFACETYPE_CROSSCOUNTRY (use if not a road or trail) 1 SURFACETYPE_SUPERHIGHWAY (super highway) 2 SURFACETYPE_PRIMARY (primary road) 3 SURFACETYPE_SECONDARY (secondary road) 4 SURFACETYPE_TRAIL (unpaved trail, or road)

[1] Words enclosed in < > are defined features or attributes in the OneSAF EDM and EDCS.

Variable Name	Value Type	Description
surfaceCondition	integer	Whether surface is wet or dry, corresponds to EDCS attribute: SURFACE_SLIPPERY- Indication that a <SURFACE> is slippery. Examples: wet grass, wet clay soil, wet roads. 1 Surface is not slippery or dry (false) 2 Surface is slippery or wet (true)
debrisSpacing	integer	The average spacing (ft) of pieces of debris or possibly small rubble piles in a debris field. This value should come from the Structural Weapons Effects (SWE) API. Expected values are in the range of 0–6 ft. Although not currently in the ONESAF EDM, they could be an attribute of "RUBBLE AREA," "RUBBLE POINT." Use 0 for no effect.
debrisRoughness	double	The RMS roughness (in.) of the debris field. Similar to The EDCS attribute: TERRAIN_ROUGHNESS_ROOT_MEAN_SQUARE - The roughness of <TERRAIN> based on elevation variations in the debris field, calculated using the root-mean-square (RMS) value of the detrended <TERRAIN_ELEVATION>. This value should come from the Structural Weapons Effect API. Expected values are in the range of 0.0–5.0 in. Use 0 for no effect.
surfaceRoughness	float	The EDCS attribute: TERRAIN_ROUGHNESS_ROOT_MEAN_SQUARE - The roughness of <TERRAIN> based on elevation variations, calculated using the root-mean-square (RMS) value of the detrended <TERRAIN_ELEVATION>s measured at a spatial frequency of approximately 0.3 meter. If the feature does not have a TERRAIN_ROUGHNESS_ROOT_MEAN_SQUARE attribute, set to 0.
iceThickness	float	This thickness (cm) of the ice from the terrain characteristics. This thickness is used to determine whether the vehicle can withstand when crossing the ice.
waterDepth	float	The depth (m) of the water (m) from the terrain characteristics. This depth is used to determine whether the vehicle can safely cross the water.
snowDepth	float	The depth (cm) of the snow cover, there are two EDCS attributes which describe snow depth: SNOW_DEPTH The depth of <SNOW> and/or <ICE> on the <TERRAIN>. SNOW_ONLY_DEPTH The depth of the <SNOW>, which may be over <TERRAIN>, <ICE>, or floating <ICE>. Use SNOW_ONLY_DEPTH, if both are provided for a terrain feature.
snowDensity	float	The average density of the snow cover (g/cm^3), EDCS attribute: SNOW_DENSITY - The density of accumulated <SNOW> on an <OBJECT>.
soilMoisture	float	The soil moisture content by volume (%) use the EDCS attribute SOIL_WATER_VOLUME - The <WATER> lost from the <SOIL> upon drying to constant mass at 105 °C, expressed as the fractional volume of <WATER> per unit bulk volume of wet <SOIL>. Multiplied by 100.
soilWetness	string	The expected input is one of the enumerations of the EDCS attribute SOIL_WETNESS - The categorical (coded) <SOIL> <WATER> content, whether liquid or solid, for the feature. The ONESAF EDM enumerations and description are shown in Table A2.
soilDensity	float	The dry soil density (kg/m^3), use the EDCS attribute SOIL_DENSITY_DRY - The average density of the <SOIL> between the <SURFACE> and the <BEDROCK> after it has been dried to a constant <<MASS>> at 105 °C.
frozenDepth	float	The depth (cm) of frozen soil from surface use the EDCS attribute: FROZEN_SOIL_LAYER_BOTTOM_DEPTH, the depth from the <TERRAIN> to the base of a layer of frozen <SOIL>.

Variable Name	Value Type	Description
thawedDepth	float	The depth (cm) of thawed soil from surface, use the EDCS attribute: FROZEN_SOIL_LAYER_TOP_DEPTH, the depth from the <TERRAIN> to the top of a layer of frozen <SOIL>.
vegetationAverage-StemSpacing	double[]	The array of average stem spacing (ft) for the eight stem size classes. Use the EDCS attribute: "MEAN_STEM_SPACING_QB_STEM_DIAMETER <MEAN_STEM_SPACING> of all stems of <STEM_DIAMETER>: (0.0, OPEN], (2.5, OPEN], (6.0, OPEN], (10.0, OPEN], (14.0, OPEN], (18.0, OPEN], (22.0, OPEN], (25.0, OPEN]" mapped to the array indices as shown in Table A3.
obstacleHeightIngress	float	The obstacle ingress height (in.), see Figure A1 and the discussion of obstacles below.
obstacleHeightEgress	float	The obstacle egress height (in.), see Figure A1 and the discussion of obstacles below.
obstacleWidth	float	The obstacle width (in.), see Figure A1 and the discussion of obstacles below.
obstacleApproach-AngleIngress	float	The obstacle approach angle (radians), see Figure A1 and the discussion of obstacles below.
obstacleApproach-AngleEgress	float	The obstacle egress angle (radians), see Figure A1 and the discussion of obstacles below.
obstacleMaterialType	integer	For obstacle features have the attribute: PRIMARY_MATERIAL_TYPE The type of primary <MATERIAL> composition of an <OBJECT>. If the obstacle has 0 width and height, then this value is ignored. 0 CONCRETE 1 GLASS 2 MASONRY 3 STEEL 4 WOOD 5 VINYL_SIDING
stabilityRubble	integer	For the features that have the attribute RUBBLE_STABILITY - The ability of <RUBBLE> to resist sliding or collapsing under stress; rubble stability. 0 CONSOLIDATED 1 LOOSE
radiusCurvature	float	The radius (meters) of the path a vehicle is following, calculated outside of STNDMob using 3 points (previous location, current location and projected location), or the attribute of a road.
initVelocity	double	The initial velocity (mps) of the vehicle at the beginning of the time step.
time	float	The time step in seconds.
brakePos	float	The percentage (0–100) amount applied to the brake.
driverName	String	An identifier a specific driver which corresponds to a driverState XML file supplied with STNDMob. New drivers can easily be added
driverCommandSpeed	float	The speed (kph) limit set by the selected driver.

Table A2. Enumerations of soil Wetness and suggested integer mapping.

EDCS Attribute: SOIL_WETNESS Enumerations	Potential Wetness	Depth to Water Table	Depth of Wetting	General Characteristics of Sites	Integer Values Consistent with NRMM
PERENNIALLY_DRY	Arid	Indeterminable	Less than 1 ft	Located in desert regions.	0
	Dry	Indeterminable	1–4 ft	Steeply sloping denuded or severely eroded and gullied.	1
MOIST	Average	More than 4 ft	More than 4 ft	Well-drained soil with no restricting layers or pans; fair to good internal and external drainage. Slope may be flat to steep.	2
WET	Wet	1–4 ft	To water table	Soil not well drained. Restricting layers or deep pans may be present. May occur at base of slopes, on terraces, upland flats, or bottom lands.	3
SATURATED	Saturated	Less than 1 ft	To water table	Sites waterlogged or flooded at least part of the year. Bottomlands subject to frequent overflow. Upland with poor drainage or shallow pans. Slopes with very poor drainage.	4
WATERLOGGED	Saturated	Zero (surface)	Complete	Areas perennially waterlogged. No change in water content or soil strength.	5

Table A3. Stem size classes mapped to MEAN_STEM_SPACING_QB_STEM_DIAMETER.

Array Index	Stem size class, in.	MEAN_STEM_SPACING_ QB_STEM_DIAMETER (stem sizes, cm)
0	0 < 0.98	(0.0, OPEN)
1	≥0.98 and <2.36	(2.5, OPEN)
2	≥2.36 and <3.94	(6.0, OPEN)
3	≥3.94 and <5.51	(10.0, OPEN)
4	≥5.51 and <7.09	(14.0, OPEN)
5	≥8.66 and <9.84	(18.0, OPEN)
6	≥15 and <99	(22.0, OPEN)
7	≥99	(25.0, OPEN)

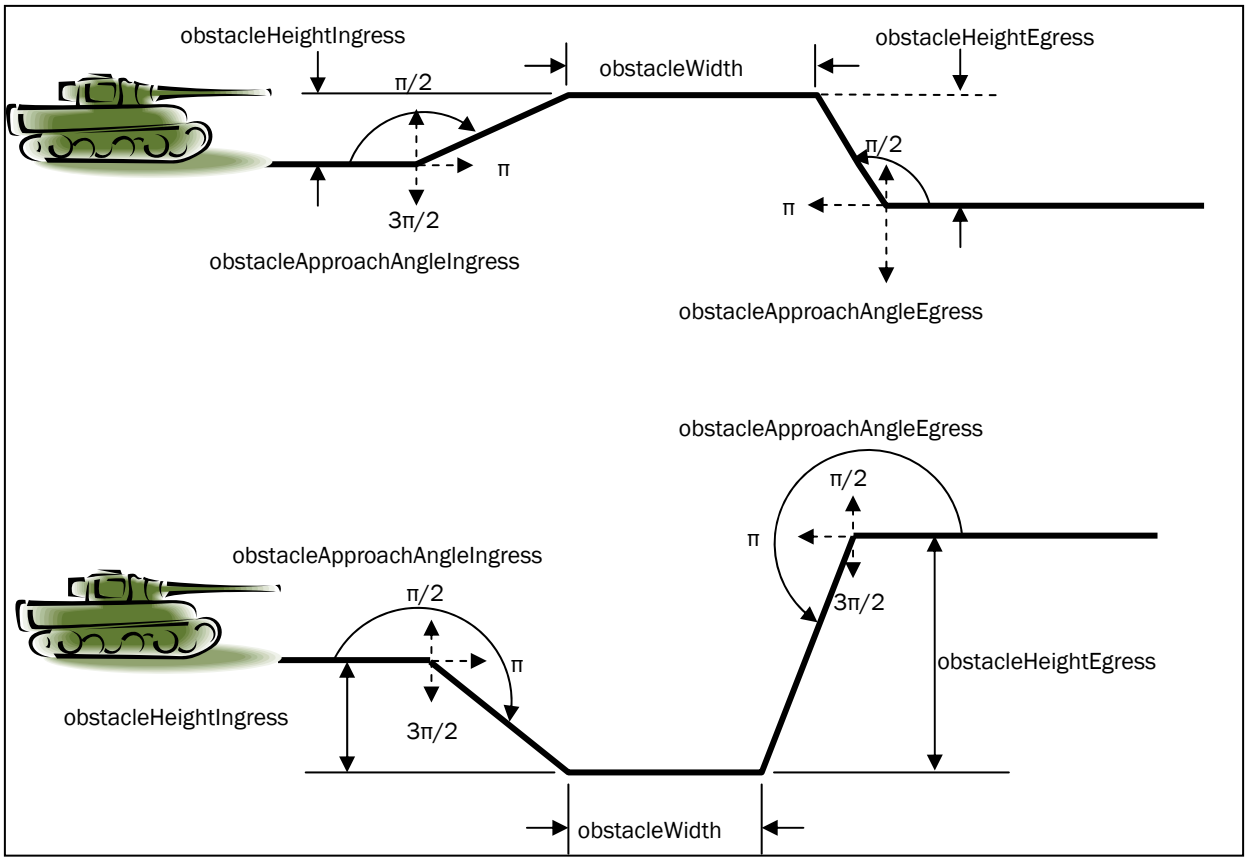

Figure A1. Standard Mobility obstacle parameter descriptions.

Obstacles

Figure A1 shows how obstacles are modeled in Standard Mobility. Ingress and egress are dependent on the direction of vehicle travel, while the EDCS features generally have left and right. Vehicle heading and relation to the feature need to be considered when mapping the left/right attributes to ingress/egress. For STNDMob egress, angles are the angles the vehicle would encounter as if they were ingress angles and the vehicle was approaching from the opposite direction. That is, egress is not the angle the vehicle would encounter during egress.

The OneSAF EDM features that have attributes of bank heights, slopes, heights, and widths, and which may be driven over, may be considered obstacles.

Table A4 describes some of these types of features. Each one needs to be examined individually, using its attributes to determine how to define the Standard Mobility parameters.

Table A4. Sample OneSAF EDM features that are obstacles for STNDMob.

Feature Name	Feature Description
AQUEDUCT AREA	A <PIPE> or artificial channel designed to transport <WATER> from a remote source, usually by gravity; an aqueduct.
CROSS_COUNTRY_BARRIER LINE	A permanent or semi- permanent <BARRIER> placed across any <TERRAIN> to prevent <VEHICLE> or<PERSONNEL> traffic
ENGINEER_TRENCH DIRECTED_LINE	An engineered <TRENCH>, or combination trench/berm, usually placed to turn, slow, or stop the movement of <MOTOR_VEHICLE>s.
FIELD_EXPEDIENT_OBSTACLE POINT	A <TERRAIN_OBSTACLE> constructed from various materials in an urban environment.
FORD NODE	A shallow place in a <WATER_BODY> used as a <CROSSING> by <VEHICLE>s or <ANIMAL>s; a ford.
INFANTRY_TRENCH LINE	A <MILITARY_TRENCH> typically integrated into a complex obstacle <SYSTEM>, that is used to provide cover, concealment, protected fighting positions and communications capability for infantry.
LOG_OBSTACLE POINT	A <TERRAIN_OBSTACLE> constructed primarily of <LOG>s.
RIVER AREA	A natural flowing <WATERCOURSE>; a river or stream.
RIVER DIRECTED_LINE	A natural flowing <WATERCOURSE>; a river or stream.
RIVER_CENTRELINE DIRECTED_LINE	The <CENTRELINE> of a <RIVER>.
ROCK_DROP POINT	A massive assemblage of <MATERIAL>, usually in the form of large concrete blocks or cylinders, suspended above or beside a <TERRAIN_TRANSPORTATION _ROUTE>, ready to be activated as a potential <BARRIER> to an advancing enemy ground force, when needed; a rock drop.
TERRAIN_CRATER POINT	A localized <TERRAIN_DEPRESSION> surrounded by higher <TERRAIN>, resulting from an explosion or the impact of a large or high velocity projectile upon the <TERRAIN>; a crater.
VEHICLE_BARRIER POINT	An obstruction placed across a <TERRAIN_TRANSPORTATION _ROUTE> to prevent the passage of <VEHICLE>s; a vehicle barrier.
WADI DIRECTED_LINE	The dry bed of an intermittent <RIVER>, often with steep walls or at the bottom of a <CANYON>, <GULLY> or <GORGE>; a wadi, wash, or arroyo.

Figures A2 and A3 show an aqueduct and OneSAF attributes associated with the obstacle, respectively.

Figure A2. An aqueduct.

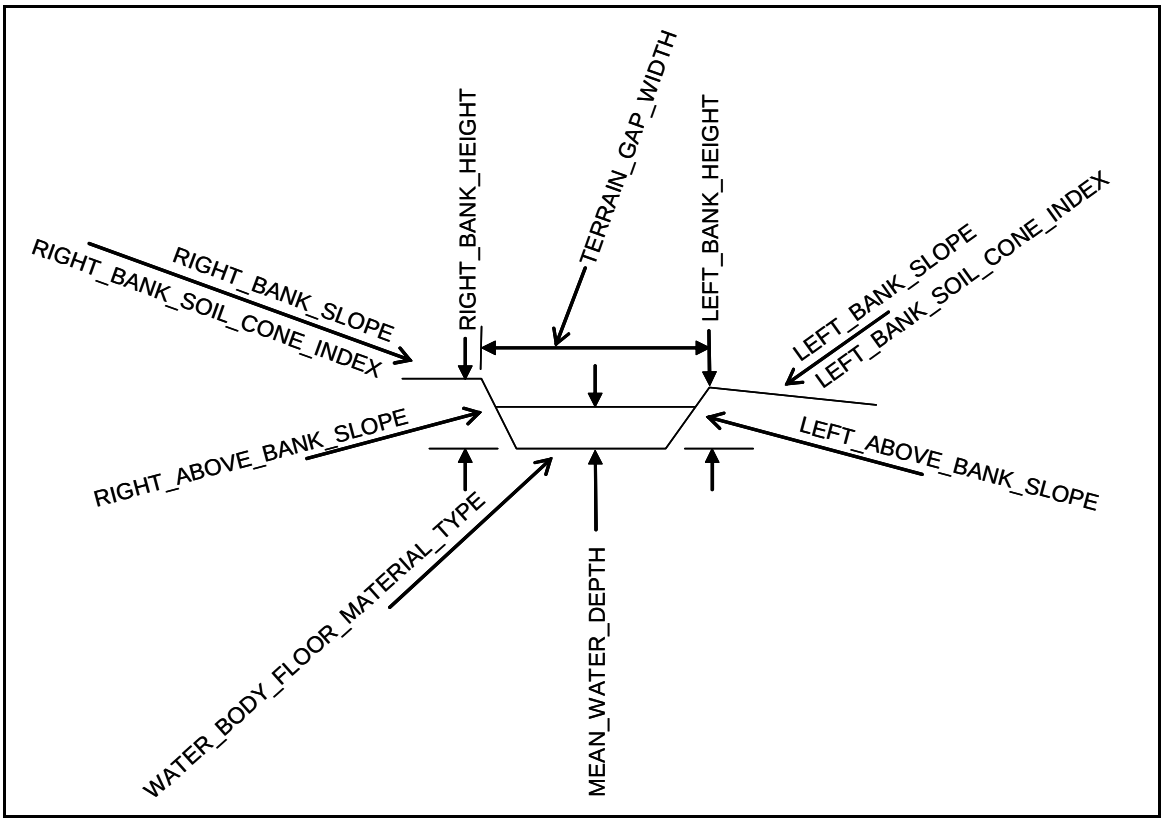

Figure A3. Diagram of OneSAF geometric aqueduct attributes.

Appendix B: ERDC SUGV Performance Tests

Introduction

During the time frame of November 2004 through mid March 2005, three small unmanned ground vehicles were tested by the Engineer Research and Development Center. The vehicles were supplied through the U.S. Navy's Space and Naval Warfare Systems Center (SPAWAR) Robotic Vehicle Loan Program. During the first 2 months, testing was conducted at the ERDC Geotechnical and Structures Laboratory, Mobility Systems Branch, in Vicksburg, MS.

This appendix details the experiments, data collected, and the analysis of those data. The third month of testing was conducted by the ERDC Cold Regions Research and Engineering Laboratory and these tests are mentioned by Lever and Shoop (2006). No significant analysis of the data collected was conducted, although Lever did use his observations of SUGV performance to support his design of a SUGV for over-snow operations (Lever et al. 2006). The three vehicles arrived at the test facilities at different times, so the various tests conducted did not always include all vehicles.

The initial testing was conducted in part to validate NRMM relationships of drawbar pull and Vehicle Cone Index (VCI) calculations. Because of the size of the vehicles (less than 100 lb), test equipment and procedures were modified from those normally used to test full-sized vehicles. Small unmanned vehicles have been used by the Army as early as World War II, and miniature versions of larger vehicles have been built to test various configurations in an effort to reduce labor and costs associated with testing the larger counterparts. However, testing procedures for small unmanned ground vehicles are relatively recent, and a standard test operating procedure for testing small unmanned ground vehicles (Aberdeen Test Center 2002) was used to guide the conduct of the tests described herein.

Vehicles

The three vehicles tested were the TALON, MATILDA, and PackBot (Figure B1). In each figure, the forward direction is shown marked, and this direction was matched to controller logic. The direction of travel

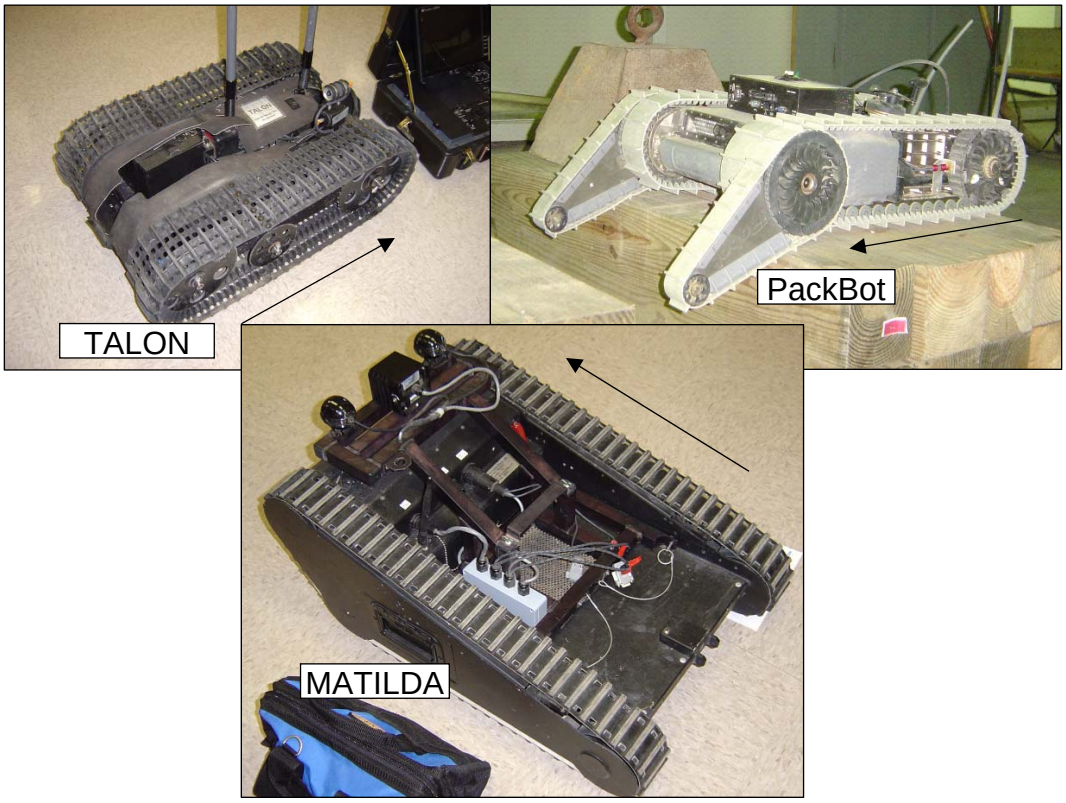

Figure B1. Test vehicles and direction definition during testing.

played an important role during obstacle crossing tests. Table B1 presents basic vehicle parameters (as tested). Figure B2 shows the control unit for the PackBot.

Each vehicle had its own control unit, which was similar to this one. The location of the controller relative to the vehicle and vehicle direction of movement were not specifically recorded. The MATILDA was received after the others and therefore was not available for all the tests.

Table B1. Specifications as measured for testing.

Vehicle	Weight, lb	Height, in.	Width, in.	Length, in.
PackBot	40	18	41	69
TALON	83	11	22	35
MATILDA	61	12	21	30

Figure B2. Control unit for teleoperation of the PackBot.

The specifications for the currently available MATILDA[1] are as follows:

Size: 21 in. W × 12 in. H × 30 in. L
Weight: 61 lb
Batteries: 12 VDC NiMH
Operating Time: 6–10 hr
Speed: 2 mph
Payload Bay Dimensions: 13.5 in. W × 16.5 in. L
Payload Capacity: 125 lb
Towing Capacity: 225 lb
Fording Depth: 6 in.
Ground Clearance: 3 in.
Turn Radius: 0
Stairs: Climbs 50 deg

Additionally, three track types are available: Embassy, Standard, and Ice Track Sets for use on Slick (Marble) Floors, Multi-Purpose–All Surfaces; and Ice and Snow, respectively. Additionally, "long" track sets are available. The track set used for the tests reported herein was the standard. It should also be noted that the towing capacity stated in these specifications does not indicate the coefficient of friction related to the towed load.

[1] http://www.mesa-robotics.com/matilda_spec.pdf.

The specifications for the currently available TALON (with a manipulator arm)[1] are as follows:

Height (arm stowed): 11 in.
Height (arm extended): 52 in.
Width: 22.5 in.
Length: 34 in.
Horizontal reach: 52 in.
Below grade reach: 24 in.
Ground clearance: 2.75 in.
Deployable mast height from ground: 40 in.
Weight: 115 to 140 lb (mission profile dependent)
Maneuverable Speed: 0 to 5.2 mph, variable speed settings: 0 to 7.6 ft/sec
Obstacle Navigation: 43 deg stairs, 40 deg slide slope, 15 in. of snow, demolition rubble
Payload Capacity: 100 lb (45 kg)
Drag Capacity with Gripper: 100 lb (45.3 kg)
Tow Capacity: 200 lb (90.7 kg)
Robot Battery Endurance: Two Lead Acid, 300 W-hr, 36 VDC, 2hr/battery at typical operational speed (rechargeable) or One Lithium Ion (optional) 750 W-hr, 36 VDC, 4.5 hr at typical operational speed

A similar set of specifications for the PackBot is not available from the iRobot Web site.[2] However, the following measurements were obtained from data files created to support the study by Haueisen et al. (2005), as these represent the vehicle as tested.

Width: 20.25 in.
Weight: 45 lb
Max Speed: 4.05 mph
Track length (flipper at 180 deg): 21.25 in.
Track length (flipper at 0 deg): 31.13 in.
Track width: 4.84 in.

[1] http://www.foster-miller.com/literature/documents/TALONBrochure.pdf.

[2] http://www.irobot.com.

Slalom tests

A slalom course was laid out, as shown in Figure B3, with cones staggered at 15-ft-spacing, 4-ft-amplitude, and a total distance of 120 ft. Times to

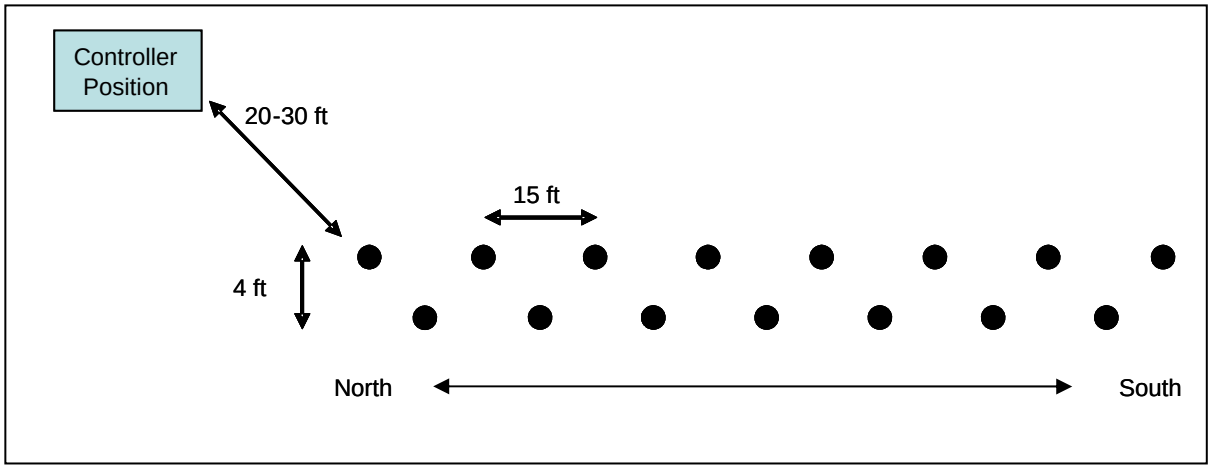

Figure B3. Layout of slalom course.

traverse the course were measured with the vehicle operated with direct operator view as shown in the figure. Table B2 illustrates the time to negotiate the course in the directions indicated. Straight implies that the cones were ignored and the vehicle traveled in a straight line, 120 ft. The PackBot travel time was not measured during this sequence of tests. Tests were run by operating the vehicles from the controller position shown in Figure B3. The vehicles were always within sight of the operator.

Table B2. Slalom test results.

Vehicle	Direction	Time, sec
TALON	North–south	19.88
TALON	South–north	18.91
TALON	Straight	15.38
MATILDA	North–south	53.0
MATILDA	South–north	53.8
MATILDA	Straight	42.0

Gap crossing

Tests were conducted on obstacles by varying the width or gap dimension of the obstacle (shown in Figure B4) until a No-Go was achieved. The obstacles were constructed of 4- by 4-in. (nominal) wooden timbers,

assembled as shown in Figure B4. Vehicles were driven over the obstacles and videotaped for Go and No-Go results. Maximum gap crossing width is a function of the track length with longitudinal center-of-gravity location. Table B3 summarizes the results and obstacle sizes.

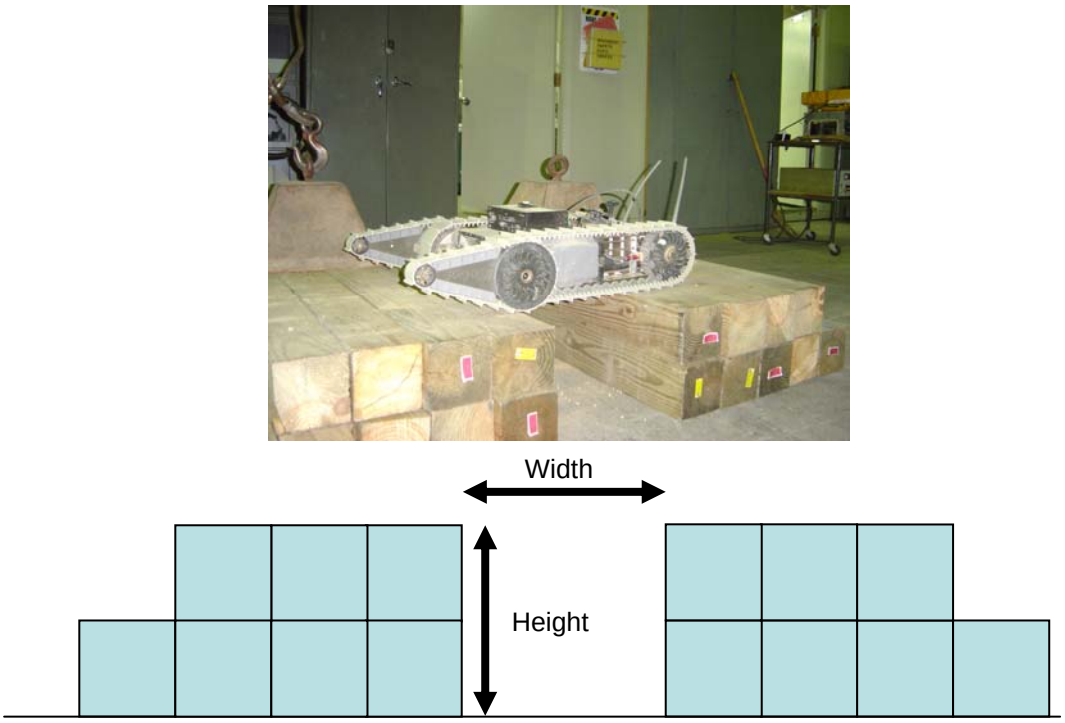

Figure B4. Obstacle crossing configuration.

Table B3. Results of obstacle tests.

Vehicle	Width, in.	Height, in.	Results	Direction
TALON	12.0	11.25	Go	Forward
TALON	14	11.25	Go	Forward
TALON	16	11.25	Go	Forward
TALON	18	11.25	No-Go	Forward
PackBot without flippers	14	11.25	Go	Forward[1]
PackBot without flippers	14	11.25	Go	Backward
PackBot without flippers	16	11.25	No-Go	Forward
PackBot with flippers	16	11.25	Go	Backward
PackBot with flippers	16	11.25	No-Go	Forward

[1] Forward for PackBot indicates flippers were in front; backwards is flippers in rear.

Slope tests

An “adjustable” slope, constructed of plywood and a concrete “board,” was used to determine the maximum slope the vehicles could climb on these surfaces. Table B4 presents the results. WonderBoard® cement backerboard, a common construction material, was used to create the concrete “slopes.” It has a smooth side and a rough side. Interestingly, the rough concrete caused reduced slope climbing performance. This was attributed to reduced contact area between the vehicle and the surface. The weight of the vehicle did not provide adequate grip on the rough surface of the concrete; however, it was an improvement over the plywood.

Table B4. Slope test results.

Vehicle	Materiel Type	% Slope
PackBot	Plywood	58
PackBot	Concrete (smooth)	85
PackBot	Concrete (rough)	76

Stair tests

Stair climbing tests were conducted with the PackBot, MATILIDA, and TALON. The TALON was the only vehicle recorded as a No-Go. The concrete stairs had a vertical step of 8 in. and a horizontal step of 5.5 in. (Figure B5).

Figure B5. Stairs used for tests.

Soft soil tests

Bearing and traction capacities of soils are functions of their shearing resistance. The U.S. Army measures soil strength, as related to vehicle performance, with the cone penetrometer. Cone penetrometer readings are expressed in terms of cone index (CI). The strength of fine-grained soils (silts and clays) may increase or decrease when loaded or disturbed. Therefore, remolding tests were developed to measure any loss of soil strength expected after traffic. The fine-grained soil CI multiplied by the remold index (RI) produces the rating cone index (RCI), which is used to denote soil strength corrected for remolding. A comparison of the RCI with the vehicle cone index (VCI) indicates whether the vehicle can negotiate the given soil condition for a given number of passes. The procedures for measuring cone index, remold index, and their application to the prediction of vehicle mobility is defined in U.S. Army Field Manual (FM) 5-430-00-1 (Headquarters, Department of the Army 1994).

Vehicle immobilization after the first pass as compared to soil strength is illustrated in Figure B6. The mobility index is shown on the x-axis of Figure B6, as defined by FM 5-430-00-1. Mobility index is highly correlated to contact pressure. Soil strength predictions or measurements provide quick assessments of a vehicle's performance off-road. If a soil has a CI of 120 psi and an RI of 0.60 in its critical layer, the soil strength may be expected to fall to 120 times 0.60, or an RCI of 72 psi, under traffic. Therefore, such soil is not trafficable by vehicles that require strengths of 72 RCI or above to operate.

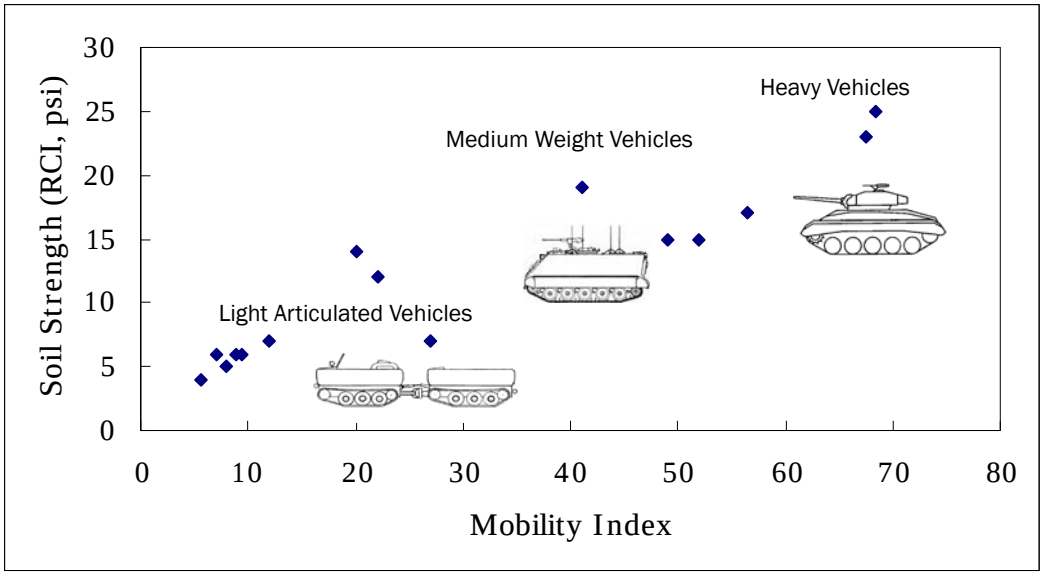

Figure B6. Soil strength conditions immobilizing Army vehicle types.

The predicted ranges of one-pass vehicle cone indexes (VCI_1) for MATILDA, TALON, and PackBot are provided in Table B5 (based on vehicle parameters and NRMM calculations). The SUGV tested in this study were predicted to operate in soil strengths between 5.15 and 9.93 as defined by RCI in fine-grain soils. For comparison purposes, the measured one-pass RCI for a walking soldier reported by Rush and Rula (1967) was 6 RCI, with the speed of the soldier increasing to 4.67 mph for an 11 RCI.

Table B5. Summary of NRMM-predicted VCI_1.

Vehicle	Fine Grain (RCI)	Coarse Grain (CI)	Organic (CI)
PackBot without flippers	9.95	0.57	13.21
PackBot with fippers	8.88	0.42	13.18
MATILDA	6.18	0.22	13.09
TALON	5.13	0.16	13.16

This suggests that the SUGV will operate within the minimum required soil strength for a foot.

Limited field testing was conducted on the TALON and MATILDA in a highly plastic clay soil having a CI of 15 with an RCI of 10. The TALON and MATILDA vehicles operated without immobilization.

Traction

Vehicle traction values are determined by drawbar pull tests. These are conducted using a load cell, string payout, and wheel speed encoders. The load cell measures the pulling force of the vehicle, and the string payout measures the actual distance traveled and vehicle velocity. These values, in conjunction with the wheel speeds, were used to calculate wheel slip (Equation B1). Slip of the wheels (or track) is related to changes in velocity at high pulls (resisting forces) and efficiency or work generated by the vehicle.

$$slip = 1 - \frac{V_{vehicle}}{V_{wheel}} \quad \text{(B1)}$$

Plotting load cell output divided by vehicle weight versus slip combined with an engine/transmission or motor performance curve provides a means of constructing tractive force speed curves for different terrain

surfaces. Alternatively, a drawbar pull test on a hard smooth surface plotted with respect to speed provides a first approximation of the engine/transmission or motor performance curve (i.e., dynamometer test). Typical methods were used to calibrate the load cell and other instrumentation.

PackBot

Results of traction tests of the PackBot are summarized in Table B6. Tests were conducted at several speeds to define the traction relationships on a smooth level concrete surface. The test nomenclature (data file names) consisted of SUGVxxxx, indicating a small unmanned ground vehicle with test number xxxx (a random number selected by the data acquisition system). A plot of the vehicle speed and load (or tractive pull) versus time is shown in Figure B7. In test SUGV731, the PackBot reached a maximum velocity of 4.1 mph and a load approaching 38 lb. As shown in Figure B7, the maximum loads and velocities do not occur at the same time.

Table B6. PackBot drawbar pull tests at various velocities.

Vehicle File	Maximum Load, lb	Maximum Speed, mph	Remarks
Drawbar on Hard Concrete Surface			
SUGV387	52.03	2.84	Slow speed
SUGV453	45.0	2.4	Slow speed
SUGV524	50.1	6.15	High speed
SUGV731	38.0	4.1	High speed
Drawbar on Compacted Dirt Surface Hangar 4			
SUGV659	52.1	2.8	Compacted dirt surface CI ~750+
SUGV781	45.9	2.8	Compacted dirt surface CI ~750+
SUGV549	51.2	6.2	Top 2 in. ~50 CI hard pan below 2 in.
SUGV039	59.7	6.2	Top 2 in. ~50 CI hard pan below 2 in.
SUGV953	28.0	3.8	Top 2 in. ~50 CI hard pan below 2 in.
SUGV616	13.4	3.3	Top 2 in. ~50 CI hard pan below 2 in.
SUGV101	27.4	3.31	Top 2 in. ~50 CI hard pan below 2 in.

Plotting drawbar pull versus velocity of the test SUGV731 is illustrated in Figure B8. In this plot, at stall, the vehicle achieves an average maximum 38-lb pull with the load dropping to zero at a maximum speed of 4.1 mph.

Slower drawbar pull tests were conducted on the hard surface to get higher resolution of the pull and speed relationship. Test SUGV453 illustrates the

relationship observed between speed and drawbar pull for the PackBot in (Figure B9). Filtering of the data to create this plot caused a slight difference in peak load. Figure B10 illustrates results from test SUGV524, that is, a peak load of 50.1 lb and peak speed of 6.15 mph (as reported in Table B6) for a high-speed test on dry concrete.

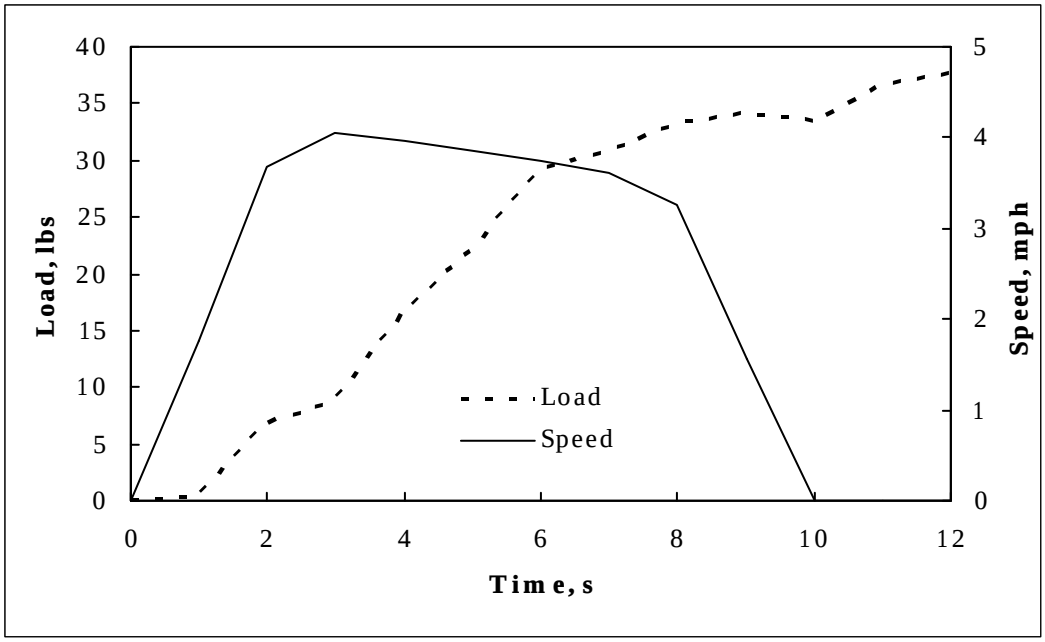

Figure B7. PackBot speed and load versus time (SUGV731).

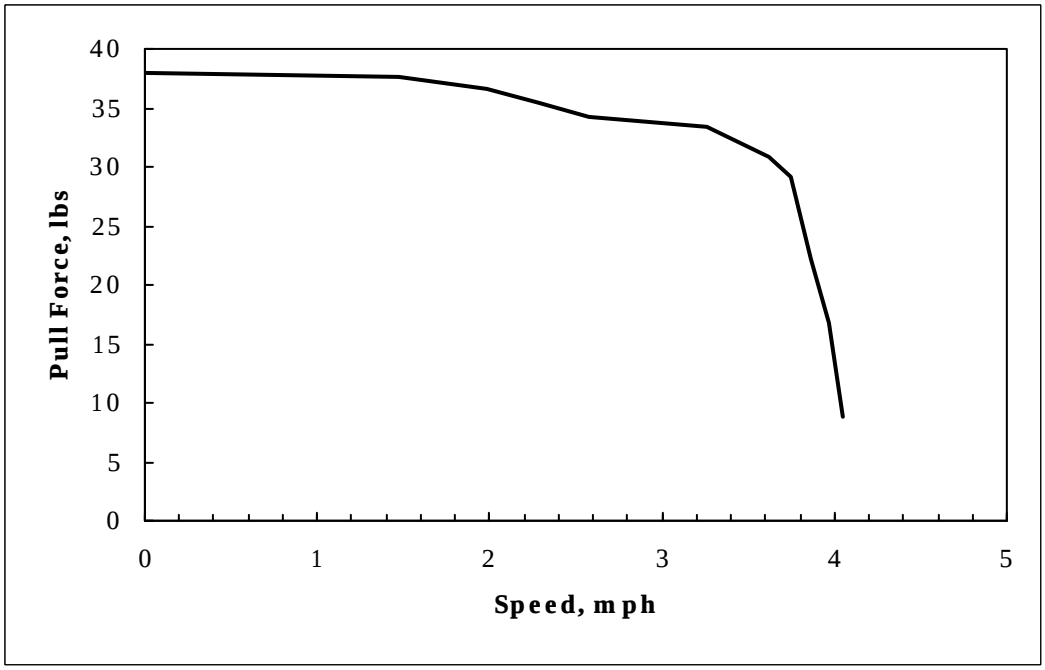

Figure B8. High-speed DBP curve for PackBot (SUGV731).

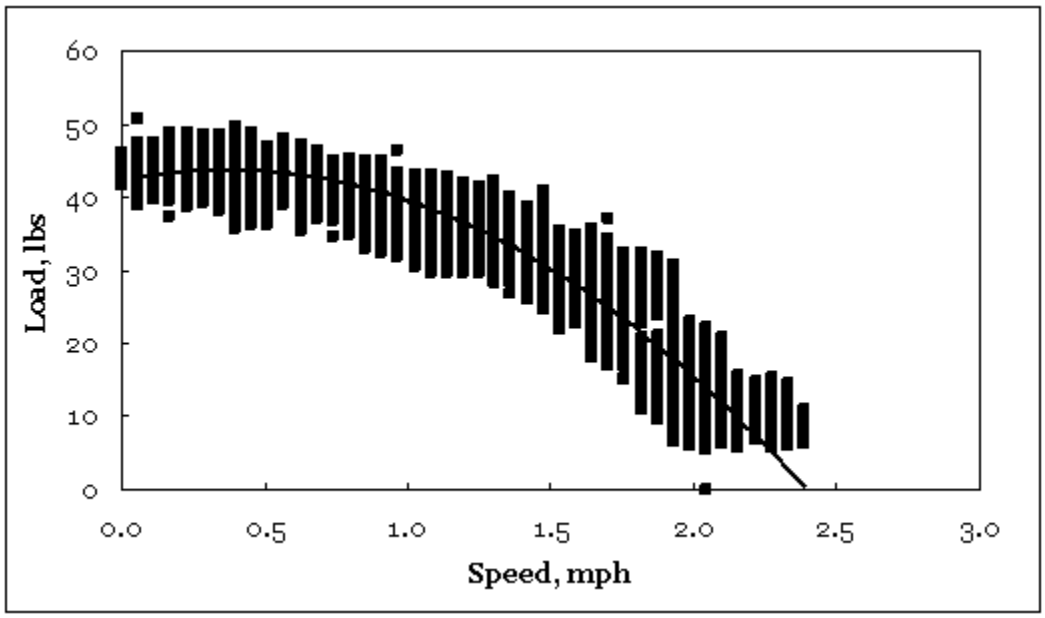

Figure B9. Relationship between vehicle pull and speed (SUGV453).

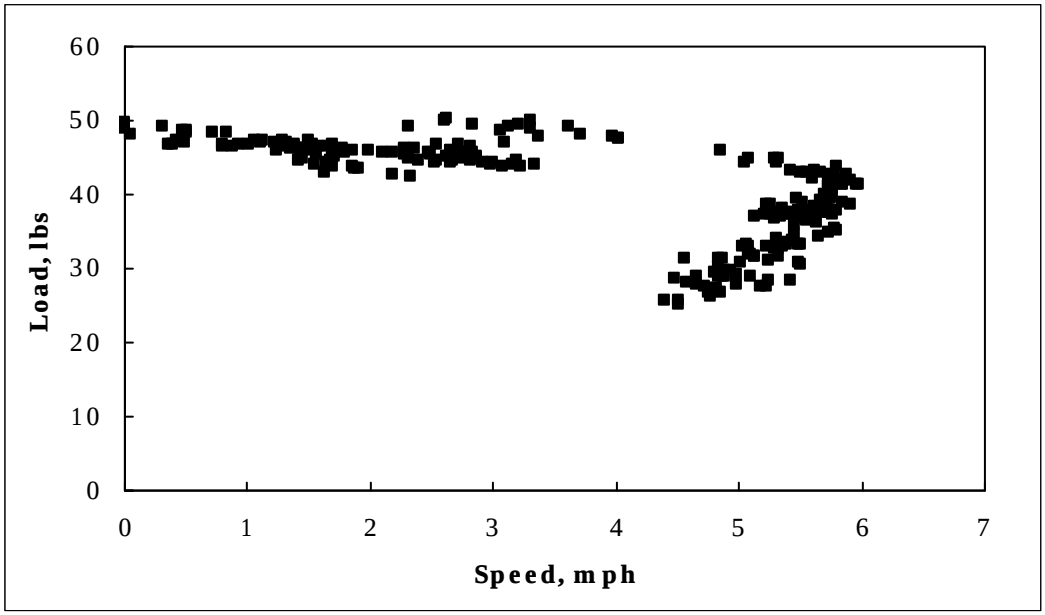

Figure B10. Relationship between speed and load for the PackBot during a hard surface test (SUGV524).

The PackBot was moved to a large hangar, and tests were conducted on loosely packed sandy clay. Three scenarios are depicted in Table B6: a hard dirt surface where the cone index was 750 CI or above, a loose surface with hard underpan where the top inch was less than a 50 CI, and below the top inch where there was a hard pan with a cone index greater than 300.

From these tests, there appears to be a drop in average of peak drawbar pull performance of the PackBot between the loose and compacted dirt surfaces. There is more variability in the "loose dirt" values, an indication of surface strength and loose material variability.

TALON

The TALON remained at the laboratory longer than the other two SUGV systems; therefore, more extensive tests were conducted. Drawbar pull tests were done on hard surface, soft sand, and tall grass areas. Hard surface pull data plotted against speed are shown in Figure B11. Maximum pull was near 100 lb with a maximum speed of 6 mph.

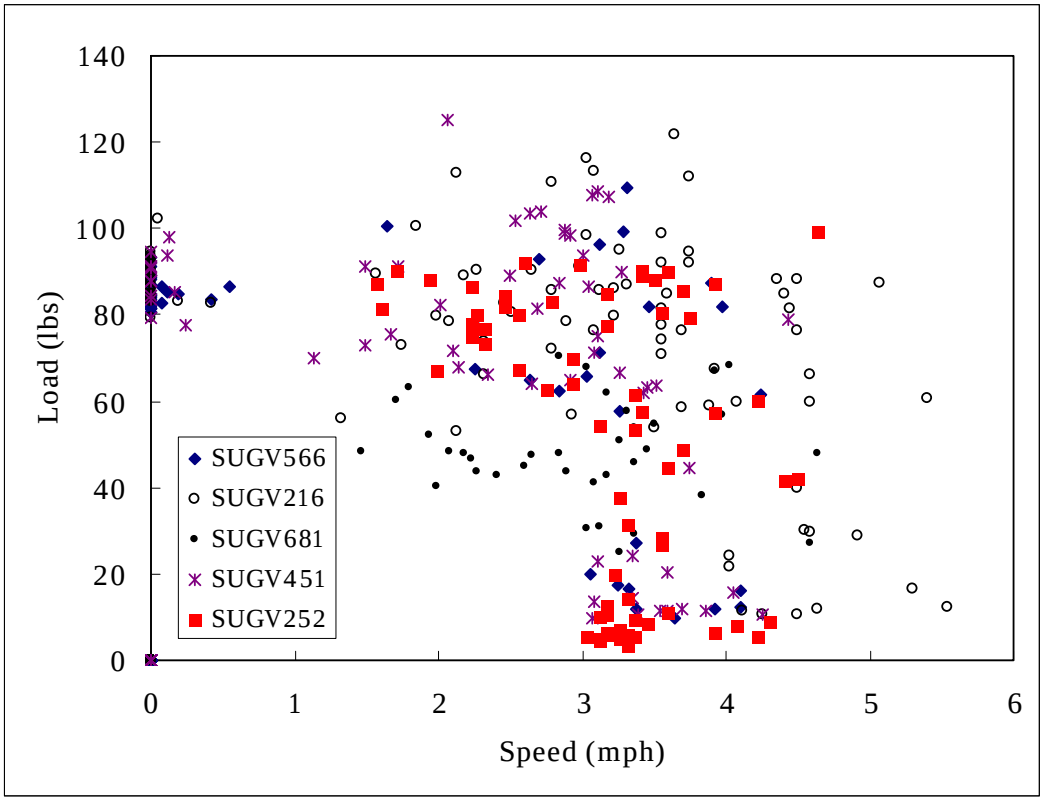

Figure B11. High-speed drawbar pull tests hard surface.

Tests run on the TALON on 20 Feb 2004 consisted of drawbar pull in sand and tall grass (Table B7). Two sand courses were established that were 500 ft long. Soil strength data are depicted in Table B8. The sand was relatively low strength until about 5 in. with an average cone index of 231. A hardpan was encountered at 5 to 6 in. Peak drawbar pulls on the sand course ranged from 108 to 137 lb. The maximum speed was measured at 6.14 mph.

Table B7. TALON drawbar pull test data.

Vehicle File	Max Load lb	Maximum Speed mph	Notes
Tests Conducted on Smooth Concrete Surface			
SUGV566	119.00	4.8	
SUGV681	116.48	4.5	Left track at or near 100-percent slip
SUGV216	127.44	5.6	Vehicle stalled out
SUGV252	108.46	4.5	Rope broke before end of test
SUGV451	137.21	4.5	
TALON_DBP_012704 Tests Conducted on Compacted Dirt Surface			
SUGV193	125.97	5.21	Vehicle stalled at 20 ft
SUGV057	116.70	5.68	
SUGV013	106.93	5.21	
SUGV502	117.33	5.68	
TALON_DBP_012904 Tests Conducted on Compacted Dirt Surface			
SUGV289	117.72	4.26	
SUGV621	111.45	6.15	
SUGV377	130.26	5.68	
TALON_DBP_013004 Tests Conducted on a Combination of Hard and Soft Dirt Surfaces Location: Hangar 4			
SUGV929	94.00	6.15	Top 2 in. ~50 CI hard pan below 2 in.
SUGV688	106.25	5.68	Top 2 in. ~50 CI hard pan below 2 in.
SUGV773	69.93	6.15	Top 2 in. ~50 CI hard pan below 2 in.
SUGV076	115.35	5.68	Surface 750+ CI hard pan below 2 in.
SUGV185	129.98	5.68	Surface 750+ CI hard pan below 2 in.
SUGV178	13.11	4.26	Surface 750+ CI hard pan below 2 in.
SUGV804	112.92	5.68	Surface 750+ CI hard pan below 2 in.
TALON_DBP_020204 Tests Conducted in Poorly Graded Sand			
SUGV486	107.44		Sandy site
SUGV970	105.41		Sandy site
SUGV443	106.76		Sand site
SUGV734	114.16		Sand site
Tests run in 1-m-high Johnson grass			
SUGV371	87.16		Stalled out after 30 ft; ran through grass that is packed down
SUGV558	76.15		
SUGV628	95.75		Vehicle stalled out at about 30 ft
SUGV927	89.08		Battery appeared low
SUGV414	90.38		Vehicle stalled out at about 30 ft
SUGV144	80.72		

Table B8. Sand/grass site DBP tests, soil strength, CI (psi).

	Depth, in.								
Readings	0	1	2	3	4	5	6	7	Average 0–6 in.
	Sandy clay area								
1	25	50	150	250	250	300	350	325	196
2	0	50	75	200	650				195
3	0	50	50	150	300	650	350	300	221
4	0	25	50	200	350	350	325	400	186
5	0	25	50	150	400	400	700		246
6	0	50	75	200	600	750			279
7	25	50	75	300	750				240
8	0	50	100	300	750				240
9	25	50	150	250	350	650			246
10	0	25	75	175	550	750			262
Average									231
	Grass Area								
1	50	75	50	75	150	150	200	750	107
2	75	150	50	50	50	350	175	750	129
3	50	200	50	50	50	200	150	200	107
4	50	100	50	50	25	150	100	200	75
5	50	100	50	25	25	75	100	175	61
6	75	50	25	50	50	100	250	750	86
7	50	25	50	25	0	100	100	150	50
8	50	50	50	25	100	150	150	175	82
9	50	25	50	75	75	125	75	100	68
10	25	50	50	50	25	150	150	400	71
Average									84

Tests were conducted along the length of the course and then in 40-in.-high grass. Maximum speed achieved on the sand course was from 4 to 6 mph. The maximum drawbar pull on the 40-in. Johnson grass was measured at 86.5 lb with a standard deviation of 7.0 lb. The soil in this area was lean clay with a soil strength cone index of 84 for the top 6 in.

Summary

Figure B12 provides a summary of the speed and load characteristic curve for each of the three vehicles. Table B9 presents the performance data used to create NRMM vehicle data files, which in turn are used to create the Standard Mobility vehicle files needed to run the combat models such

as OneSAF. A tractive force speed curve (Haueisen et al. 2005) was used to make predictions and is plotted in Figure B12 as the "predicted" curve. The predicted data were based on scaling the tractive force curve from an M113 to represent the smaller SUGV. The tractive force speed curve shape in Figure B12 appears to identify well with the PackBot, the difference being attributed to motion resistance. Figure B13 illustrates the tractive force divided by weight or drawbar pull coefficient of each vehicle. The predicted values were obtained by Haueisen et al. (2005) and, once again, the shape compares well with all vehicle types.

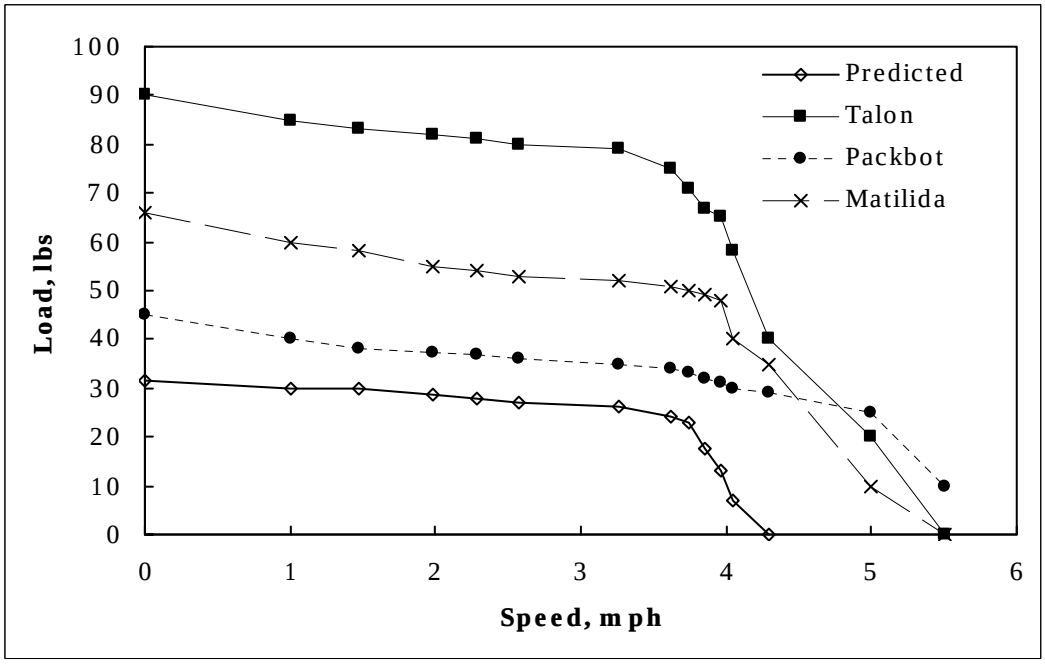

Figure B12. Comparison of drawbar pull versus speed curves for SUGV.

Table B9. Tractive force data for NRMM vehicle file.

	Vehicle			
	Predicted[1]	TALON	PackBot	Matilida[2]
Speed, mph	Load, lb			
0	31.6	90	45	59.5
1	30.1	85	30	49.5
2	28.9	80	37	40.5
3	27	78	35	0
4	13.2	65	30	0

	Vehicle			
	Predicted[1]	TALON	PackBot	Matilida[2]
Speed, mph	Load, lb			
5	0	20	30	0
5.5		0	10	0
6.0			0	

[1] Vehicle file created to support Haueisen et al. (2005) analysis. Predicted data are actually extrapolated data from an M113 that was scaled down to represent the SUGV.
[2] MATILDA was damaged during soft soil tests; data reflect expected performance curve.

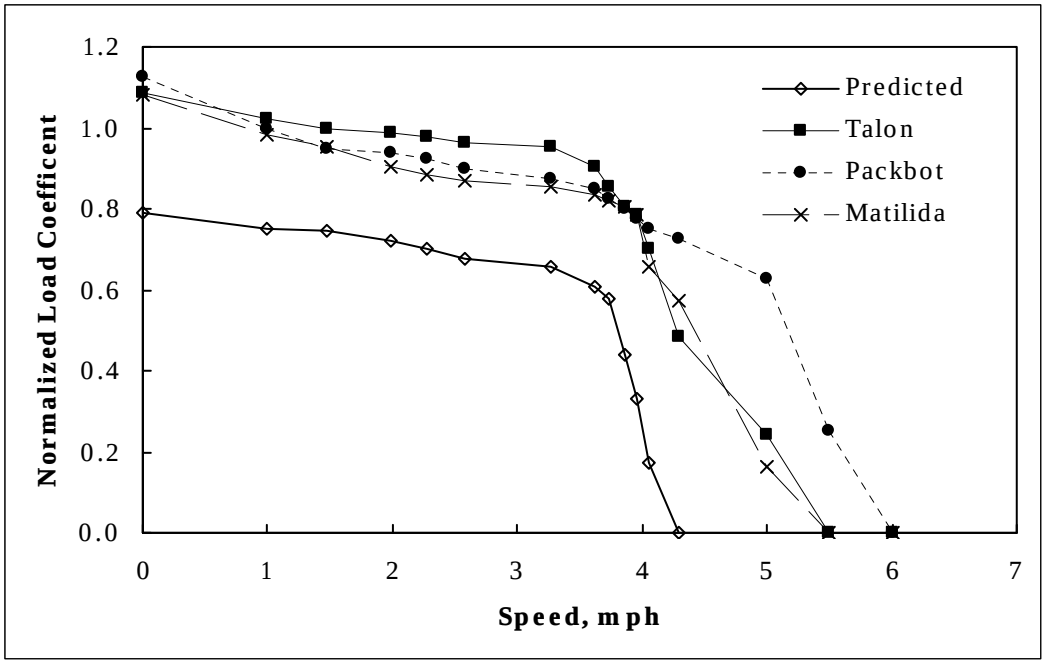

Figure B13. Comparison of normalized (DBP/weight) load.

Appendix C: Electric Motor Modeling for SUGV Trafficablity

Part I. Steady-state conditions

Purpose

This appendix reviews the basic governing equations for small electric motor-powered wheeled or tracked ground vehicles. The intent is to examine the equations and measured results and to develop procedures and algorithms for simulation of SUGV trafficability. Ehsani et al. (1997) also discusses the use of electric motors and tractive force speed curves in the design of electric-powered vehicles.

It is common for small robotic vehicles to use permanent magnet direct current (PMDC) motors. These motors are also used in home appliances, and the representation of PMDC motor performance is well standardized for steady-state conditions. For varying operation conditions as would be seen by a small vehicle, vehicle performance becomes a function of the motor performance, vehicle design, the environment, and operator control. While some of the nonsteady performance parameters can be calculated in a manner similar to full-sized (internal combustion) vehicles, other parameters are directly related to the electric motor performance (for example, skid steering and braking). It should be noted that other motor types (e.g., Wies et al. 2000) can be used, perhaps providing higher efficiencies, particularly in nonsteady conditions.

Theoretical tractive force speed relation

Full-sized vehicle performance, modeled using the STNDMob API, is based on the steady-state theoretical tractive force speed table as represented in an NRMM vehicle data file. In the optimal case, the data are collected for an engine-transmission system on a dynamometer and reported as output torque and drive shaft speed. However, these data are not always available and, thus, have often been developed from field tests (U.S. Army APG 1980).

Figure C1 shows tractive force speed data from NRMM vehicle data files for an M151, an M1084, and an M1A1. The force data values have been normalized by vehicle weight (traction coefficient). Based on terrain type

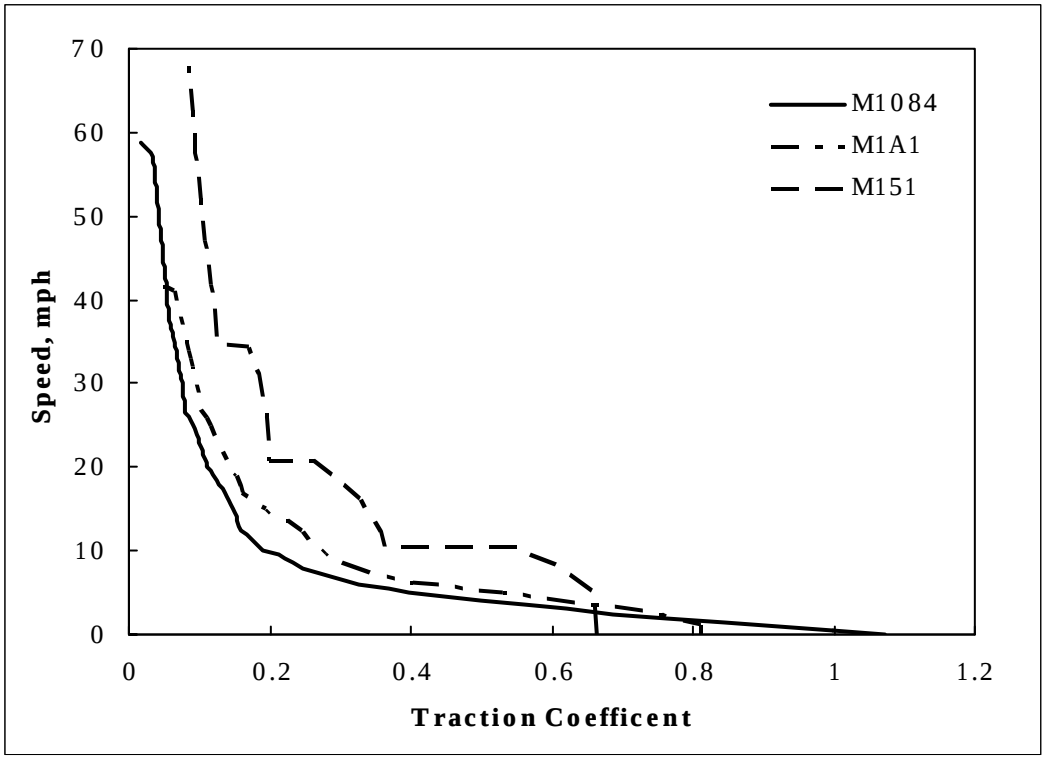

Figure C1. Traction coefficient speed curves for three full-sized combustion-powered vehicles.

and throttle position, these data are adjusted to reflect available traction and fitted to a hyperbolic curve, resulting in a series of curves for all anticipated terrain types. (An example for dry sandy clay was shown as Figure 4 of the main text.) What is important to note is that the curves fall to the left of a tractive force coefficient of 1, and the curves have a hyperbolic shape.

Permanent magnet DC motors

Table C1 presents a list of motor parameter nomenclature and basic performance equations. The units shown are consistent for the equations shown. These parameters and equations can be temperature dependent, and published specifications generally report the temperature at which the data were collected or calculated. At least one manufacturer (Mabuchi Motor Co., Ltd.[1]) provides an on-line design tool that allows the user to change both input voltage and temperature and then recalculates the motor performance curves and parameters.

[1] http://www.mabuchi-motor.co.jp/en_US/product/p_0300.html.

Table C1. Nomenclature and useful equations.

Symbol	Units	Description
τ_m	Newton meter (Nm)	Torque at the motor shaft
ω_m	rad/sec	Radial speed of the motor shaft
R_m	ohms (Ω)	Motor resistance (constant) = V_{in} / I_s
I_o	amps (A)	Motor no-load current[1]
ω_n	rad/sec	Motor no-load speed[1]
I_s	A	Motor current at stall[1]
T_s	Nm	Motor shaft torque at stall[1]
V_{in}	volts (V)	Voltage input to motor
I_{in}	A	Current input to motor
P_{in}	watts (W)	Power input to motor = V_{in} I_{in} (C1)
P_{out}	W	Power output from motor = τ_m ω_m (C2)
K_T	Nm/A	Motor torque constant = T_s / I_s (C3)
K_V	V/rad/sec	Motor speed constant = V / ω. Note that if K_v is not given, it can be shown that it is approximately equal to K_T
r	m	Vehicle wheel radius or, if a tracked vehicle, the effective radius of the drive sprocket.
η	none	Gear ratio = number of motor rotations / number of wheel rotations >>1
F	N	Force tangent to wheel or track edge: $F = \frac{\eta \tau_m}{r}$ (C4)
V	m/sec	Velocity of wheel, or track: $V = \frac{r\omega_m}{\eta}$ (C5)
τ_m	Nm	Torque at the motor shaft: $\tau_m = K_T\left(I_{in} - I_o\right)$ (C6) $\tau_m = k_T\left(\frac{V_{in}}{R_m} - I_o - \frac{K_V \omega_m}{R_m}\right)$ (C7)
ω_m	rad/sec	Speed of motor shaft: $\omega_m = \frac{V_{in} - I_{in}R}{K_V}$ (C8) $\omega_m = \frac{\left(V_{in} - I_o - \frac{\tau_m R_m}{K_T}\right)}{K_V}$ (C9) Note that Equation C9 is equivalent to Equation C7

[1] At a given input voltage (usually the rated voltage).

Theoretical tractive force versus speed curves should be developed at a constant, maximum power. However, as can be seen from Equations C6 and C9 (in Table C1), speed and torque are related through the input current and voltage. Solving Equations C6 and C8 for I_{in} and V_{in}, respectively, and combining with the input power (Equation C1) yields

$$P_{in} = V_{in} I_{in} = \left(\omega_m K_V + I_{in} R_m\right)\left(\frac{\tau_m}{K_T} + I_o\right) \tag{C10}$$

Solving for torque:

$$\tau_m = \frac{V_{in} I_{in} - \omega_m K_V I_o - I_{in} I_o R_m}{\omega_m + \frac{I_{in} R_m}{K_T}} \tag{C11}$$

This provides the relationship among input voltages, current, motor speed, and torque. Ignoring transmission losses, motor speed and torque can be converted to wheel speed and force using Equations C4 and C5.

Barnett (2005) presented the motor specifications for the RS-775SF Mabuchi motor used in the MATILDA robot (motor not currently in Mabuchi on-line catalog), as shown in Table C2, along with applicable vehicle parameters. Using these values, ignoring driveline losses, and noting that the MATILDA has two motors resulted in Figure C2. The maximum motor speed and stall torque are adjusted for gear ratio and wheel diameter so that curve represents the maximum theoretical vehicle speed based on the motor and drive train. The use of 12 V in Equation C12 is based on the MATILDA specification of a 12-V NiMH battery pack, and produces results that agree with the published top speed of 2 mph, if mechanical and minor voltage losses are taken into account. Reducing the voltage to about 10.2 will force the maximum theoretical vehicle speed to 2 mph.

Also shown in Figure C2 is an estimated tractive force speed curve, limited by a traction coefficient of 1 and the vehicle's weight. This is theoretically the highest value that would be measured in field tests. Dry pavement is generally considered to have a traction coefficient of 0.9 for full-sized wheeled and tracked vehicles.

Table C2. MATILDA robot parameters (after Barnett 2005).

Parameter	Value[1]
R_m	0.139 Ω
I_o	2.2 A
ω_n	9350 rpm
I_s	43.1 A
T_s	0.2501 Nm
K_T	0.006114 Nm/A
r	0.0732 m
η	134.17
[1] At 6 V and 25 °C.	

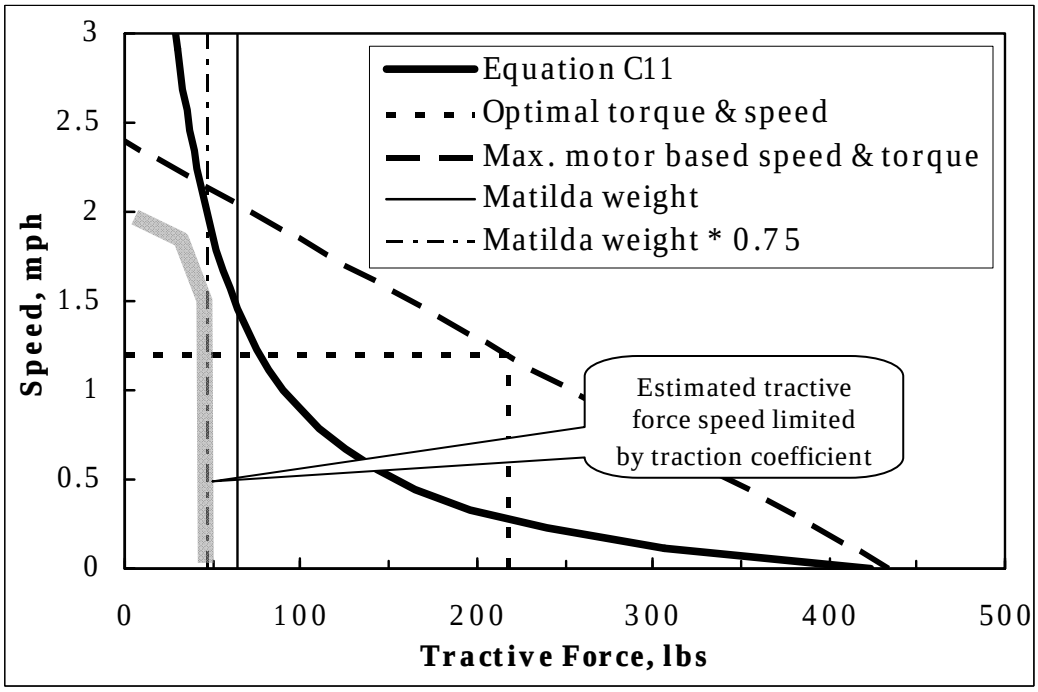

Figure C2. Estimated MATILDA tractive force versus speed at 12 V and 11 A.

Barnett (2005) described the development and testing of a drawbar pull testing device for small vehicles and presents some of the data collected. Figure C3 shows plots of the equations, parameters, and data similar to Figure C2, but at a half-speed setting. From Barnett's analysis, it appears that this is represented by 6 V applied to the motors. He did not, however, report the motor current or input power, nor did he plot Equation C11 or an equivalent. Equation C11 is shown using 6 V and 11 A for the voltage

and current values. Notice how Barnett's range of tractive force data (in Figure C3) is limited by the traction coefficient and vehicle weight.

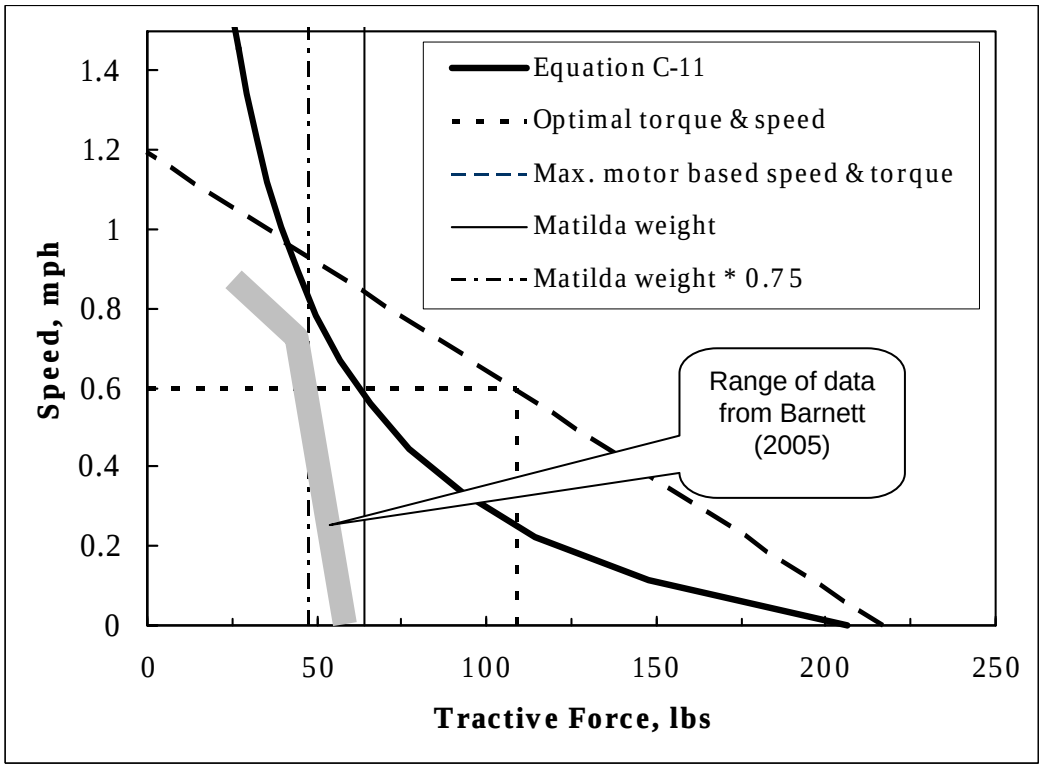

Figure C3. Tractive force speed curves, based on MATILDA parameters at half speed.

Comparing the shape of the tractive force speed curves among Figures C1, C2, and C3 raises an issue associated with the applicability of representing the small electric vehicle data with a hyperbolic curve as done with STNDMob. Haueisen et al. (2005), in order to conduct their case study of the PackBot, created NRMM data files that included a tractive force speed curve. By processing this file with NRMM to create the STNDMob vehicle file, the hyperbolic curve fit for all the terrain surfaces was obtained. Figure C4 shows the NRMM data and hyperbolic curve fit for a primary road, indicating that this curve shape can be represented satisfactorily with a hyperbola.

Summary

From the above analysis, it can be seen that, based on PMDC motor and vehicle design parameters, an estimate of the tractive force speed curve can be obtained. Depending on where the theoretical force speed curve is, in relation to the vehicle weight, will influence its shape. Combustion

engine-powered vehicles have tractive force speed relations that are represented in the STNDMob API as hyperbolas and, for small electric-powered vehicles, this representation is also appropriate.

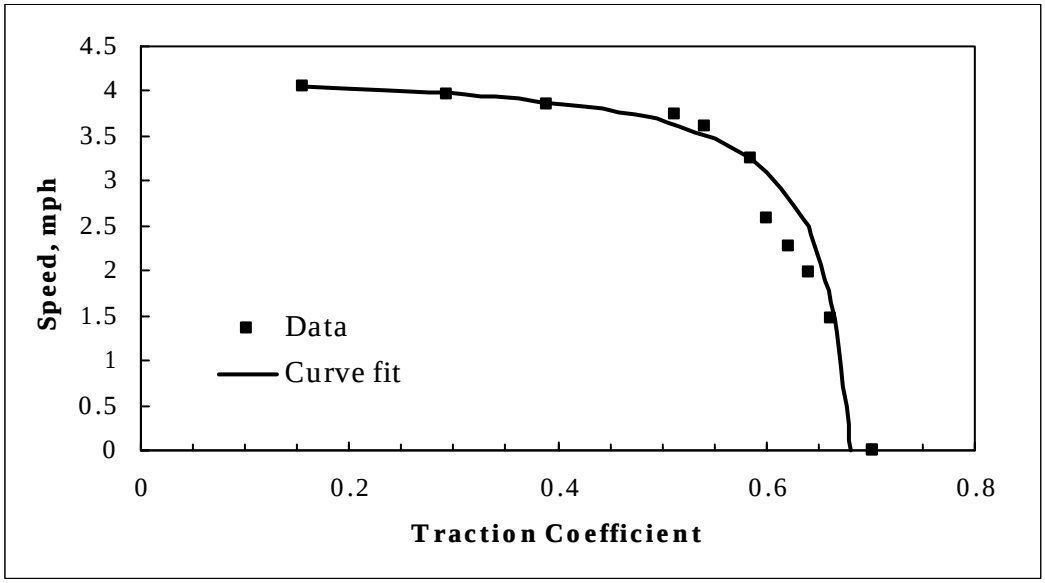

Figure C4. Hyperbolic curve fit to the PackBot tractive force speed data.

Part II. Nonsteady conditions

Purpose

Vehicle acceleration and braking capability are also dependent upon terrain conditions, and while whole vehicle body motion for both full-sized and small vehicles is represented by Newton's law ($F = ma$), acceleration and braking for a small electric-powered vehicle will also be very dependent on the motor characteristics. Previously unpublished improvements to the STNDMob allow available acceleration capability to be calculated based on the tractive force speed curves and current vehicle speed. This section reviews that methodology and its applicability to SUGV.

Available acceleration based on tractive force speed curves

To determine the maximum speed a vehicle is capable of, the STNDMob application calculates the resistance coefficient for the current vehicle location, orientation, driver parameters, and terrain parameters (see Richmond et al. 2005). Using the resistance coefficient T and the tractive force speed curve coefficients for the appropriate terrain surface material and a specified percent throttle value, a maximum vehicle capable speed

(V_{max}) is calculated. If the current vehicle speed is less than this value, the vehicle is capable of acceleration. At the current vehicle speed (V), the effective tractive force is

$$F_{effective} = Wc\left[\frac{ab_0}{(V + b_1)} + ab_2\right] \tag{C12}$$

where:

W = total gross vehicle weight
a and c = horsepower and soil traction correction coefficients for vehicles that are plowing (set to 1.0 if not plowing)
b_0, b_1, b_2 = tractive force speed curve-fit parameters.

The available force is then

$$F_{available} = F_{effective} - T \tag{C13}$$

where T is the traction force (pounds) at the current speed obtained from the 100% throttle tractive force speed curve (regardless of the current throttle setting and is in part used to represent the gear ratio and applied torque relative to the maximum engine torque[1]). The effective vehicle mass is

$$M = \frac{W}{g}\left(R_1 + R_2 T^2\right) \tag{C14}$$

where:

g = acceleration due to gravity
R_1, R_2 = rotating mass coefficients, defined below.

These coefficients are vehicle- and engine-dependent values and account for the inertia of rotating masses, which also need to be accelerated or decelerated. Knowing available force and effective mass, the available acceleration is

[1] A reference for the development of this form of R_2 and T does not appear to exist (personal communication with Richard Ahlvin, ERDC Geotechnical and Structures Lab, May 2007).

$$acceleration = \frac{F_{available}}{M} \tag{C15}$$

Rotating mass coefficients

Currently, the STNDMob API depends upon the vehicle file to contain the rotating mass factors, which are calculated by the NRMM, and are based on rules of thumb for vehicle configuration (R_1) and an empirical equation for the engine/transmission contributions (R_2) (see also McKinley 1988; Smith 1970).

$$R_1 = \begin{cases} 1.14 \text{ if are any track assemblies} \\ 1.03 \text{ if there are no track assemblies} \end{cases} \tag{C16}$$

$$R_2 = \sum_{i=1}^{N} \frac{0.002 I d_i^{1.68} C}{n_i W} \left(\frac{r Q_i}{\eta} \right)^2 \tag{C17}$$

where:

N = number of engines
i = engine index
I = 1.0 for all gas and four-stroke cycle diesel piston engines
= 2.0 for all two-stroke cycle diesel engines
= 3.0 for turbine engines
d = engine displacement (cubic inches) for piston engines (or rated horsepower for turbine engines)
C = 0.125 if engine is a turbine, otherwise = 1.0
n = number of cylinders, use 8 for gas turbines
W = total gross weight (pounds)
r = rolling radius (inches) or sprocket pitch (if there is a track assembly)
Q = maximum engine torque (inch-pounds)
η = 0.7 if there are any track suspension assemblies
= 0.9 if there are no track suspension assemblies.

The R_2 values and a sample effective mass value for the three vehicles discussed in the main text are shown in Table C3.

Table C3. Effective mass of three vehicles at 10 mph and full throttle on dry pavement.

Vehicle (Mass), lbm	R1	R2 (1/lbf²)	Effective Traction Force lbf	Effective Mass, lbm
M1084 (1050.72)	1.03	0.19E-08	8086.9	1212.9
CIV (162.55)	1.03	0.38E-07	3516.1	243.8
M151 (98.0)	1.03	0.705E-07	1344.3	113.4

The rotation mass factors for electric-powered vehicles may be significantly different, and cannot be calculated from Equations C16 and C17. Electric motor specifications often provide the rotor inertia, which is a component of a rotating mass factor. An "Electric Drive Train Simulator (Demo[1])" includes effective mass calculations. The manual shows some sample moment of inertia calculations, but it is not clear how the overall effective mass is calculated. Ehsani et al. (1997) recognized the need to use an effective mass in calculating acceleration, but only estimated the rotating mass factor with a value of 1.0 for their passenger car-sized electric vehicle example. Further analysis and development of a simple rotating mass model for small electric-powered vehicles is required.

[1] www.enigmaindustries.com (15 May 2007).

REPORT DOCUMENTATION PAGE

Form Approved
OMB No. 0704-0188

1. REPORT DATE *(DD-MM-YYYY)*
May 2009

2. REPORT TYPE
Final report

3. DATES COVERED *(From - To)*

4. TITLE AND SUBTITLE
Mobility Performance Algorithms for Small Unmanned Ground Vehicles

5a. CONTRACT NUMBER

5b. GRANT NUMBER

5c. PROGRAM ELEMENT NUMBER

6. AUTHOR(S)
Paul W. Richmond, George L. Mason, Barry A. Coutermarsh, Jason Pusey, and Victoria D. Moore

5d. PROJECT NUMBER
UO-2005-37

5e. TASK NUMBER

5f. WORK UNIT NUMBER

7. PERFORMING ORGANIZATION NAME(S) AND ADDRESS(ES)

U.S. Army Engineer Research and Development Center, Geotechnical and Structures Laboratory, 3909 Halls Ferry Road, Vicksburg, MS 39180-6199;
U.S. Army Engineer Research and Development Center, Cold Regions Research and Engineering Laboratory, 72 Lyme Road, Hanover, NH 03755-1290;
Army Materiel Systems Analysis Agency, U.S. Army Research, Development and Engineering Command, 392 Hopkins Road, Aberdeen Proving Ground, MD 21005-5071

8. PERFORMING ORGANIZATION REPORT NUMBER

ERDC TR-09-6

9. SPONSORING / MONITORING AGENCY NAME(S) AND ADDRESS(ES)

Headquarters, Department of the Army
Office of the Deputy Chief of Staff, ATTN: DAMO-SB
400 Army Pentagon
Washington, DC 20310-0400

10. SPONSOR/MONITOR'S ACRONYM(S)

11. SPONSOR/MONITOR'S REPORT NUMBER(S)

12. DISTRIBUTION / AVAILABILITY STATEMENT
Approved for public release; distribution is unlimited.

13. SUPPLEMENTARY NOTES

14. ABSTRACT

Future Combat Systems will include Small Unmanned Ground Vehicles (SUGV). Several have already been deployed, including the TALON®, an 80-lb SUGV; PackBot® at 50 lb, and Gator™ at 2500 lb. As doctrine, tactics, techniques, and procedures continue to evolve, there exists a need to represent the performance of these vehicles in Army models and simulations. Army simulations such as COMBAT^{XXI} and OneSAF will use the Standard Mobility Application Programmers Interface (STNDMob API) for estimating vehicle performance. Currently, only the Gator can be represented by a STNDMob vehicle class, and it is modeled as a manned vehicle.

This report describes the results of a study undertaken to identify and discuss mobility performance algorithms applicable to SUGV in the weight range of 10 to 5000 lb. Algorithms used by the NATO Reference Mobility Model and the STNDMob were examined. Most of the algorithms currently used in STNDMob were found to be applicable to SUGV. However, it was found that vehicle performance data and algorithms for additional material surfaces and obstacles need to be developed; specifically, models and data for wheeled vehicle skid steering, interior building floor and roof surfaces, and stair climbing are needed. Previously unreported SUGV test results for TALON, MATILDA, and PackBot are presented, and performance estimates described herein compared well using currently available algorithms in STNDMob. Recommendations for new algorithms and improvements to current mobility algorithms are presented.

15. SUBJECT TERMS
Mobility
Mobility modeling
Modeling and simulation
SUGV
Tractive-force relationship
Unmanned vehicle
Unmanned vehicle performance

16. SECURITY CLASSIFICATION OF:			**17. LIMITATION OF ABSTRACT**	**18. NUMBER OF PAGES**	**19a. NAME OF RESPONSIBLE PERSON**
a. REPORT	**b. ABSTRACT**	**c. THIS PAGE**			**19b. TELEPHONE NUMBER** *(include area code)*
UNCLASSIFIED	UNCLASSIFIED	UNCLASSIFIED		110	